NETS 2020

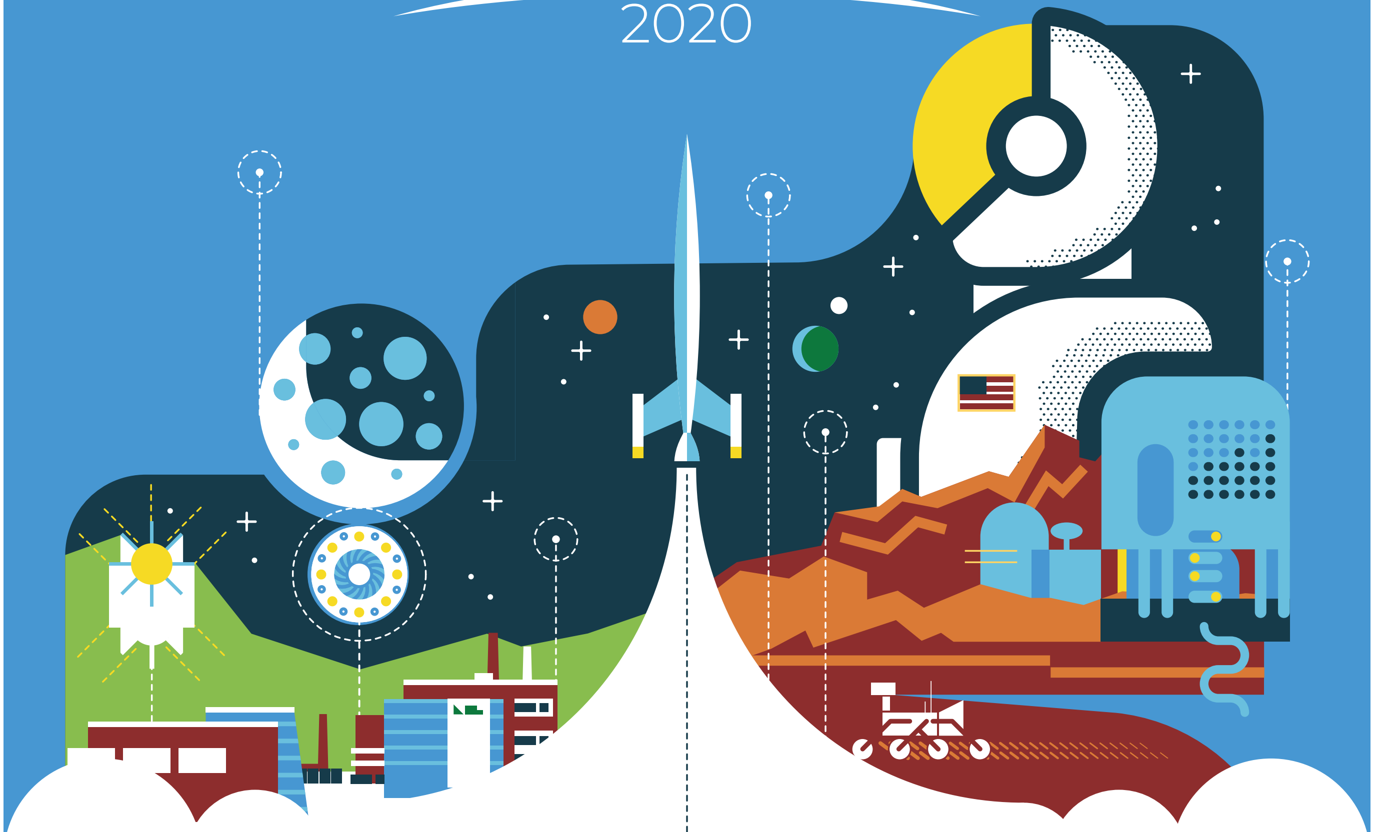

CONFERENCE PROCEEDINGS

NUCLEAR and **EMERGING TECHNOLOGIES** for **SPACE**

Knoxville, TN 2020, April 6th – 9th

Track 4: Advanced and Emerging Technologies for Nuclear Space Applications

Technical Track Chairs: Steve Howe & Gerry

Jackson

Oak Ridge National Laboratory

U.S. Department of Energy

Author	Title
Adams, Robert	Pulsed Fission Fusion (PUFF) Propulsion Crewed Mars Vehicle - Preliminary Results
Greason, Jeffrey K.	Fusion Pellet Runway Revisited
Greason, Jeffrey K.	Nuclear Fission With Supersonic Isothermal Expansion
Greason, Jeffrey K.	Solar-Wind Powered Reaction Drive
Howe, Troy	Affordable Deep Space Nuclear Electric Propulsion Spacecraft
Jackson, Gerald P.	Antimatter-Based Propulsion For Exoplanet Exploration
Jackson, Gerald P.	Antimatter-Based Spacecraft Power Generation
Morris, Nicholas A.	Stay Cool - Alternatives For Long Term Storage of Large Quantities of Liquid Hydrogen on a Mars Transfer Vehicle
Raju, Rittu S.	Modeling an Open Cycle Gas Core Nuclear Rocket: Current Status and Challenges
Schillo, Kevin	Modeling of Pulsed Fission Fuel Target Compression
Tarau, Calin	Advanced Thermal Management Concept For Nuclear-Powered Ice Melting Probe
Wang, Jianjian	Advanced Waste Heat Recovery Technology by Thermo-Radiative Cell for Nuclear Space Power Applications
Weed, Ryan W.	Radioisotope Breeding for Positron Microfusion Propulsion

Nuclear and Emerging Technologies for Space
Knoxville, TN, April 6 – April 9, 2020, available online at https://nets2020.ornl.gov

PULSED FISSION FUSION (PUFF) PROPULSION CREWED MARS VEHICLE – PRELIMINARY RESULTS

Robert Adams[1], ,Magdalena Allen[1], Nathan Blaylock[3], Augustin Demonceaux[1], Glen Doughty[1], Patrick Giddens[2], Kimberly Gonzalez[1], Troy Howe[3], Steve Howe[3], John Kuczek[1], Nathan Schilling[2], Kevin Schillo[2], William Siedler[2], Brian Taylor[1], Rosemary Williams[1]

[1]Marshall Space Flight Center, Huntsville, AL, 35806
[2]University of Alabama in Huntsville, Huntsville, AL, 35899
[3]Howe Industries, LLC, Tempe, AZ, 85281

Primary Author Contact Information: 256-544-3464, Robert.b.adams@nasa.gov

The PuFF (Pulsed Fission Fusion) project aims to revolutionize space travel through nuclear propulsion. PuFF will produce both high specific impulse (I_{sp} 5,000-30,000 sec) and high thrust (10-100 kN), enabling quick (~1 month) transit times to Mars, the outer planets and exiting the solar system (~5 years).

I. INTRODUCTION

Several efforts were made to improve the vehicle design concepts during this performance period. First we worked with the trajectory department at MSFC to create some performance parametrics for a crewed Mars mission. Second we developed a spreadsheet to calculate 0th order parameters for engine performance as a function of target size, composition and some other parameters. Finally we've contemplated using influence diagrams to evaluate the numerous variables feeding PuFF performance and to manage our quest to find the optimal parameter set. All of these efforts are in a state of progress and will only be summarized here, anticipating a more detailed description in a later report.

Each of the subsystem below, as well as mission trajectories, will be discussed in a separate section below.

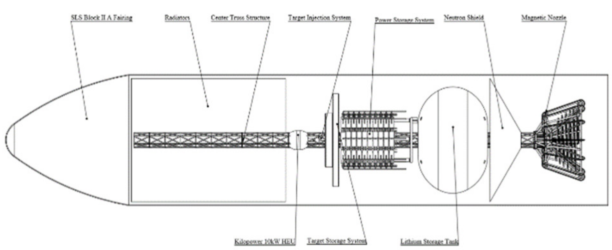

II. TRAJECTORIES TO MARS

The trajectory department incorporated decks supplied by the team for a PuFF powered mission to Mars in 180 days. The plots below show the first parametric calculations for final mass to Mars as a function of the thrust to weight and specific impulse. Future efforts will create these plots for faster trip times, incorporate a round trip analysis, and evaluate other missions of interest. The team anticipates that these curves, combined with performance curves created for a variety of target sizes and other performance parameters, will allow optimization of the PuFF concept engines to be further evaluated.

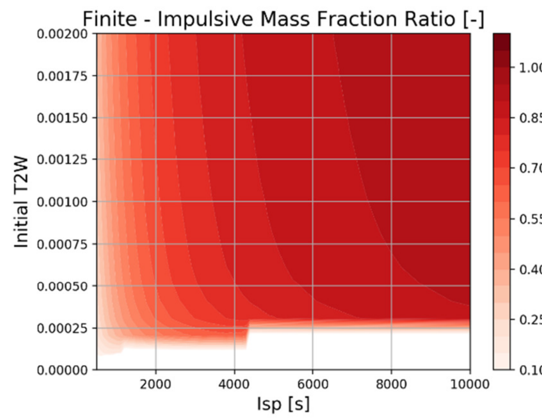

Fig 1. Final Mass fraction ratio vs Thrust to Weight and Specific Impulse for a 180-day one-way trip to Mars.

III. PULSER SUBSYSTEM

The pulser subsystem is responsible for delivering the pulse to power the Z-pinch for target implosion. The pulse must deliver 10-25 MA within a width of 2-15 μs. Linear Transformer Drivers (LTDs) are an advantageous option for supplying the pulse due to their compact design (and therefore reduced size and mass) compared to traditional pulsed power systems. LTDs can also be constructed using off-the-shelf capacitors. The pulse is delivered from the LTDs to a central line (bus) that carries it to the injected lithium liner for target implosion.

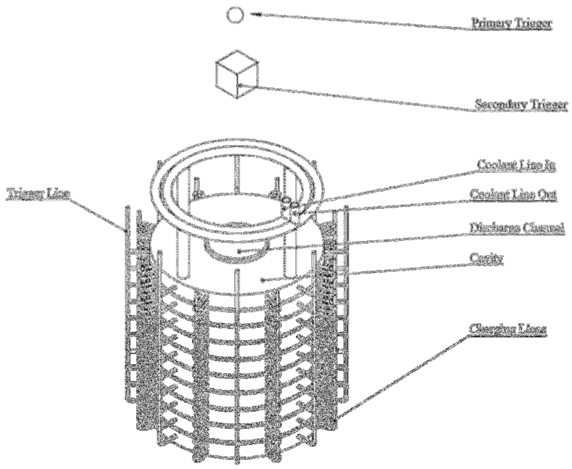

The LTDs provide the pulse for the Z-pinch. LTDs are an array of capacitors and switches used to deliver a high-current, narrow pulse. The base subassembly of the LTDs is called a brick. A brick consists of two capacitors charged to opposite voltages (most likely 100 kV for this application) and separated by a spark-gap switch. The switch closes a circuit that builds opposing voltages across a dielectric (either gas or oil), aided by ferromagnetic cores. This pulse is inductively transmitted to a central transmission line that runs axially along the ship and delivers to the Z-pinch. See Figure 1.[i]

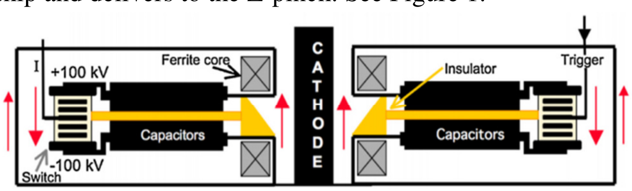

Figure 1 – Cross-section of an LTD cavity.[i] A brick is shown on each side of the central bus (cathode).

Brick are arranged into “pizza pie” circular arrangement, called a cavity, with the central bus running along the center axis. Multiple cavities can be stacked vertically along this axis, creating what is called an LTD stack. The LTDs fire for each target implosion, thus at a rate of 10 Hz when the engine is in operation.

IV. LITHIUM INJECTION SUBSYSTEM

The gas pressurized system is considered to be the most attractive for the storage and injection of lithium. The gas pressurized system is commonly used in conventional modern chemical rockets today and is well understood. An inert gas, such as helium, is kept in a highly pressurized storage tank and pumped into the main liquid fuel tank. The pressure from the helium forces the liquid’s movement through an exit in the fuel tank. The lithium is then pumped to the manifold for injection. Heating elements wrapped around the fuel tank will melt the lithium.

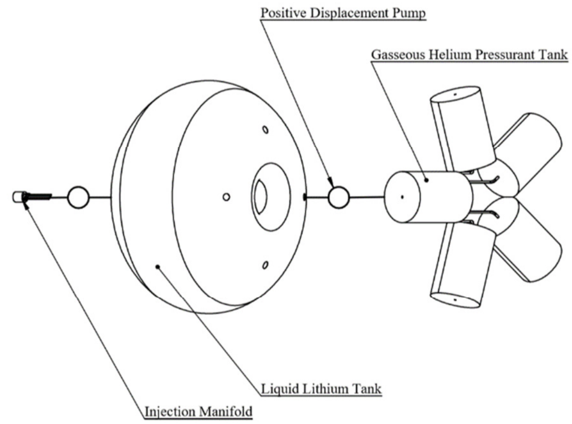

Previous work by the University of Maryland[Error! Bookmark not defined.] on LH2 cylindrical tank mass estimations was used. 60 MT was given for the mass estimation of lithium propellant. Assuming the lithium will begin as a solid, a volume of 112.4 m^3 is expected. Accounting for ullage and residuals, the volume of the lithium tank is assumed to be about 10% larger than the lithium propellant volume. The mass and volume relation (y=12.158x) for the LOX tank (red) is shown in **Error! Reference source not found.**. A factor of 20% is added to the mass estimation to account for the change from a cylindrical tank to a toroidal tank. An additional estimating factor of 20% is included for the tank. The equation used to find the tank mass estimate is shown below.

$$m_{Li\ tank} = 9(1.2)(1.2)V_{Li\ tank}$$

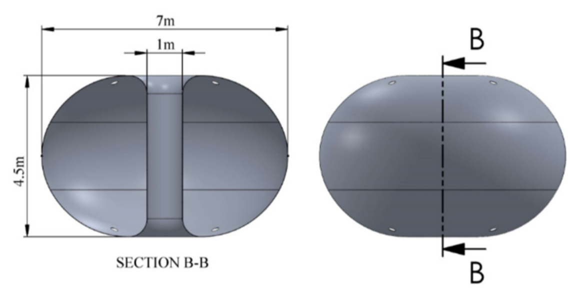

V. TARGET SUBSYSTEM

The PuFF system centers on a fission fusion reaction in a uranium target, which is injected by a railgun or a mechanical assembly with a frequency up to 10 Hz. Before injection, targets must maintain a subcritical configuration in flight and in failure mode (such as being dropped in the ocean, or a jammed injection system.

The figure below illustrates a three-capacitor system that allows two capacitors to recharge while the third one fires into the rail gun. The normally open switch connecting the power source to the capacitor prevents charging in case of power failure, as does the normally-closed ground switch that only opens during firing.

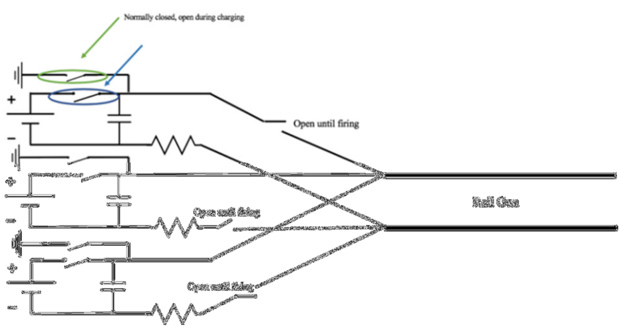

For pellet storage, a compact arrangement of 100,000 highly enriched cylindrical Uranium pellets must be computationally modeled to determine if the assembly will go critical while waiting for injection and implosion. The maximum anticipated target has a diameter of 3 cm and a height of 2.77 cm. The ratio of length to diameter used to optimize *k*-effective (k_{eff}) for a right circular cylinder can be shown to be is L = 0.924D.

MCNP models simulated 100,000 pellets arranged in a hexagonal lattice resting on boron plates. The general design for the storage container is a cylinder with a hole down the middle to make way for the structure. The design stores two layers of Uranium pellets and consists of a cylinder with an outer diameter of eight meters and an inner diameter of one meter.

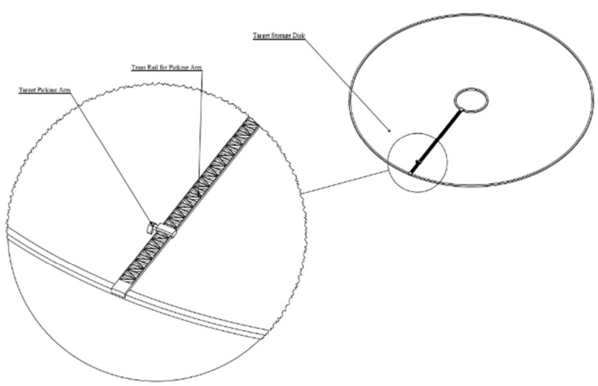

25 MA, *r* = 10 cm		25 MA, r = 15 cm		50 MA, *r* = 10 cm	
Hollow (%)	k_{eff}	Hollow (%)	k_{eff}	Hollow (%)	k_{eff}
0	1.3108	0	1.93996	0	0.41346
25	0.14971	25	2.20935	25	0.42152
50	0.12029	50	1.99138	50	1.8355
90	0.92591	90	1.85358	90	0.33288

VI. MAGNETIC NOZZLE SUBSYSTEM

After the target is imploded, hot plasma expands within the magnetic nozzle. The nozzle uses High Temperature Superconducting (HTS) thrust coils to produce a strong magnetic field (1-40 T within 10 cm of the coils). These field lines direct the plasmoid out of the nozzle and produce thrust. The nozzle will be heated by the photon and neutron radiation from the plasma and cooled by molten salt, likely FLiBe (Fluorine-Lithium-Beryllium), and the HTS coils will be additionally cooled by a cryogen, likely liquid nitrogen (LN_2; 77 K) or liquid helium (4.2 K or less).

The magnetic nozzle subsystem consists of the thrust coil assembly, quench protection assembly, power supply assembly, molten salt coolant assembly, and cryogenics assembly.

For the fields required for PuFF (1-40 T) indicate the use of HTS, whether a LN_2 cooling system or LHe is required. Mostly likely, to get high enough current densities and to handle its own self field, LHe temperatures will be necessary even with the use of HTS (SuperPower Inc. lists their REBCO tape as withstanding only up to ~1 T applied field at 77 K**Error! Bookmark not defined.**). MagLab provides a quantitative map of the critical surface for Yttrium Barium Copper Oxide (YBCO), shown in **Error! Reference source not found.**.[ii]

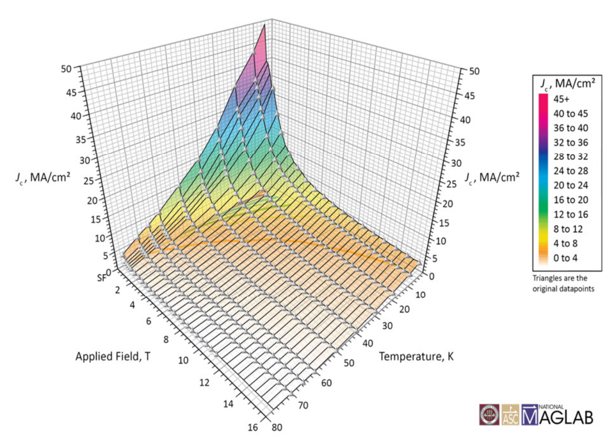

A second model of the thrust coil to account for evolving thermal designs is also presented. It is a circular model that keeps the superconductor in the center of the assembly surrounded by layers of insulation and thermal mediums to facilitate the steep temperature gradient that will be required to maintain superconducting temperatures. See **Error! Reference source not found.**.

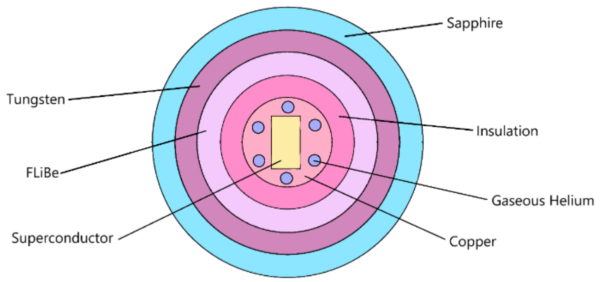

VII. POWER GENERATION SUBSYSTEM

Power required for charging the LTDs and target ignition is quite high – 10 MJ per target ignition is needed. This power could be provided by a fission reactor, and is for system start-up and shut-down but for the majority of system operation is it advantageous to use some of the energy that would normally be lost during target ignition and expansion. The primary loss mechanism of the target during expansion is radiation losses, as most of the energy generated by the target goes into high-energy gamma ray photons or neutrons that speed away from the target and do not provide thrust or specific impulse. An important secondary loss mechanism is inductive losses, as the target expands and rapidly changes the magnetic field in the magnetic nozzle, this induces eddy currents in conductors in the nozzle.

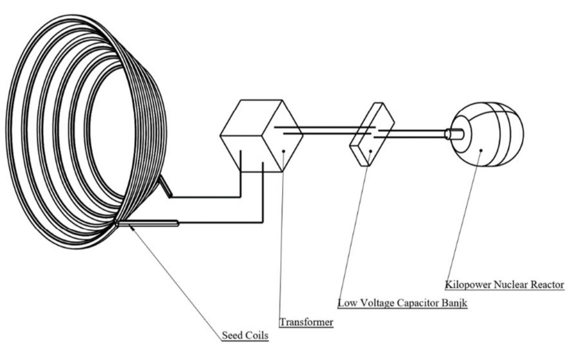

VIII. THERMAL SUBSYSTEM

In this advanced propulsion engine, the difference in temperature between the magnetic nozzle subsystem and the superconductor assembly is significant. The superconductor assembly remains at approximately 77 Kelvin or below while the magnetic nozzle subsystem goes to temperatures of up to 1,500 K. If the temperature of the superconductor assembly exceeds 77 K, it will no longer operate correctly. There are two main designs being considered to solve this problem.

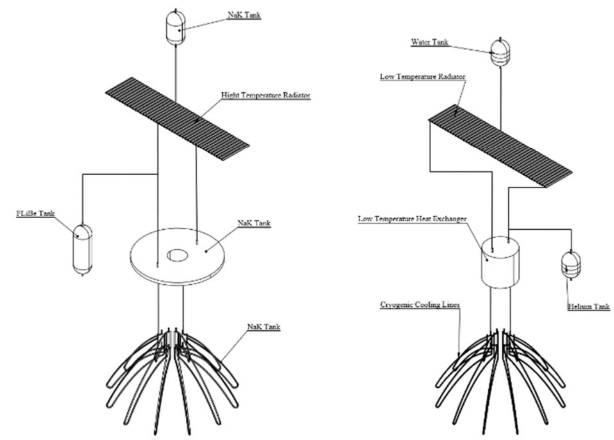

In this advanced propulsion engine, the difference in temperature between the magnetic nozzle subsystem and the superconductor assembly is significant. The superconductor assembly remains at approximately 77 Kelvin or below while the magnetic nozzle subsystem goes to temperatures of up to 1,500 K. If the temperature of the superconductor assembly exceeds 77 K, it will no longer operate correctly. There are two main designs being considered to solve this problem.

(a) To mediate the differences in temperature, a system of coolant pipes, heat exchangers, and radiator assemblies will be used. A Brayton cycle will be used to moderate the flow from the heat exchanger to the superconductor coolant pipes and vice versa. One heat exchanger will suck heat from the superconductor assembly, and also the flow from the Brayton cycle. The radiators will radiate heat from the engine to deep space.

(b) The second design eliminates the connection between the magnetic nozzle coolant flow and superconductor coolant flow. The Brayton cycle is replaced by a second set of radiators that only interact with the superconductor flow. The edited flow chart can be seen in **Error! Reference source not found.**.

V. CONCLUSIONS

While the vehicle described herein is not complete or closed, substantial progress has been made on the design of the individual subsystems. There are several system to system interactions that need to be resolved before vehicle closure. Work continues on this design.

REFERENCES

[i] Mazarakis, M. G. et al., "High current, 0.5-MA, fast, 100-ns, linear transformer driver experiments," Physical Review Special Topics (2009).

[ii] Applied Superconductivity Center, National High Magnetic Field Laboratory (MagLab), "Plots: Critical Surface of YBCO Tape," https://nationalmaglab.org/magnet-development/applied-superconductivity-center/plots. Accessed: 2019.

Nuclear and Emerging Technologies for Space
Knoxville, TN, April 6 – April 9, 2020, available online at https://nets2020.ornl.gov

FUSION PELLET RUNWAY REVISITED

Jeffrey K. Greason[1]

[1]*Tau Zero Foundation, Midland, TX 79707*

jgreason@tauzero.aero 805-508-4437

The concept of the "seeded Bussard ramjet" or "Fusion Pellet Runway" has been long discussed in the community but seldom published in technical papers. Modern capabilities in "chipcraft" smart pellets make the technical realization of this capability more attainable. Meanwhile, modern pulsed fission or fission-fusion concepts for high thrust rocketry face specific power limits driven in part by the "internal" energy flows required to capture, store, and switch the energy for igniting each pulse, a limitation which can be overcome with a pellet runway. The literature on the concepts is summarized and reasons for its reexamination in modern propulsion discussed.

I. BACKGROUND AND MOTIVATION

High performance missions such as interstellar probes require very high mission velocities and for that reason, fusion reactions, as the highest specific energy reaction next to antimatter, have long drawn attention. However, realistic considerations of power conversion lead to practical exhaust velocity limits in the range of 10^6-10^7 m/s. When combined with a desire for practical acceleration times (a few years, say ~10^8 seconds), very high specific power is required (0.015-1.5 MW/kg overall, or ~0.6-60 MW/kg for the drive alone). These are daunting challenges that have provoked a search for alternatives.

I.A. Beam and Pellet Propulsion

The use of external power overcomes these limits. Beam velocities of a few percent of lightspeed are quite simple for elementary charged particles; more daunting for macroscopic pellets, but in principle attainable with long accelerators or laser-driven lightsails.[1,2,3]

The challenge for any form of beam propulsion is the divergence of the beam, which limits the range over which acceleration can take place. While the limits for beam propulsion are subject to technological improvement, there will always be some limit.

G. Nordley[2] suggested that if the macroscopic pellets include some form of onboard navigation, control, and a way to apply steering forces, the pellet range can be extended without limit. Jordin Kare[3] greatly expanded on these themes, including discussion of how external reference beams can provide the required navigational accuracy.

However, the power requirements for the beam are significant and beam cost tends to scale with power. To drive even a 1000 kg probe to 5% of c would call for a beam with pellet velocity on the order of 10% of c. Achieving that velocity in 10^8 seconds is a beam power (even with 100% efficiency) of 1.5 GW, for years.

I.B. Bussard Ramjet

Bussard[4] suggested that fusion could be powered by hydrogen scooped from the interplanetary or interstellar medium which would also form the reaction mass for a ramjet propulsion system. Unfortunately attempts to design effective magnetic scoops have been plagued with high inlet drag[5,6], though work continues[7,8].

I.C. Fusion Pellet Runway

Whitmire and Jackson[9] appear to have been the first to realize that ramjet limitations could be overcome by seeding the path in front of the ship by reaction mass or by fusion fuels from a space-based pellet launcher, discussed further by Matloff[10]. Jordin Kare appears to have been the first to realize that self-steering smart pellet and impact-triggered fusion could be combined, in a presentation at a workshop on robotic interstellar probes in the mid 1990's titled "Impact Fusion Runway for Interstellar Propulsion"[11] which unfortunately did not include published proceedings. He presented that work informally at many other space conferences through the late 1990's and 2000's, and it has been called the "Bussard Buzz Bomb" and the "Fusion Pellet Runway." [12]

In this approach, a pellet launcher launches smart pellets, preceding the spacecraft which are primarily fusion fuel rather than inert reaction mass. The impact energy of the spacecraft overtaking the pellet provides the ignition energy for a pulsed fusion system.[13,14]

Unfortunately, Dr. Kare passed away suddenly in 2017 before he could republish his original notes. However, his solution to the problem of navigation and acceleration of fusion pellets was essentially the same as that envisioned for pellet propulsion.[3]

Dr. Kare also had worked out the "starting problem", which is that a fusion system which relies on the impact energy of the incoming pellet has to get up to speed somehow. So long as the pellet launcher can launch at more than twice the minimum impact energy, starting can be achieved by laying down most of the runway with high speed pellets, then tapering off the speed so the last few pellets are slow, then launching the spacecraft, and then switching back to high speed "chasing" pellets to start the ship. As the ship accelerates, the closing velocity of the chasing pellets drops, and then it begins to overtake the low-speed pellets on the runway … accelerating further until the full speed pellets can be overtaken with ignition, and then accelerating down the runway.

II. APPLICATION TO PROPULSION TODAY

First, many of the challenges which appeared so difficult back in the 1990's for "pellet propulsion" systems of all types would appear to merit reexamination. Today the entire field of "chip craft" is far advanced, with examples having flown[15], and serious efforts to design entire spacecraft in the 2-gram range[16] which could provide high-fraction fusion fuel pellets in the 10 gram and higher range. The laser-beam propulsion system envisioned for Breakthrough Starshot[17] could, rather than launching thousands of gram-sized spacecraft, launch thousands of gram-sized pellets to push a more conventionally sized spacecraft. And since pellet speeds as low as a few hundred km/s may be sufficient[18], a wide range of other launching techniques, more affordable than large laser installations, can be considered.

The side forces required for steering require both a suitable source of power and actuation, but quite small forces suffice over the long coast distances of the pellets. The present author has discussed use of differential drag on small coils acting as magnetic sails to provide both the forces lateral to the course and the torques needed to trim the magnetic sails in a lifting configuration, with a low power mm-wave beam based at the pellet launcher providing the small onboard power required by the pellet.[19]

II.A. Pulse Energy and Pulsed Nuclear Systems

Today, we have a richer array of pulsed fusion and fission-fusion systems in design and in various stages of laboratory test than we had in the 1990s[20,21,22]. These systems as conceived today can potentially scale to high Isp but not to the high specific power involved in interstellar-class missions. Private communication with these workers indicate that the two large drivers of the system mass are the magnetic nozzle and associated systems, and the systems that capture part of the energy of each nuclear pulse, store it in some fashion, and switch it in the controlled fashion needed to ignite the next pulse – what some have termed the "internal energy flow" of the fusion reactor. Note that an alternative approach to the magnetic nozzle, the electrostatic nozzle[23] may have promise for reducing mass, leaving the internal power flow as the fundamental limitation.

Pulsed fusion systems of this type discuss the "Q", or ratio between the released power and this internal power flow. Shear-Flow Stabilized Z-Pinch[21] hopes for a Q in the range of 50 or so. PuFF, being a fission/fusion system that is easier to ignite, has much higher Q in the range of 1000. Still, these are large internal power flows, and the specific power of those systems, like other space power systems, tends to be more in the kW/kg range than in the MW/kg range, making MW/kg system masses difficult even at Q of 1000 and impossible at Q of 50.

However, the energy of an incoming pellet is significant. Even a 0.01 kg pellet (probably the minimum scale), at 100 km/s, has 50 MJ of kinetic energy. That could be used as a direct impactor, steered on to the fusion target by systems on the spacecraft, in which case the peak power can be very high (at that speed, collision is a 10ns process, so peak power is ~ 5000 TW during impact). Or for systems requiring a specific shaped energy input, the pellet can be charged by electron beam a it approaches the spacecraft and then braked by magnetic coils, capturing the kinetic energy as an electric pulse that can be shaped by conventional electrical techniques and delivered to the ignition system – eliminating the energy storage, capture, conversion, and switching systems.

The details of how this would apply to each nuclear pulse system vary, but this is such a powerful technique that it merits serious examination.

III. EFFECT ON MISSION ENERGETICS

If the pellet is braked by coils on the ship and used as a source of energy, the fusion pellet mass being added to the onboard fusion fuel, and if the fusion pellet mass is negligible compared to the onboard mass, the result is essentially a fusion rocket of enhanced thrust/weight.

However, that need not be the case. Two other modes of operation are of interest. First, the ship can operate in the "mostly rocket" mode when getting up to runway ignition speed and then, if the pellet launcher can handle a higher mass flow of pellets, the runway can be made dense enough that most, or even all, of the fusion fuel is ingested from the runway. That essentially is a "ramjet mode", and it relieves the ship of the need to carry onboard mass.

In the limit of nearly pure rocket propulsion, ideal thrust power is:

$$Power = \frac{1}{2} Thrust \times V_{exhaust} \tag{1}$$

While in the limit of nearly pure ramjet power, ideal thrust power is:

$$Power = Thrust \times V_{overtake} \tag{2}$$

Since a fusion propulsion system is likely limited to a maximum power, this implies it is favorable to use ramjet power from the onset of "runway ignition" speed up until the speed at which the ship overtakes the pellets is half of the exhaust velocity in "rocket mode", so long as the pellet launching system can preposition enough mass on the "runway" to support that mode.

Just to show what that can do, consider a system with exhaust velocity of $5x10^6$ m/s, trying to develop a velocity of 10^7 m/s (3.3% of c) at a mass ratio of 7.4 for pure rocket operation. By using the ramjet mode from $3x10^5$ m/s to $2.5x10^6$ m/s, the onboard mass ratio drops to 4.75. Of course, the extra mass still had to be sent from the pellet launcher, but that may have a much greater tolerance for higher mass throughput as a fixed installation.

ACKNOWLEDGEMENTS

Jordin Kare and I shared many stimulating conversations about his work in advanced propulsion and our shared interest in beam riding propulsion over more than two decades. Because of the fundamental character of his work, I had persuaded him to republish his original groundbreaking work in this area when he suddenly passed away. I hope that I can draw some attention to the benefits of his pioneering work in the field.

REFERENCES

1. C. SINGER, "Interstellar Propulsion Using a Pellet Stream for Momentum Transfer," *JBIS*, v. 33, pp 107-115 (1980)
2. G.D. NORDLEY, "Particle Beam Propulsion and Two-Way EML Propulsion", *NASA/OAST Fourth Advanced Space Propulsion Workshop,* April 5-7, 1993, JPL D-10673, pp. 463-474, R.H. FRISBEE, Ed., Jet Propulsion Laboratory, Pasadena, CA (1993). Retrieved Feb 2020 from http://www.gdnordley.com/_files/2way%20EML%20&%20PB%20prop.pdf
3. J. KARE, "High-acceleration Micro-scale Laser Sails for Interstellar Propulsion," *NIAC Final Report, Grant# 07600-070*, (2002). Retrieved Feb 2020 from http://www.niac.usra.edu/files/studies/final_report/597Kare.pdf
4. R. W. BUSSARD, "Galactic Matter and Interstellar Spaceflight," *Astronautica Acta*, Vol. 6, p. 170-194, (1960).
5. T. A. HEPPENHEIMER, "On the Infeasibility of Interstellar Ramjets", *JBIS*, Vol 31, p. 222-224, (1978)
6. D. G. ANDREWS & R. ZUBRIN, "Magnetic Sails and Interstellar Travel", IAF-88-553 (1988)
7. D. WHITMIRE, "Relativistic Spaceflight and the Catalytic Nuclear Ramjet", *Acta Astronautica*, Vol. 2, p. 497-509, (1975). DOI 10.1016/0094-5765(75)90063-6
8. G. L. MATLOFF & A. J. FENNELLY, "Interstellar Applications and Limitations of Several Electrostatic/Electromagnetic Ion Collection Techniques," *JBIS*, Vol 30, p. 213-222, (1977)
9. D. WHITMIRE & A.A. JACKSON, "Laser Powered Interstellar Ramjet", *JBIS*, Vol 30, p. 223-226 (1977)
10. J. KARE posted a short summary on the USENET newsgroup sci.space.tech on 6 September 1997. Retrieved Feb 2020 from https://yarchive.net/space/exotic/bussard_buzz-bomb.html
11. G. L. MATLOFF, *Deep-Space Probes*, p. 110-112, Springer-Praxis, Chichester, UK (2000). ISBN 1-85233-200-X
12. P. GILSTER, *Centauri Dreams: Imagining and Planning Interstellar Exploration*, Chapter 6, "Of Lightsails, Ramjets, and Fusion Runways", Copernicus Books, New York (2004). ISBN 0-387-00436-X
13. A. T. PEASLEE, ed., *Proceedings of the Impact Fusion Workship*, LA-8000-C, Los Alamos Scientific Laboratory, Los Alamos, New Mexico, July 10-12, 1979. Retrieved Feb 2020 from https://fas.org/irp/agency/dod/jason/impact2.pdf
14. F. WINTERBERG, "Circular macroparticle accelerator: Impact fusion propulsion", *Acta Astronautica*, Vol 32, No. 2, p. 107-111 (1994). DOI 10.1016/0094-5765(94)90061-2
15. S. KACAPYR, "Cracker-Sized satellites demonstrate new space tech", Cornell University, June 3 2019. Retrieved Feb 2020 from http://news.cornell.edu/stories/2019/06/cracker-sized-satellites-demonstrate-new-space-tech
16. J. E. MOORES & H. PODMORE, "Starchips in solar system planetary exploration: an opportunity for Canada", International Journal of Space Science and Engineering, Vol. 5 No. 2, p. 181 (2019). DOI 10.1504/ijspacese.2019.097444
17. W. HETTEL, P. MEINHOLD, P. KROGEN & P. LUBIN, "Beam Propagation Simulation of Large Phased Laser Arrays", *Proceedings SPIE 11107, Laser Beam Shaping XIX* (9 September 2019). DOI 10.1117/12.2528931
18. F. WINTERBERG, *The Physical Principles of Thermonuclear Explosive Devices*, Fusion Energy Foundation, New York, (1981). DOI 10.1002/piuz.19830140511
19. J. GREASON, presentation as International Space Development Conference, Los Angeles, CA (2018)

20. R. ADAMS, J. CASSIBRY, D. BRADLEY, L. FABISINSKI, G. STATHAM, Pulsed Fission-Fusion (PuFF) Phase I Report, NIAC (2013). Retrieved Feb 2020 from https://www.nasa.gov/sites/default/files/files/Adams_2013_PhI_PuFF_inProgress.pdf

21. U. SHUMLAK et. al., "The Sheared-Flow Stabilized Z-Pinch", *Transactions of Fusion Science and Technology,* v. 61, p. 119-124. (2012)

22. H. U. RAHMAN, P. NEY, N. ROSTOKER, & F.J. WESSEL, "Fusion in a Staged Z-pinch", *Astrophys Space Sci*, v. 323, p. 51-55 (2009)

23. G. JACKSON & S. HOWE, "Antimatter Driven Sail for Deep-Space Missions", *Proceedings 2003 Particle Accelerator Conference*, Portland, IEEE, p. 705 (2003)

Nuclear and Emerging Technologies for Space
Knoxville, TN, April 6 – April 9, 2020, available online at https://nets2020.ornl.gov

NUCLEAR FISSION WITH SUPERSONIC ISOTHERMAL EXPANSION

Jeffrey K. Greason[1]

[1]*Tau Zero Foundation, Midland, TX 79707*

jgreason@tauzero.aero 805-508-4437

In spite of decades of promise and a high technical maturity, nuclear fisson propulsion has not flown. One potential barrier to adoption has been that the capability improvements over chemical propulsion have not yet been sufficient to justify the investment and overcoming psychological barriers. A combination of high thrust/weight and high Isp is required to achieve those revolutionary capabilities. A possible route to achieving both at once is supersonic isothermal expansion of rocket propellant, which permits in principle a nuclear-thermal rocket to directly heat rocket exhaust to stagnation temperatures well above the temperature limits of the reactor construction materials. Since no energy conversion steps are required, the large radiators of nuclear-electric concepts are dispensed with, while Isp ~1.5-2.0x that of a conventional nuclear-thermal design appears attainable. A review of the relevant literature is followed by conceptual design calculations showing that such a rocket appears feasible and worthy of more detailed design study.

I. ADVANCED PROPULSION & FISSON

Nuclear fission has been the advanced propulsion system of the future since the early days of space transportation research[1]. The energy content of nuclear fission reactions, millions of times greater than the specific energy of chemical energy, gave reason for that promise, and has led to a vast literature and a very successful hardware development program for nuclear-thermal rockets[2], serious work on nuclear-pulse propulsion[3], and many proposals for nuclear-electric rockets[4]. In spite of all this effort and mature development, the promise has not been realized. And while there are certainly non-technical reasons for this, such as public sentiment and the Nuclear Test Ban Treaty, there are also technical reasons.

A game-changing space propulsion capability would offer revolutionary improvements in mission cost, travel time, or, ideally, both. If a given mission can be done with a long travel time, various forms of low-thrust but high specific impulse propulsion already exist (solar-electric, multiple-gravity assist or weak-stability-boundary trajectories, solar sails). Therefore, a technology that beats existing propulsion has to offer both lower initial launch mass for a given mission (higher specific impulse) AND travel times as fast as, or faster than, chemical propulsion. Nuclear fission reactors provide power at temperatures fixed by materials limits to 2200-2400K in the NERVA program[2] with hopes of approaching 3000K with more modern designs[5]. While improved materials can push these limits, we cannot look to materials changes to double the absolute temperature. That limits the Isp of conventional nuclear-thermal reactors to 850-1200 seconds with hydrogen reaction mass. Nuclear-electric cycles, of course, can offer much higher Isp, but the conversion from heat to electricity to thrust involves considerable waste heat for Carnot efficiency reasons, hence large radiators, with attendant mass. This has led to an extensive literature on gas-core nuclear concepts in the attempt to make a dramatic increase in reactor temperature[6].

For missions such as a human Mars mission, the performance of nuclear thermal rockets offers potential reductions in launch mass on the rough order of two-fold, with comparable trip time. This has not been enough to justify the investments required. However, another factor of two improvement in Isp (four-fold over chemical rockets), would be enough to offer missions which are both faster and cheaper (and in the case of human missions, faster missions are also smaller missions, further decreasing mass and cost and reducing astronaut health risks).

II. SUPERSONIC ISOTHERMAL EXPANSION

Familiar rockets, both chemical and nuclear-thermal, heat the exhaust gases to a temperature limited by the chemical reaction or, for nuclear-thermal, by reactor materials, and then expand that gas through a nozzle isentropically (without change in entropy or enthalpy), converting the random molecular motion of the hot gas to the directed supersonic flow of much cooler gas.

It has been known since 1946 [Ref 7], that if energy could be added to the gas during supersonic expansion, then rather than the gas cooling during expansion, it could be maintained at a nearly constant temperature – isothermal expansion – which would imply that the "stagnation temperature" of the gas would be ever-increasing. This was discussed further in [Ref 8]. However, the added energy required is significant, and it cannot be added by conduction from hot walls – the same boundary layer which limits heat transfer from gas to wall limits the heat transfer from wall to the gas. It is necessary to heat the gas by some means that heats the expanding supersonic gas in the bulk.

Nuclear rocket proponents found this same principle, calling it “reheat”, and considered using the neutron flux to heat the working fluid after initial supersonic expansion and proposed to use the neutron flux from the reactor to isothermally expand a neutron-multiplying reaction mass doped with fissile material, but that leaves fission products in the exhaust stream[9].

If a suitable heat transfer mechanism exists, the equations of the gas expansion are, in the case where chamber velocity is negligible:

$$\frac{1}{2}v^2 = R_s T_c \ln\left(\frac{p_c}{p}\right) \quad (1)$$

II.A. Heating by Blackbody Radiation

If the walls of the expanding nozzle are kept warmer than the expanding gas, they will emit black-body radiation thermal photons. If the gas is not “optically thin”, it can then absorb those photons, which pass freely through the boundary layer.

Chemical rockets demonstrate clearly that the addition of quite small fractions (under one part per thousand by mass flow) of agglomerated carbon nanoparticles (“soot”), dramatically increase the optical thickness of exhaust gases. Doping hydrogen with such particles can be done in many ways, for example by injecting a small fraction of carbon-containing gases which decompose to free carbon at the working temperature of the reactor. Therefore, it should be possible to tailor the optical thickness of the gases as desired.

The challenge of course is that the black body radiation is determined by:

$$Heat\ Flux = \epsilon\sigma T^4 \quad (2)$$

And therefore, large heat transfer areas are required.

II.A.1. Many Parallel Converging/Diverging Tubes

By dividing the flow in to a large number of parallel chambers, the heat transfer area can be greatly expanded. The does lead to very small throat dimensions, but the chamber and throat can then be of annular design to further increase area. Because the areas are so small, doping of the working fluid to improve optical thickness will likely be required.

II.A.2. Vortex Heater

To improve the residence time for heating and avoid the problems of small throats, a vortex flow can be used, with the heat serving to increase the tangential vortex velocity, which can then be recovered as linear velocity. Initial calculations by Colgate[10] look promising for undoped working fluid.

II.A.3. Light Bulb

If the working fluid has sufficient optical thickness without doping, then heating can take place in a tube made of material which is transparent in the relevant infrared range, and is surrounded by a larger radiating surface. In this way, the radiation limit can be overcome, because large radiating areas can be used to focus heat on a smaller stream of fast-moving gas. At high pressure and temperature, undoped hydrogen may be optically thick enough for this method[11].

II.B. Independence of heating method

While the technological maturity of supersonic isothermal expansion is low, if a separate coolant loop carries the heat from the reactor to the supersonic isothermal expansion means, it can be tested independently from any reactor (for example, in electrically heated test devices), and avoids the issue of potential escape of fission products through the exhaust (making the reactor a completely closed-loop system). This potentially offers a route to a system which can be adequately tested on the ground at reasonable cost.

III. ISOTHERMAL EXPANSION ROCKET

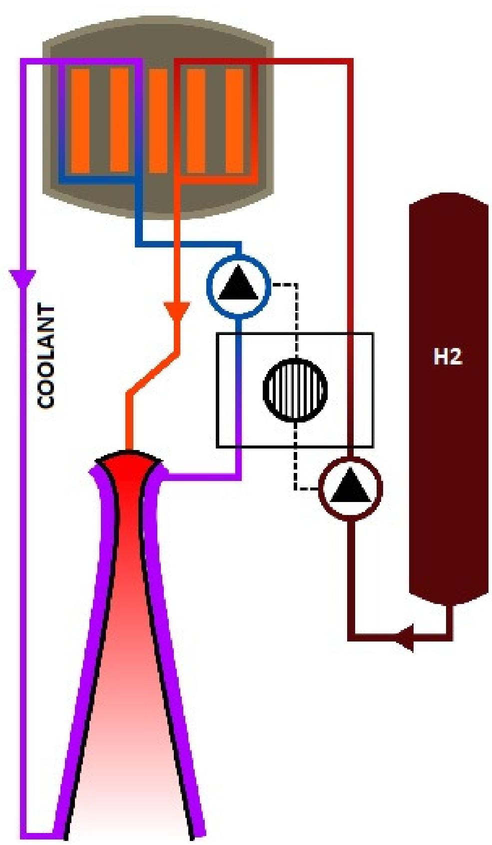

Figure 1: Cycle Diagram of Isothermal Heating

Consider a reactor which is cooled both by the flow of hydrogen and by a circulating coolant, in which both the hydrogen and the coolant are brought near the reactor operating temperature less heat exchanger losses. Pumping power and housekeeping electricity is generated by a heat engine that vaporizes the liquid hydrogen and warms it to ~300K while working across the large temperature difference from coolant return. Coolant flow rate must be high enough to minimize temperature losses through its circulation loop.

A conceptual design using these parameters for a 1200MW reactor (NERVA-class)[12], using the bundle-of-parallel-chambers method was able to package the reactor and expansion system in an Atlas 5m fairing and still achieve, with 2450K temperature limits ~15000 m/s exhaust velocity. If a deployable "conventional" nozzle were used to recover the remaining enthalpy by supersonic isentropic expansion, velocity approaching ~19000 m/s appears possible.

IV. CONCLUSIONS

The principle of supersonic isothermal expansion offers ~1.5 to 2.0 fold increases in specific impulse of nuclear thermal rocket systems, without requiring the massive heat exchangers of nuclear-electric systems, and while permitting closed-loop reactor solutions. Technical maturity is low but simple, electrically heated gas flow experiments could quickly improve readiness.

For hydrogen propellant and Mars missions, this potentially offers enough improvement over conventional nuclear thermal to make the difference in whether the technology makes the cutoff for implementation.

In looking ahead, there has long been awareness[13] that for cislunar operations, a nuclear-thermal rocket with sufficient thrust/weight for Lunar landing and takeoff offers tremendous improvement in logistics cost. While the attainable exhaust velocity for non-hydrogen propellant will of course be lower than for hydrogen, a Lunar-derived propellant in the 5000-6000 m/s with long-term storability would revolutionize Lunar and cislunar operations. Further work should explore water and sodium-vapor reaction mass using supersonic isothermal expansion to see if useful Isp, affordable Lunar logistics, and long-term storability can be combined.

.

REFERENCES

1. W. DORNBERGER, *V-2*, Ballantine, New York, New York, 1954.
2. W.H. ROBBINS & H.B. FINGER, *An Historical Perspective of the NERVA Nuclear Rocket Engine Technology Program*, NASA Lewis Research Center, NASA, CR-187154/AIAA-91-3451, 1991.
3. G. DYSON, *Project Orion: the true story of the atomic spaceship*, Holt, New York, New York, 2002.
4. E. STUHLINGER, "Electrical Propulsion System for Space Ships with Nuclear Power Source," *Journal of the Astronautical Sciences*, Vol. 2 No. 1, pp 149-152, (1955).
5. H. LUDEWIG et. al., "Design of particle bed reactors for the space nuclear thermal propulsion program," *Progress in Nuclear Energy*, Vol. 30 No. 1, pp 1-65, (1996)
6. T. LATHAM, "Criticality Studies of a Nuclear Light Bulb Engine," *Journal of Spacecraft & Rockets*, AIAA, Vol. 6 No. 10, (1969)
7. F. ZWICKY, "Morphological Features of the Isothermal Conversion of Chemical Energy Into Propulsive Energy," *ARS Journal*, American Rocket Society, Vol. 22, p. 339-342, November-December 1952.
8. H. S. SEIFERT & D. ALTMAN, "A Comparison of Adiabatic and Isothermal Expansion Processes in Rocket Nozzles," *ARS Journal*, American Rocket Society, Vol. 22, p. 159-161, May-June 1952.
9. C. LONGMIRE, F. REINES, & S. ULAM, "Some Schemes for Nuclear Propulsion", Los Alamos National Lab, New Mexico, LAMS-2186, March 1958.
10. S. COLGATE, "Vortex Gas Accelerator," *AIAA Journal*, AIAA, Vol. 2 No. 12, p. 2138-2142 (1964).
11. R.W. BUSSARD & R.D. DELAUER, Fundamentals of Nuclear Flight, Mc-Graw Hill, New York, p. 133 (1965)
12. S. BOROWSKI, "Nuclear Thermal Rocket Workshop Reference System Rover/NERVA", *Nuclear Thermal Propulsion: A Joint NASA(DOE)DOD Workshop*, NASA 92N11091, p. 53-92 (1991)
13. "Project Rover, U.S. Nuclear Rocket Development Program", *Project Rover*, U.S. Congress, House Committee on Science and Astronautics, U.S. Government Printing Office, 1961.

Nuclear and Emerging Technologies for Space
Knoxville, TN, April 6 – April 9, 2020, available online at https://nets2020.ornl.gov

SOLAR-WIND POWERED REACTION DRIVE

Jeffrey K. Greason[1]

[1]*Tau Zero Foundation, Midland, TX 79707*

jgreason@tauzero.aero 805-508-4437

A new class of reaction drive is discussed, in which reaction mass is expelled from a vehicle using power extracted from the relative motion of the vehicle and the surrounding medium, such as the solar wind. The physics of this type of drive are reviewed and shown to permit high velocity changes with modest mass ratio while conserving energy and momentum according to well-established physical principles. A comparison to past propulsion methods and propulsion classification studies suggests this is a new type of reaction drive not described in the prior literature. An example of how this principle might be embodied in hardware suggests accelerations sufficient for solar system missions, with shorter trip times and lower mass ratios than chemical rockets.

I. Nomenclature

NOTE: Variables with an arrow above, such as $\overrightarrow{v_e}$, are defined in the reference frame of the moving ship

I_{sp}	specific impulse, m/s
P	power, (positive if supplied from ship, negative if supplied to ship), W
$\overrightarrow{T_{net}}$	net thrust of the ship, thrust minus drag, N
m_e	reaction mass expelled, kg
m_{ship}	mass of the ship, kg
m_{wind}	mass of the surrounding medium that interacts with the ship, kg
v_{ship}	velocity of the ship in the rest frame, m/s
$\overrightarrow{v_e}$	exhaust velocity of the reaction mass, relative to the ship, in the ship frame, m/s
$\overrightarrow{v_\infty}$	freestream velocity; velocity of the surrounding medium in the ship frame, m/s

II. Introduction

Substantial reductions in trip times to the outer solar system or for interstellar precursor missions are difficult for fundamental physical reasons. Fast trips imply high velocities: a constant speed of 100 km/s is only ~20 AU/year, beyond any demonstrated capability (though achievable with a close-solar flyby Oberth maneuver). Fast trips also imply that acceleration cannot be too small: a 29 AU trip (Neptune from Earth) of 100km/s peak velocity requires a constant acceleration of at least 0.005 m/s^2 to achieve a two-year flight time (ignoring Solar gravity), otherwise too much time is spent in acceleration and braking to take advantage of high speed.

With rocket propulsion, high velocity implies either high mass ratio (expense) or high exhaust velocity (high specific energy of the propellant). High acceleration implies high specific power, which is why electric rockets have not been able to overcome these limitations. Nuclear propulsion systems offer high specific energy, but whether they can combine high specific energy with high specific power remains to be demonstrated. Given those limits, a new approach would be beneficial.

By using large external magnetic fields (Plasma Magnet[1]) to harvest the drag power of the passing solar wind, and using that to run a reaction drive expelling reaction mass, a new class of propulsion opens up new mission capabilities. Because such power harvesting intrinsically involves both significant drag and thrust, the equations of motion differ from more familiar propulsion systems.

III. Review of Propulsion Principles

While interplanetary space is a thin vacuum, it is not completely empty, and that has led to a variety of proposals for ways to interact with the interplanetary or interstellar medium for propulsion[1-6]. Conventional forms of propulsion push on the surrounding medium as reaction mass to be accelerated by onboard energy (propellers and jets), ignore it (rockets), or use it as a source for drag (sails and aerobrakes).

It is also possible to harvest energy from the dynamic pressure of the surrounding medium and use that energy to expel onboard reaction mass. This was first considered in special case of mixing gathered reaction mass with a rocket, the Ram Augmented Interstellar Rocket[7], and more recently in the general case of any form of wind-power extraction, by the present author[8].

From the conservation of energy and momentum (see appendix of (Ref 8) for derivation), it can be seen that in the simple case where there are no inefficiencies in the system and where the minimum of expended reaction mass is used:

$$|\overrightarrow{v_e}| = \overrightarrow{v_\infty} \tag{1}$$

$$I_{sp} = \frac{1}{2}\overrightarrow{v_\infty} \tag{2}$$

$$\frac{(m_{ship\,(final)}+\Delta m_e)}{m_{ship\,(final)}} = \frac{(v_{\infty(initial)}+\Delta v)^2}{(v_{\infty(initial)})^2} \tag{3}$$

Contrast eq. 3 with the rocket equation and three dramatic differences are apparent, all favoring a reaction drive powered by external dynamic pressure in high velocity flight. First, in cases where $v_{\infty(initial)}$ is large compared to a rocket exhaust velocity $\overrightarrow{v_e}$, the scaling is more favorable for the wind-powered case. Second, mass ratio scales with the square of velocity rather than the exponential of velocity. Third, in cases where Δv is much less than $v_{\infty(initial)}$ the required mass ratio is smaller still (bearing in mind that the wind-driven drive is only useful in situations where $v_{\infty(initial)} \gg 0$).

While a detailed discussion of the numerical results with losses is beyond this paper, it is clear that the dominant parameter, as in other wind-energy-extraction devices, is the parasitic drag – in other words, the element of drag which does not result in useful power extraction. However, a cursory examination of the physics gives reason for optimism. Even if the parasitic drag were equal to the useful drag, for example (50% efficiency), this would double the required thrust per unit power of the expelled reaction mass, cutting the effective I_{SP} in half.

IV. Thrust At Angle to Drag

To accelerate downwind, one need only use a sail or other pure drag device; to accelerate sunward, one uses the principle above of coaxial thrust, expelling reaction mass downwind to thrust sunward. For outer solar system missions the required maneuvers for fast transits fall largely in to these categories. For operations in the inner solar system, thrust directions with a significant component perpendicular to the wind (prograde or retrograde) are needed.

If a purely prograde or retrograde thrust is desired, sufficient thrust must be used to cancel the drag associated with the power extraction. Again, in the lossless, ideal case, from simple vector mathematics, in order for the sunward component of thrust to just cancel the drag, the axis of thrust can be 60 degrees off the windward direction (so that cosine of the angle is 0.5). The component of thrust prograde or retrograde in that case is then the sine of 60 degrees or 0.866. In other words, in this idealized case where the prograde or retrograde velocity is negligibly small, the effective specific impulse for maneuvers using this principle rises from the case of equation 2 to:

$$I_{SP} = 0.866\overrightarrow{v_\infty} \tag{4}$$

In real maneuvers, of course, once prograde or retrograde components of velocity are built up which are significant compared to the solar wind speed, the vector direction of the apparent wind changes and the real maneuver requires numerical computation rather than analytical methods. The principle remains, however, that such maneuvers are even more efficient than braking.

V. Nomenclature

The nomenclature for such a device is not obvious. While it might be classified under the broad heading of 'jet propulsion' since it expels reaction mass, a classification that also includes propellers, which are broadly recognized as different from rockets. As will be seen, the governing equations are also different from rockets (the rocket equation does not apply), so calling them some form of 'rocket' seems misleading. And since they produce thrust and consume propellant mass, 'sail' hardly seems appropriate. Following Zwicky[9], one might think of them as a 'dynamic-pressure-powered mass driver', but that is rather clumsy. Bond[7] suggests this as the high-speed, inert reaction mass limit of a ram-augmented interstellar rocket, but since in the general implementation there is neither ram-pressure recovery, nor a rocket, nor augmentation, nor interstellar flight, so that nomenclature seems ill-suited to the general case. This propulsive principle might be called a "wind drive" or a "ram drive", but using the common abbreviation *q* for dynamic pressure[10] suggests the name q-drive – which is the name used in the balance of this text. It has also been referred to in more popular accounts as the "Plasma Clipper"[11].

VI. Applications of the Principle

Some applications of how this principle might be applied to enable useful missions within the Solar system are helpful in understanding the principle.

At first glance, the q-drive principle appears to offer "something for nothing". Propellant is expended but where does the energy come from? The answer is that the energy comes from the loss of velocity of the reaction mass to the surrounding medium. One may think of it as an inelastic collision between the expended reaction mass and the surrounding medium, where the resulting change in energy is carried away by the ship. In this sense, it is very reminiscent of the Oberth effect [18], in which there are also three masses involved: the ship, the exhaust mass, and a planet. The q-drive principle is much more flexible, however, since it uses the surrounding medium as the third mass, and so the q-drive is not restricted to operation near a gravitating body.

VI.A. Neptune Fast Transit & Orbiter (Coaxial Thrust)

Starting from near the Earth, but outside the Earth's magnetosphere (for example, in a cislunar staging point), use a plasma magnet in simple drag mode to accelerate away from the Sun to a heliocentric velocity of 150km/s. No propellant is required for the acceleration. To brake from that outward velocity to achieve a state of rest in heliocentric coordinates is then a Δv of 150km/s, where the relative 'wind' speed $\overrightarrow{v_\infty}$ is initially 300 km/s and rises during the maneuver to 450 km/s. (When the vehicle is at rest in heliocentric coordinates, it has $\overrightarrow{v_\infty}$ equal to the wind speed.) In this case, the mass ratio required is 2.25 from equation 11. By comparison, to achieve the same maneuver with the same mass ratio using a rocket, an exhaust velocity of 185 km/s would be required, which is far beyond any chemical rockets' capability, and if based on an onboard power plant, would require a very high power-to-mass ratio. By using the q-drive principle, the result can be achieved with inert reaction mass and with power harvested from the motion of the ship through the surrounding medium.

VI.B. Fast Mars Transit (Non-Coaxial Thrust)

While a detailed exploration of the design of a Mars trajectory using these capabilities is beyond the scope of this paper, by inspection, both the thrust and the specific impulse exceed the capabilities of "Direct Fusion Drive"[14] systems that offer 310 day round trip with 30 day stays to Mars. Even faster trajectories may be possible.

VII. Example Implementations

For accelerations that enable fast transits, a method of extracting power from the solar wind is needed that provides a high drag-to-mass ratio, and it seems likely that a low parasitic drag is also important. In atmospheric applications, rotating devices (windmills, anemometers) are used to draw power from the wind, and magnetic field analogies of both are possible, but the relatively low lift-to-drag ratio of magnetic fields in plasma suggests these approaches may have high parasitic drag. A useful approach may lie in a linear, reciprocating motion of a magnetic field, where essentially all the drag goes into pushing on a moving field. High drag-to-mass is achievable using the plasma magnet approach[1].

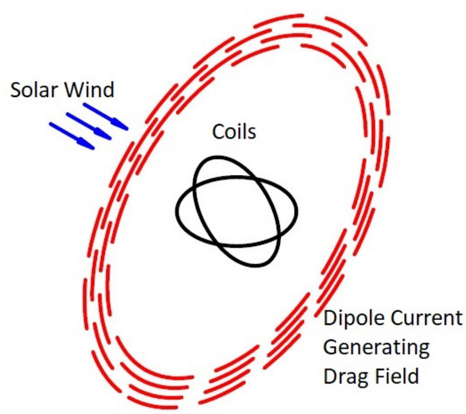

Fig. 1. Operating Principle of a Plasma Magnet

The basic principle of the plasma magnet, illustrated in Figure 1, is that a rotating magnetic field, driven by alternating current in a crossed pair of coils, creates a circulating current in the plasma, and that current then expands in radius until it creates a dipolar magnetic field much larger than the physical coils.

If such a field is turned on and the generating coils are attached to a tether, the tether will be pulled by the solar wind, which could rotate the shaft of a conventional generator. Then, the field could be turned off, the tether reeled back in, and the cycle repeated. In principle this approach of mechanically moving the field coils in a reciprocating manner would extract power, and it illustrates the principle involved, but the mechanical motions would be too slow to provide adequate power-to-mass ratio. We need a more rapid motion of the field, which can be achieved by replacing the reciprocating motion of the coils carrying the magnetic field with the reciprocating motion of the magnetic field itself.

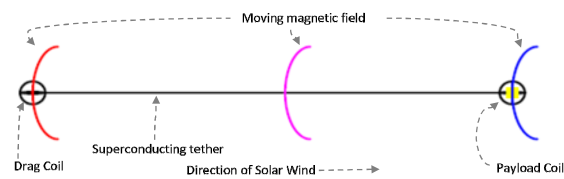

Fig. 2. Oscillating Magnetic Piston for Power Extraction

In this approach, a pair of plasma magnet generating coil sets are used, separated by a tether with wires to transfer power from one set of coils to the other. Initially, the windward coil set is energized and the solar wind pushes on it, transferring the energy in the dipole field to the leeward coils. During the power stroke, energy is extracted from the wind, which can be used to power an electric thruster to expel reaction mass. A third coil set, omitted from the illustration for clarity but located at the windward end with a closed (toroidal) configuration that does not generate a magnetic field outside the coils, receives the energy on the return stroke, so that drag is only pushing on the field during the power stroke. Then, the energy is again transferred to the windward coil, and the cycle repeats.

A detailed design would be required to estimate mass but a sizing study, based on peak currents in superconducting MgB_2 tapes at 20K (Ref. 15-17) of 2.5×10^8 A/m^2, suggests that accelerations in the 0.025-0.05 m/s^2 range may be feasible using this approach. The long tether, carrying oscillating currents in the 1 KHz range from end to end, modulated by a reciprocating frequency in the 20 Hz range, is admirably suited to form a Wideröe style[18] ion accelerator, thus providing an integrated method for converting the resulting electric power to thrust. However, any form of high-power electric thruster can be employed.

VIII. Conclusion

A new class of reaction drives appears capable of generating vehicle velocities greater than those practical for propeller or rocket devices. A conceptual design suggests that, by using plasma magnet techniques, such a drive could offer accelerations and mass ratios sufficient for rapid transits to the outer solar system.

To explore further, the analysis of the physics involved needs to be extended in two ways. First, the analysis needs to include the effects of efficiencies in power conversion and parasitic drag, to assess whether the approach is practical. Second, to extend the application of this technique for inner solar system missions, the theory needs to be extended to include thrusts that are not parallel to the drag vector, which would enable a wider range of maneuvers.

This paper begins to examine routes for embodying this type of reaction drive in hardware. To assess the achievable accelerations, designs will need to be carried to a level of detail at which masses can be estimated credibly.

ACKNOWLEDGMENTS

Thanks to the Tau Zero Foundation for providing the initial challenge which led to this work, and to TVIW for providing stimulating discussions which have helped to shape it.

REFERENCES

1. J. Slough and L. Giersch, "The Plasma Magnet", *41st AIAA/ASME/SAE/ASEE Joint Propulsion Conference*, AIAA 2005-4461, AIAA, Washington, D.C. 2005. DOI: 10.2514/6.2005-4461
2. R. Zubrin and D. Andrews, "Magnetic Sails and Interplanetary Travel," *25th AIAA/ASME/SAE/ASEE Joint Propulsion Conference*, AIAA 89-2441, AIAA, Washington, D.C., 1989. DOI: 10.2514/6.1989-2441
3. P. Janhunen, "Electric Sail for Spacecraft Propulsion," *AIAA Journal of Propulsion and Power*, v 20 no 4, 2004, pp 763-764. DOI: 10.2514/1.8580
4. R. Zubrin, "Dipole Drive for Space Propulsion," *JBIS*, **70**, 2017, pp. 442-448
5. D. Brisbin, "Spacecraft with Interstellar Medium Momentum Exchange Reactions: The Potential and Limitations of Propellantless Interstellar Travel," *JBIS*, **72**, pp 116-124, 2019
6. J. Gilland & G. Williams, "The Challenges of Ambient Plasma Wave Propulsion", *49th AIAA/ASME/SAE/ASEE Joint Propulsion Conference,* AIAA 2013-3876, AIAA, Washington D.C, 2013. DOI: 10.2514/6.2013-3876
7. A. Bond, "An Analysis of the Potential Performance of the Ram Augmented Interstellar Rocket", *JBIS*, **27**, 1974, pp. 674-685.
8. J. Greason, "A Reaction Drive Powered by External Dynamic Pressure", *JBIS*, **72**, 2019, pp. 146-152. (electronic copy retrieved from https://tauzero.aero/wp-content/uploads/JBIS-May-2019-Greason.pdf on October 20, 2019)
9. F. Zwicky, "Fundamentals of Propulsive Power," *International Conference for Applied Mechanics*, Paris, September 1946. Collected in *Morphology of Propulsive Power,* Society for Morphological Research, Pasadena, 1962, p. 37-47.
10. M. Munk, "Notes on Propeller Design – IV", NACA Technical Note No. 96, May, 1922, p. 6
11. K. Hebden & J. Greason, *ROOM*, being prepared for publication.
12. A. Lavoie, "Tethered Satellite System (TSS-1R) Post Flight (STS-75) Engineering Performance Report", Report JA-2422, Document ID 20010022502, NASA, Huntsville, August 01, 1996. (electronic copy retrieved from https://ntrs.nasa.gov/archive/nasa/casi.ntrs.nasa.gov/20010022502.pdf on October 20, 2019)
13. M. Kruijff, E. van der Heide, W. Ockels, and E. Gill, "First Mission Results of the YES2 Tethered SpaceMail Experiment", *AIAA/AAS Astrodynamics Specialist Conference and Exhibit*, AIAA 2008-7385, AIAA, August 2008. DOI: 10.2514/6.2008-7385
14. M. Paluszek et. al., "Direct Fusion Drive for a Human Mars Orbital Mission", *Proceedings of the 65th International Astronautical Congress*, 2014. (electronic copy retrieved from https://www.osti.gov/biblio/1182281 on February 6, 2020)
15. C. B. Eom et. al., "High Critical Current Density and Enhanced Irreversibility Field in Superconducting MgB_2 Thin Films", *Nature*, **411**, 31 May 2001, p. 558-560.
16. A. Matsumodo et. al., "Evaluation of connectivity, flux pinning, and upper critical field contributions to the critical current density of bulk pure and SiC-alloyed MgB_2," *Applied Physics Letters*, **89(132508)**, 2006.
16. M. Ranot and W.N. Kang, "MgB_2 coated superconducting tapes with high critical current densities fabricated by hybrid physical-chemical vapor deposition," *Current Applied Physics*, **12(2)**, 2012, pp 353-363.
18. S. Humphries, *Principles of Charged Particle Acceleration*, Wiley, New York, 1986, p. 453

AFFORDABLE DEEP SPACE NUCLEAR ELECTRIC PROPULSION SPACECRAFT

Dr. Troy Howe[1], Dr. Steve Howe[1], and Jack Miller[1]

[1]*Howe Industries, LLC, 1435 E. University Drive Ste C-108, Tempe, Arizona, 85281*

Primary Author Contact Information: Troy@howeindustries.net ,480-967-5660

The space industry is expanding at an increasing rate. While most efforts are currently focused on Earth and lunar orbits, it is only a matter of time before affordable exploration missions into deep space become more prevalent. Howe Industries has conceptualized a deep space probe capable of transporting CubeSats and other payloads to deep space utilizing nuclear electric propulsion and an advanced thermoelectric generator power conversion system. This probe can be utilized for affordable exploration of Europa in the search for extraterrestrial life.

I. MISSION ARCHITECTURE

Swarm-Probe Enabling ATEG Reactor (SPEAR) will utilize nuclear electric propulsion to travel from Earth to deep space under its own power. A 15 kWt nano-reactor with advanced thermoelectric generators will extract a minimum of 3 kWe of power for use with the electric thruster and various systems throughout its voyage. A specific mission to study the icy moon of Europa has been devised to demonstrate the capabilities of the SPEAR system and search for life amongst the plumes of Europa.

I.A. Motivation for Europa Mission

The exploration of Europa has gained significant popularity due to its potential to harbor alien life. A potentially massive subsurface ocean could harbor this life[1]; however, access to this ocean to study its environment is a complex engineering challenge requiring a probe to melt through kilometers of ice before reaching the ocean.

However, access to the material within this ocean may be easier than once thought. Plumes have been observed on Europa possibly originating from fissures formed on Europa's icy crust[2], expelling large amounts of subsurface material. These plumes have been documented several times by the Hubble Space Telescope[1]. Most recently in 2019 water vapor was confirmed around Europa with its origins suspected to come from a plume.[3]

While plumes have been observed there is still much debate as to their frequency, size, and location on Europa's surface. Missions slated to study the Europa environment such as the Europa Clipper, have included instruments necessary to study this environment and capture plume particles.[4] To avoid the harsh radiation environment associated with Europa the Europa Clipper will not orbit Europa, instead opting for several low altitude fly-bys of the moon.[4] This severely limits the spacecraft's ability to intercept a plume and collect particles for analysis.

I.B. SPEAR Probe Design

The SPEAR spacecraft has been uniquely designed to investigate the plumes of Europa for traces of life. Utilizing several novel technologies SPEAR will act as an inexpensive follow-on for the Europa Clipper mission or be the first mission dedicated to study Europa's plumes.

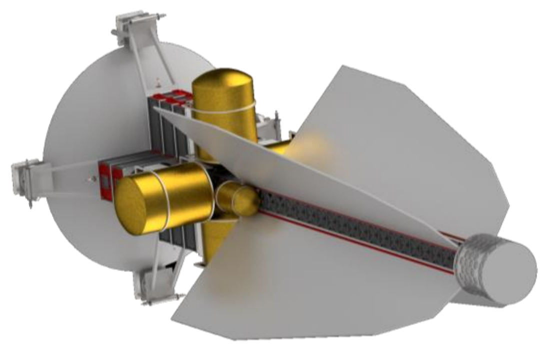

Fig. 1. Artist rendition of the SPEAR spacecraft with a CubeSat constellation payload for the exploration of Europa and the possibility of extraterrestrial life within its potentially large subsurface ocean.

Utilizing Nuclear Electric Propulsion (NEP), SPEAR will traverse its way to Europa to deploy a constellation of CubeSats equipped with instruments to study Europa. This mission is made possible by the highly efficient advanced thermoelectric generator (ATEG) power conversion system. Utilizing advanced technologies these thermoelectric generators would be capable of 20-36% efficiency, far beyond the capabilities of current thermoelectric technologies. Paired with a 15 kWt nano-reactor SPEAR would have an unprecedented 3000-5400 We power in deep space for NEP and science objectives around Europa.

Four large radiators will be used to control the cold side temperature of the ATEGs to maintain optimal performance. SPEAR will operate with a 600K hot side, and 350K cold side temperature. These radiators are visible in figure 1 and span most of the spacecraft's length.

Situated behind these radiators are four large xenon propellant tanks which house all the propellant for a journey to Europa. These propellant tanks as well as the radiation shield behind them protect the electronics and CubeSat payload from the ionizing radiation originating from the nano-reactor. A large high gain antenna used for communicating with Earth via the deep space network (DSN) is situated at the rear of the spacecraft.

SPEAR has an extremely lightweight design so it can be launched on small/medium class launch vehicles, greatly reducing total mission costs. SPEAR will be capable of launching on multiple launch vehicle platforms currently under development and already in production. Under its own power and propulsion, SPEAR will navigate its way to Europa. Also leveraging the NewSpace movement and the miniaturization of spacecraft, SPEAR will be outfitted with 10 CubeSats each with a mass of 7kg that will be deployed around Europa to study its environment. Each CubeSat will be outfitted with a hyperspectral camera, Raman spectrometer, and a lab-on-a-chip device that will utilize a microscope and test for chirality of the collected samples. This included CubeSat constellation maximizes the probability of directly intercepting a plume or particles that may be suspended in Europa's atmosphere.

I.C. Mission Phases

SPEAR will have four primary mission phases that have been used to estimate costs, mission trajectories, and science objectives.

I.A.1 Earth Departure

After a ride share, or dedicated launch from a small/medium satellite launch vehicle, SPEAR will start its nuclear reactor and begin the spiral maneuver to escape Earth.

I.C.2 Interplanetary Cruise

Once outside of Earths sphere of influence, SPEAR will continue its spiral maneuver until it reaches the Jovian system. While in interplanetary space, SPEAR will place any unnecessary system into a hibernation mode. In order to mitigate costs, SPEAR will utilize an artificial intelligence-based guidance and navigation system to control its trajectory to limit ground control intervention.

I.C.3 Jovian System Capture

The NEP system will be used for a spiral maneuver to reach Jupiter's moon Europa. During this spiral transfer SPEAR will study the surface of Europa for evidence of plumes and adjust its course accordingly to enter an orbit that maximizes its probability of intercepting a plume. If previous missions have studied Europa and more accurate models of plumes exist, SPEAR will adjust its course accordingly.

I.C.4 Europa Environment Study

Upon reaching Europa SPEAR will deploy its constellation of CubeSats with the goal to intercept and analyze the material from a plume. It is expected that with the harsh radiation environment around Europa, the CubeSats will only last 30 days before succumbing to radiation. During this time SPEAR will power the CubeSats with wireless RF charging and transmit data from the CubeSats back to Earth. SPEAR and each CubeSat will continue to operate if possible.

II. ADVANCED THERMOELECTRIC GENERATORS

The key technology that makes the SPEAR mission possible is the advanced thermoelectric generators (ATEGs). These ATEGs boast efficiencies 3-4 times that of most current technologies for the same temperature gradient.

The equations governing thermoelectric generators can be found below and include the figure of merit and the overall efficiency of the thermoelectric generator.

$$Z\bar{T} = \frac{\left(S_p - S_n\right)^2 \bar{T}}{\left(\sqrt{\rho_p \kappa_p} + \sqrt{\rho_n \kappa_n}\right)^2} \tag{1}$$

$$\eta = \frac{\Delta T}{T_h} \frac{\sqrt{1 + Z\bar{T}} - 1}{\sqrt{1 + Z\bar{T}} + \frac{T_c}{T_h}} \tag{2}$$

The figure of merit, which directly effects the efficiency is dependent on the material properties of the thermoelectric. Increasing the temperature also increase the efficiency, but only to a certain degree, changing the figure of merit is a far more practical method to increase TEG efficiencies.

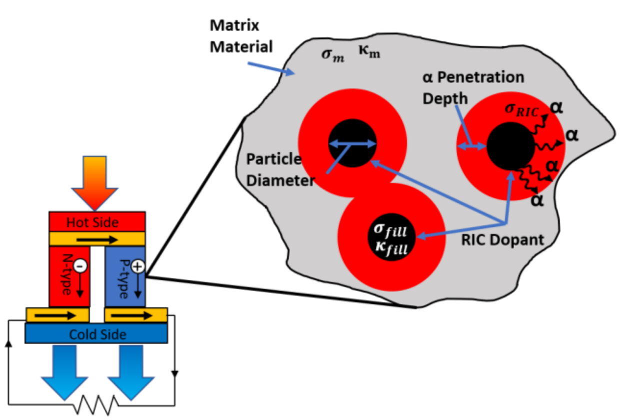

Fig. 2. Principles behind radiation induced conductivity that promotes the high efficiency of the new ATEGs in development by Howe Industries.

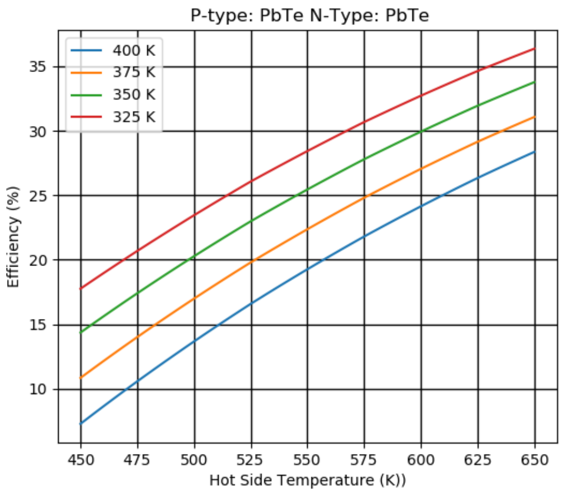

Fig. 3. This figure depicts the performance of a PbTe ATEG under various temperature gradients. Efficiency levels are well above any previous TEG technologies at the temperature gradient SPEAR will operate at.

Manipulating these thermoelectric properties is a difficult task and high figure of merit values have been difficult to achieve. The ATEGs under development by Howe Industries utilizes several different phenomena that are prevalent during ionizing radiation to manipulate the material properties of thermoelectric generators to achieve figures of merit and efficiencies that were previously thought impossible.

The primary phenomena enhancing the ATEGs performance is radiation induced conductivity (RIC). When subject to ionizing radiation, some materials have shown an increase in electrical conductivity. In one case, a greater than 10,000 times increase in electrical conductivity was observed without altering the materials geometry[6].

The Seebeck coefficient and thermal conductivity also show changes that would positively increase the efficiency, but to a lesser extent than the change in electrical conductivity.

Introducing ionizing radiation is possible through a few different methods. The first being the use of radioisotopes that emit low penetrating alpha particles. The second method must involve a neutron source and an element with a high neutron capture cross section to capture the neutron and emit an alpha particle, a (n,α) interaction.

Figure 2 shows how these particles will interact with the thermoelectric matrix they are suspended in. These particles can consist of either ^{241}Am, ^{238}Pu, or ^{10}B(n,α) and will have the effects seen above. RIC effects local areas, but with enough areas effected by RIC, the bulk materials electrical conductivity can be changed.

Figure 3 shows the performance of an PbTe ATEG with RIC effects increasing its performance to 30% within the temperature gradient specified by the SPEAR probe. The associated figure of merit would be 24.7, a value shattering any previous figure of merit.

A test was performed on boron nitride (BN), a material containing ^{10}B, to observe the effects of ionizing radiation on the materials conductivity. Figure 4 shows the change in material conductivity as the power/neutron flux increased inside of the reactor. A ~50 times decrease in electrical resistance was observed. The resistance matches almost exactly with the reactors power levels, showing a strong relationship between the neutron flux and materials electrical conductivity. These results show support the ATEG concept and paves the way for prototype unit to be produced and characterized.

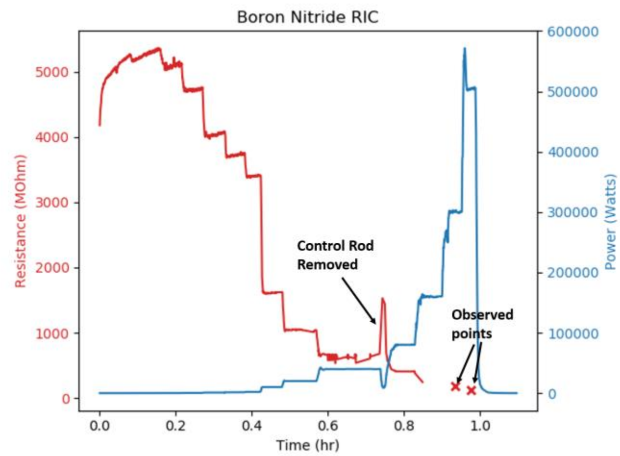

Fig. 4. Boron Nitride results from a test with Kansas State University's (KSU) Trigga Mark II reactor. There is a strong association between the reactors power and the decrease in resistance observed. Up to 50 times decrease in resistance was observed.

III. NANO-REACTOR

Supplying the thermal power for the SPEAR spacecraft is the 15 kWt reactor. This compact reactor weighs less than 150kg and utilize several unique materials making it commercially available to private companies.

Low enriched uranium (LEU) is used as the fissile material, with lithium hydride (LiH) moderators, beryllium reflectors, mercury heat pumps, and a boron control rod. A cross section view of the reactor is visible in figure 5. Enriched to 19.75% the LEU can be owned by private companies to avoid costly government intervention and security.[7] The lightweight LiH moderator, aids in reducing the weight of the LEU reactor, but reduces the maximum operating temperature of a typical reactor. The highly efficient ATEGs compensate for this decrease in temperature and can extract far more electrical power than any other nuclear power system currently in space.

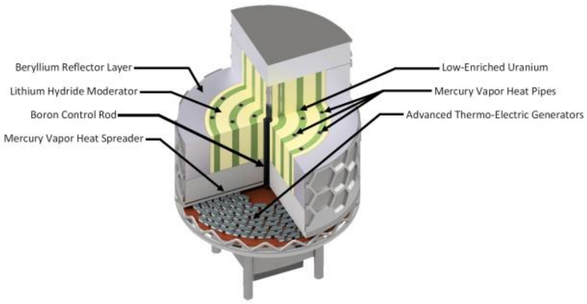

Fig. 5. SPEAR nano-reactor containing LEU and reactor materials that promote a lightweight reactor. Coupled with the ATEG power conversion system, SPEAR will have an unprecedented amount of power available in deep space.

The reactor can be used in conjunction with both radioisotope ATEGs and (n,α) ATEGs. The reactor acts as a neutron source, so ATEGs containing ^{10}B or other (n,α) particles will also be able to achieve high levels of efficiency. This may be especially important due to unknown availability and requirements of private companies owning radioisotopes.

Monte Carlo N-particle Code (MCNP6) simulations showed criticality levels 1.01437 with the control rod removed and 0.98793 with the control rod fully inserted. The ATEGs sit below the reactor with their hot side connected to a heat spreader plate and the cool side connected to the radiator assembly.

IV. CONCLUSIONS

SPEAR would be a first of its kind NEP spacecraft utilizing the revolutionary ATEG power conversion system. The exploration of Europa is of paramount importance to understanding life beyond our planet and its exploration will push current technologies to their limits. A CubeSat constellation maximizes the potential to intercept plumes and any material suspended in Europa's atmosphere that may contain traces of life.

The coupled nano-reactor and ATEG conversion technology opens deep space for affordable exploration to government agencies, universities, and private industries. With its novel and lightweight design, SPEAR can be launched for a fraction the cost of traditional deep space missions. The ATEGs being developed by Howe Industries also have far reaching terrestrial power generation applications for heat waste recovery and for remote power generation.

ACKNOWLEDGMENTS

Thank you to NASA's Innovative and Advanced Concepts (NIAC) Program for funding our study, and to Dr. Alan Cebula and the KSU Mechanical and Nuclear Engineering Department for the use of their reactor.

REFERENCES

1. K. Northon, "NASA's Hubble Spots Possible Water Plumes Erupting on Jupiter's Moon Europa," NASA (2016).
2. B.S. Southworth, S. Kempf, and J. Schmidt, "Modeling Europa's dust plumes," Geophysical Research Letters, (2015).
3. L. Shekhtman, "NASA Scientists Confirm Water Vapor on Europa," NASA (2019).
4. T. Lam, M. Ozimek, C. Scott, "A Robust Mission Tour for NASA's Planned Europa Clipper Mission," Space Flight Mechanics Meeting (2018).
5. S. Vance, W. Patterson, M. McGrath, K. Retherford, T. Hurford, B. Pappalardo, "Europa Plume Advisory Meeting Report," NASA (2014).
6. T. Shikama, et. al. "Electrical properties of ceramics during reactor irradiation," journal of Nuclear Materials (1998).
7. D. I. Poston, P. R. Mcclure, "White Paper-Use of LEU for a Space Reactor," Los Alamos National Laboratory (2017).

SYMBOLS

ρ	electrical resistivity
S	Seebeck coefficient
κ	thermal conductivity
η	efficiency
T_h	hot side temperature
T_c	cold side temperature
ΔT	temperature gradient
$\bar{T}$	average temperature
$Z\bar{T}$	figure of merit
p	denotes p-type thermoelectric
n	denotes n-type thermoelectric

Nuclear and Emerging Technologies for Space
Knoxville, TN, April 6 – April 9, 2020, available online at https://nets2020.ornl.gov

ANTIMATTER-BASED PROPULSION FOR EXOPLANET EXPLORATION

Gerald P. Jackson, Ph.D.[1]

[1]*1275 W. Roosevelt Rd., Suite 132, West Chicago, IL, 60185*

Cell: 630-710-7079, gjackson2@hbartech.com

Antimatter-based propulsion and onboard electrical power generation technologies are uniquely well suited for unmanned spacecraft sent to explore exoplanets and transmit back scientific observations. Congressional guidance calls for an interstellar coasting velocity of 10% of the speed of light (0.1c). In order to achieve such spacecraft velocities exhaust velocities commensurate with particle energies of at least 1 MeV/nucleon are required. The design of a propulsion system capable of such particle energies is presented. Early demonstration experiments are proposed.

I. PROXIMA CENTAURI

The basic relative geometry of the Alpha Centauri star system and our own solar system is shown in figure 1. The Alpha Centauri trinary star system is composed of Rigil Kentaurus, Toliman, and Proxima Centauri. The first two stars form a close binary with a combined stellar mass of two times the mass of our own sun. Their mutual orbit is highly elliptical within a distance range of 11.2 to 35.6 AU. Proxima Centauri orbits that binary with a radius of approximately 13,000 AU (0.21 LY). Assuming that Alpha Centauri has a cometary halo structure similar to our own Oort Cloud, then Proxima Centauri orbits within it. Assuming 10-year acceleration and deceleration burns and a 0.1c coasting speed, those burns begin and end within each Oort Cloud.

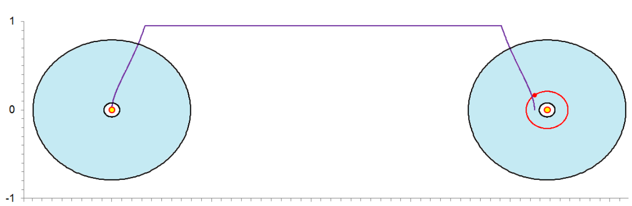

Fig. 1. Our solar system (left) and Alpha Centauri solar system (right) each surrounded by an Oort Cloud (light blue regions). Note that Proxima Centauri orbits (red orbit) within the Alpha Centauri Oort Cloud. Spacecraft velocity profile is also shown assuming 0.1c drift speed.

Proxima Centauri resides at a distance of 4.244 ± 0.001 LY from Earth. Fortuitously, a confirmed planet Proxima b has been found[1] orbiting that star in the habitable zone[2,3] of that system. Recently another candidate exoplanet Proxima c has been identified[4] that is too cold to likely harbor life

II. BASIC CONCEPT

Nuclear fission is the process by which heavy nuclei are split into smaller nuclei. The fission of uranium nuclei yields approximately 1 MeV per nucleon, primarily in the form of kinetic energy of the fission daughters. For the case of depleted uranium U238, on average fission generates two fission daughters of atomic mass 100, with 100 MeV of kinetic energy per daughter. Traditionally, fissile isotopes such as U235 are required to sustain fission chain reactions, wherein neutrons also emitted from the fission process induce other nuclei to also fission.

An alternative approach to inducing nuclear fission is to allow antiprotons to stop in a population of uranium[5]. Unenriched and depleted uranium U238 undergoes antiproton-induced fission just as easily as fissile U235. Unlike weapons-grade fissile materials such as U235, there are no regulatory controls on the handling of U238. This significantly reduces research costs and administrative overhead, allowing development of the technology to progress much faster than otherwise possible.

Instead of a solid uranium target, imagine the uranium in the form of ions trapped in an electrostatic trap[5]. Electrostatic traps provide stable containment for charged particles oscillating back and forth across the trap in the same way that magnetic storage rings confine circulating particle beams. By launching antiprotons (signified by a P with an overhead bar) in the same direction as the uranium ions and constructing the trap so that the antiprotons and uranium ions have the same velocity, the antiprotons stop with respect to the uranium ions and annihilate.

Because the uranium is in the form of a sparse cloud, the energetic fission daughters escape the trap without significant energy loss or scattering. As shown in figure 2, imagine that this electrostatic trap is at the apex of an electrostatically charged, pseudo-parabolic (blue) wire mesh. It has been experimentally determined[6] that the average fission daughter under these circumstances has a net electrostatic charge of +20e. At 1 MeV per nucleon and an average charge of +e/5 per nucleon, a 5 MV voltage difference between an inner mesh electrode (blue) and a larger outer mesh electrode (blue) can redirect random fission daughter trajectories into a collimated exhaust stream (see figure 3).

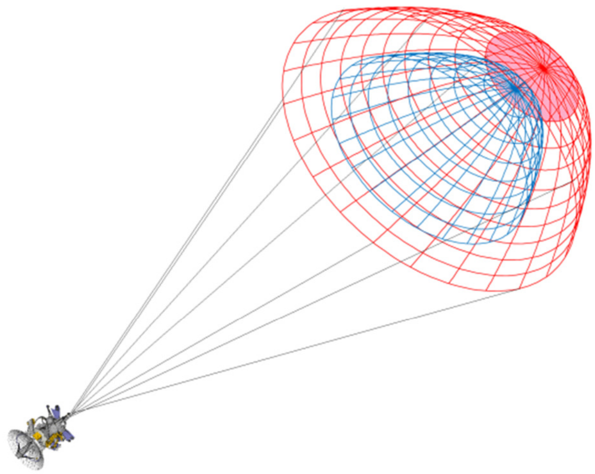

Fig. 2. Illustration of the proposed propulsion architecture, wherein exhaust particles emanate from the apex of the inner (blue) electrostatically charged wire mesh.

Note the solid region of the outer electrostatic len**s** in both figure 2 and figure 3. This region is composed of a thin electrically conducting foil just thick enough to absorb fission daughters that are close to being stopped (less than 1 MeV/amu)[5]. By varying the voltage between the two lenses, the electrical current (charged fission daughters) deposited into the outer lens can be regulated. This provides a variable supply of spacecraft electrical power capable of a megawatts of average power.

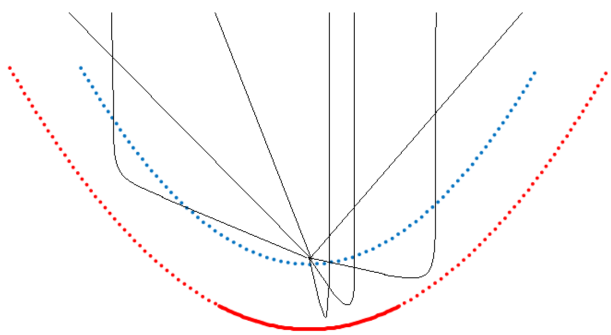

Fig. 3. Cross-section of the electrostatic sail showing focusing of the fission daughters emanating from the trap at the apex of the inner mesh electrode.

Table 1 contains assumed input values and calculated data deriving the antiproton mass required to decelerate the spacecraft to zero velocity as a function of the interstellar drift velocity. Note that the needed antiproton mass scales roughly as the square of the spacecraft drift velocity (or as the inverse square of the interstellar transit time). In the above calculations it is consistently assumed that the propulsion system would execute a deceleration burn lasting ten years due to the very high power levels associated with removing so much kinetic energy from the spacecraft. For comparison, a small nuclear power plant on the grid operating at 400 MW for an entire year puts out the same amount of energy that the antimatter propulsion system needs to generate over 10 years when the drift velocity of the spacecraft is 0.1c.

TABLE I. Antiproton mass requirements under different mission duration scenarios.

Mission Transit Time	56 Yrs	97 Yrs	200 Yrs
Spacecraft Speed	0.1c	0.05c	0.0225c
Burn Durations	10y	10y	10y
Spacecraft Dry Mass	10kg	10kg	10kg
Fuel Mass / Dry Mass	14.1	2.9	0.84
Antiproton Beam Current	180mA	37mA	11mA
Propulsion Power	40MW	8.2MW	2.4MW
Propulsion Thrust	4.9N	1.0N	0.30N
Total Antiproton Mass	590g	120g	35g

III. ANTIMATTER STORAGE

In order to enable deceleration for such a mission to Proxima b, on the order of 100 g of antiprotons will be needed. There is no known reasonable method to store this many antiprotons unless their negative electrostatic charge is neutralized with an equal number of positive charges. The obvious solution is to store the antiprotons in the form of antihydrogen. In these quantities, it is most convenient to store the antihydrogen as solid molecular antihydrogen. For temperatures below 10ºK solid molecular hydrogen is stable. Therefore solid molecular antihydrogen is also stable in solid form. The idea is to store the antihydrogen as an array of levitated "snowballs".

The problem is that even at milliKelvin temperatures the molecular antihydrogen sublimates away from the stored antihydrogen snowball, slowly dissipating the antimatter during the interstellar voyage before the deceleration burn ever occurs. Moreover, in order for the spacecraft computers to continue operating, the electronics must be maintained at an elevated temperature. Generating a temperature gradient within the spacecraft of several orders of magnitude without consuming unreasonable amounts of power would be problematic.

Sublimation occurs when the vacuum pressure outside of the material is lower than the vapor pressure associated with the material at a given temperature. In order to prevent sublimation, one method is to surround the material with a thin membrane within which the vapor pressure is in equilibrium. Since antimatter must be levitated in an extremely good vacuum in order to avoid dissipation due to annihilations with background gas molecules, the vacuum around the snowball needs to always be much lower than its vapor pressure. Therefore, the above solution requires that the membrane be composed of antimatter.

Looking at the periodic table, the lightest atom that has a reasonably high boiling point is lithium. The idea currently under study is to coat the antihydrogen snowball with a thin layer of antilithium. This is the process of encapsulation used in many industries, especially in medicine and food science. In the case of antihydrogen snowballs, preliminary calculations suggest that an antilithium coating of 1 micron thickness would be sufficient to suppress antihydrogen sublimation. For snowball masses over a gram the mass ratio of antilithium to antihydrogen is approximately three orders of magnitude. Therefore, rather inefficient antilithium production methods can be tolerated. In addition, since the propulsion system only generates one fission per annihilation, an antilithium nucleus annihilating against a U238 nucleus still only produces a single fission event. But since antilithium is only 0.1% of the overall antimatter mass, the operation of the propulsion system is effectively unaffected by the antilithium. Figure 4 contains a map of the proposed antilithium production. Many of the steps are standard nuclear fusion channels proposed for terrestrial power production. The overall efficiency of coated antihydrogen snowballs is estimated to be 99.6%.

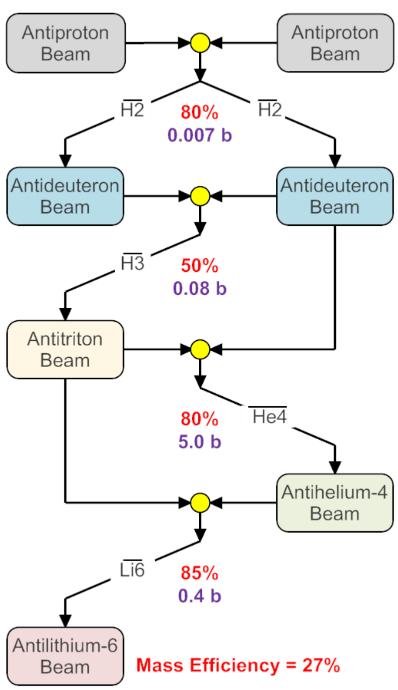

Fig. 4. Proposed antinucleosynthesis process for the formation of antilithium nuclei.

The encapsulation of a hydrogen snowball with lithium is analogous to ion implantation of silicon to form N-type and P-type semiconductors. By lowering the lithium beam energy so that the lithium nuclei stop very close to the surface of the snowball, the encapsulation process will occur. In the case the antilithium the beam will be fully-stripped nuclei (no positrons in orbit). Therefore, the encapsulation process will also require an equal current positron beam to maintain electrostatic neutrality and to form molecular bonds between the antihydrogen and antilithium.

The chemistry of cold hydrogen in contact with high temperature lithium nuclei, called hot atom chemistry[7], suggests that a thin intermediate layer of lithium hydride will also form between the solid hydrogen and the lithium coating.

IV. DISCUSSION

One priority for the development of this propulsion system is to experimentally demonstrate a lithium coating over a cryogenically maintained sample of solid molecular hydrogen, observing the formation of the lithium hydride layer and demonstrating the suppression of hydrogen sublimation. As a lower cost preliminary step, experiments have already been started encapsulating room temperature sulfur with aluminum, demonstrating suppression of sulfur sublimation and the formation of an aluminum sulfide intermediate layer.

REFERENCES

1. Anglada-Escudé, et. al., "A Terrestrial Planet Candidate in a Temperate Orbit around Proxima Centauri," *Nature* **536**, Issue 7617, pp. 437–440, 2016. doi: 10.1038/nature19106.
2. Strughold, H., *The Green and Red Planet: A Physiological Study of the Possibility of Life on Mars*, University of New Mexico Press, 1953, ISBN: 978-1258378509.
3. Huggett, R.J., *Geoecology: An Evolutionary Approach*, Routledge, Chapman & Hall. p. 10. 1995, ISBN: 978-0-415-08689-9.
4. Damasso1, M. and Del Sordo, F., "Proxima Centauri Reloaded: Unravelling the Stellar Noise in Radial Velocities", *Astronomy & Astrophysics*, submitted for publication, arXiv:1612.03786.
5. Jackson, G.P., "Antimatter-Based Spacecraft Power Generation", this conference.
6. Ajlouni, A.W., and Mahasneh, A.A., "Atom Behavior During Nucleus Fission Process", *Journal of Applied Sciences* **7**, No. 12, pp. 1664-68, 2007.
7. Willard, J., "Chemical Effects of Nuclear Transformations", *Annual Review of Nuclear Science* **3**, pp. 193-220, 1953. doi:10.1146/annurev.ns.03.120153.001205

Nuclear and Emerging Technologies for Space
Knoxville, TN, April 6 – April 9, 2020, available online at https://nets2020.ornl.gov

ANTIMATTER-BASED SPACECRAFT POWER GENERATION

Gerald P. Jackson, Ph.D.[1]

[1]*1275 W. Roosevelt Rd., Suite 132, West Chicago, IL, 60185*

Cell: 630-710-7079, gjackson2@hbartech.com

Antimatter-based propulsion and onboard electrical power generation technologies are uniquely well suited for unmanned spacecraft sent to explore exoplanets and transmit back scientific observations. For example, a mission to the habitable planet Proxima b will require 100 kW for data communication back to Earth, AI-level computing, and a LIDAR system capable of sensing Oort Cloud objects from both our solar system and the Centauri AB binary system. This paper describes a generator technology capable of on-demand electrical power generation within a mass budget of 1 kg. Early demonstration experiments are proposed.

I. BASIC CONCEPT

Nuclear fission is the process by which heavy nuclei are split into smaller nuclei. The fission of uranium nuclei yields approximately 1 MeV per nucleon, primarily in the form of kinetic energy of the fission daughters. For the case of depleted uranium U238, on average fission generates two fission daughters of atomic mass 100, with 100 MeV of kinetic energy per daughter. Traditionally, fissile isotopes such as U235 are required to sustain fission chain reactions, wherein neutrons also emitted from the fission process induce other nuclei to also fission.

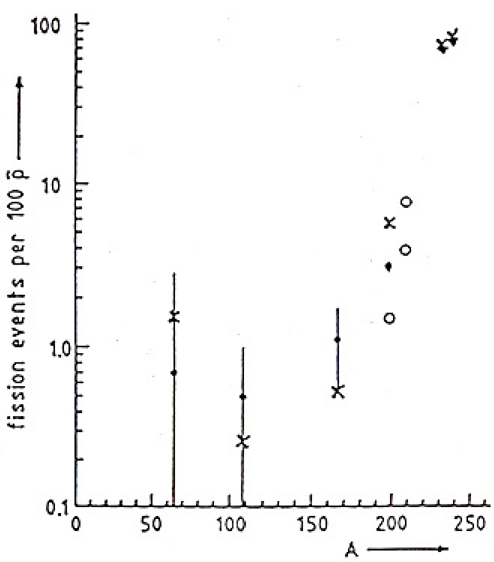

Fig. 1. Absolute fission probabilities for Cu, Ag, Ho, Au, Pb208, Bi, Th, and U targets.

An alternative approach to inducing nuclear fission is to allow antiprotons to stop in a population of uranium. Figure 1 shows the experimentally determined fission probability as a function of atomic mass[1-3]. Note that every antiproton that stops in uranium induces fission. When a low kinetic energy antiproton strikes a target, it quickly decelerates due to scattering against electrons in the target. At thermal energies the antiproton will only penetrate a few atomic layers into the target. When the negatively-charged antiprotons decelerate to kinetic energies of a few electron-Volts they displace an orbiting outer-shell electron. Because antiprotons are fermions with different quantum numbers than electrons, they quickly cascade down to the ground state and annihilate against one of the nucleons (proton or neutron) in the nucleus. The absorption by the nucleus of one of the pi-mesons that emanate from this annihilation induces the nuclear fission. Unlike neutron induced fission, the isotope of uranium is irrelevant. Depleted uranium U238 undergoes antiproton-induced fission just as easily as fissile U235. Unlike weapons-grade fissile materials such as U235, there are no regulatory controls on the handling of U238. This significantly reduces research costs and administrative overhead, allowing development of the technology to progress much faster than otherwise possible.

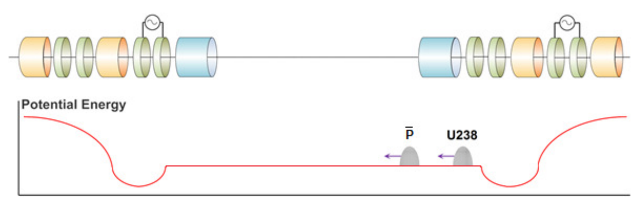

Fig. 2. Lightweight electrostatic particle accelerator that mixes U238 ions with antiprotons.

Instead of a solid uranium target, imagine the uranium in the form of ions trapped in an electrostatic trap similar to that sketched in figure 2. Electrostatic traps provide stable containment for charged particles oscillating back and forth across the trap in the same way that magnetic storage rings confine circulating particle beams. By launching antiprotons (signified by a P with an overhead bar) in the same direction as the uranium ions and constructing the trap so that the antiprotons and uranium ions have the same velocity, the antiprotons stop with respect to the uranium ions and annihilate.

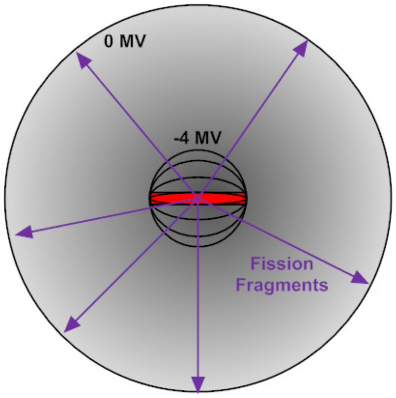

Fig. 3. Sketch of the electrical power generator architecture.

Because the uranium is in the form of a sparse cloud, the energetic fission daughters escape the trap without significant energy loss or scattering. As shown in figure 3, imagine that this electrostatic trap (red region) is in the middle of a spherical shell It has been experimentally determined[4] that the average fission daughter under these circumstances has a net electrostatic charge of +20e. At 1 MeV per nucleon and an average charge of +e/5 per nucleon, a 5 MV voltage difference between an inner mesh electrodes and the shell can convert fission daughter kinetic energy into electrical potential energy (charge a capacitor). Because of the width of the fission daughter mass, energy, and charge distributions, in figure 3 an optimum voltage of 4 MV is shown, maximizing the generated electrical power.

II. VOLTAGE BREAKDOWN

While material composition and surface smoothness play a role which is hard to quantify, the general rule of thumb for maximum electric field is the vacuum breakdown limit[5-6]

$$E_s\, V_s \;\le\; 10^{12}\ \frac{V^2}{m} \qquad . \qquad (1)$$

Using this equation as a guide, one design of the generator calls for an inner electrode radius of 4 m and an outside radius of 8 m. The surface area of the outside shell would then be 100 m^2.

There are various solar sail materials under consideration[7]. New carbon fiber sheets have attained an specific mass of 3 g/m^2, compared to 5 µm thick Mylar at 7 g/m^2 and aluminized Kapton film at 12 g/m^2. Because carbon fiber sheet is already conductive and would self-inflate with voltage applied to its surface (analogous to hair standing up on one's head), such a carbon fiber outer shell would have a total mass of approximately 0.3 kg.

The inner grid in figure 3 is illustrated as a set of wires arranged similar to lines of longitude. Another option that would be able to stand off higher voltages is to compose the inner electrode of a uniform film of carbon fiber sheet having a specific mass of 0.1 g/m^2, a target for current interstellar solar sails. At a density of 2 g/cm^3, the thickness of such sheets is only 50 nm. By comparison, a 100 MeV fission daughter such as barium would have a range through this material of over 12 µm, suffering an energy loss of 0.64 MeV traversing the material. A greater advantage of having a thin carbon membrane for the inner electrode would be the stripping of additional electrons[8] from the fission daughter. This would allow for smaller voltages and smaller generator size. More theoretical and experimental work needs to be devoted to this potential enhancement. Such work would provide guidance on the optimum thickness of such a membrane when also considering such issues as tensile strength, maximum temperature, and maximum surface electric field.

The same barium fission daughter would have a maximum kinetic energy of approximately 1 MeV by the time it impinges on the outer shell. At this energy the range of the daughter in a carbon fiber shell would only be 0.3 µm. With a specific mass of 3 g/m^2, such a shell would have a thickness of 1.5 µm, stopping all of the fission daughters and absorbing their residual kinetic energy in the form of heat.

III. ELECTROSTATIC TRAP MASS

An electrostatic trap capable of simultaneous long-term storage of both antiproton and depleted uranium ions has already been designed theoretically. Alternating focusing and defocusing electrodes are utilized to form a strong-focusing lattice[9]. It is envisioned that such an electrostatic particle accelerator could be composed of very thin tungsten wire similar to that of the ion gauge pictured in figure 4. In space the pictured vacuum flange and accompanying ceramic insulators in the bottom-right corner would be removed. A scale model of a space qualified electrostatic trap needs to be built to confirm that a mass below 100 g is achievable.

Fig. 4. Picture of a commercial ion gauge mounted on a vacuum flange.

IV. ELECTRICAL POWER

The estimated mass of the outer shell, inner electrode, and electrostatic trap is approximately 0.55 kg. This requires that the system for generating onboard electrical power has a mass budget of 0.45 kg. The solution proposed in this paper is to utilize an array of light emitting diodes coupled to optical fibers (and optical fiber amplifiers) and matched photovoltaic cells to convert the 4 MV capacitor charge into voltages suitable for onboard subsystems. The optical fibers can also be used directly as the light source to transmit scientific data back to Earth[10] and for the spacecraft LIDAR system[11].

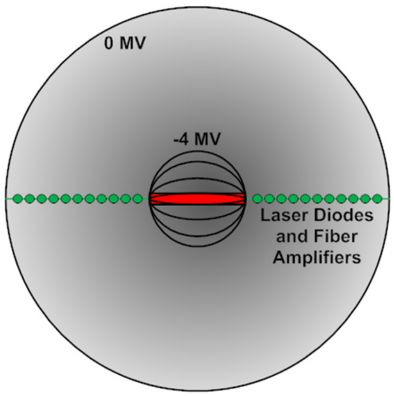

Fig. 5. Sketch of the placement of laser diodes and fiber amplifiers to convert the 4 MV into useable spacecraft power.

Fundamentally, harvesting electrical power from the architecture in figure 3 requires the extraction of residual uranium electrons remaining in the trap to the outside. This means that the electrons must either follow a conductor or be beamed. One approach to efficient energy harvesting is to transmit the electrons across many voltage drops, each drop performing work that can be transmitted outside of the generator. As illustrated in figure 5, an array of laser diodes and/or fiber amplifiers create a voltage ladder between the inside electrode and the generator shell. Since optical fibers are insulating, they provide a compact and lightweight method of energy transmission.

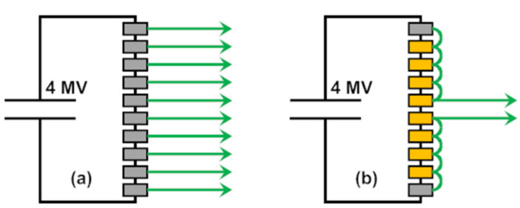

Fig. 6. Electrical circuit diagrams illustrating possible conversion architectures.

As illustrated in figure 6, there are several ways to package and distribute the light energy transmitted by the optical fibers. In scenario (a) each step in the voltage ladder is composed of a laser diode that feeds an individual optical fiber. This approach has the highest mass and the lowest power density. Scenario (b) is the preferred architecture in which primary laser diodes (top and bottom grey elements) feed optical fibers that are amplified (yellow elements) in several steps before being transmitted outside of the generator shell. The limit to this approach is the peak power capacity of the optical fiber and fiber amplifiers.

V. CONVERSION EFFICIENCY

Laser diode electrical-to-optical efficiencies can be as high as 80%. Laser diode light coupling into optical fibers can also be as high as 80%. The efficiency of converting laser light back into electrical power with a matched photovoltaic element can be as high as 90%. The efficiency of converting fission daughter kinetic energy into potential energy at the optimum inner electrode voltage is estimated to be approximately 70%. Therefore the overall estimated conversion efficiency of this generator architecture is taken to be 40%.

TABLE I. Representative generator parameters.

Generator Parameter	Value
Assumed total conversion efficiency	40%
Assumed output power level (kW)	100
Total fission energy rate needed (kW)	250
Ave. energy released per fission (MeV)	200
Needed rate of fission events (Hz)	7.8E15
Needed antiproton mass rate (g/yr)	0.41
Electrical current flowing on shell (mA)	25
Surface area of outer shell (m^2)	100
Emissivity of outer shell	1
Thermal power emitted by shell (kW)	150
Equilibrium shell temperature (°K)	403

Table I contains a summary of representative generator parameters. For a continuous electrical output power of 100 kW (worst case scenario) the consumption rate of antiprotons would be 0.41 g/year. Also assuming continuous peak power operation, the expected temperature of the shell is 403°K. The shell would operate at room temperature if the generator were operated continuously at 30% capacity. More likely, the generator will be run at very low duty cycle for peak power levels (LIDAR scans and transmission pulses to Earth) and very low levels (<1%) for computing and powering scientific instruments.

VI. ELECTRON MANAGEMENT

The depleted uranium electrons liberated by fission events along with secondary electrons generated from the inner electrode, either via field emission or created by passage of fission daughters through the inner electrode material, will be accelerated to 4 MeV when they strike the outer generator shell. In order to maintain efficient generator operations this flow of electrons must be avoided. These electrons start off at very low energies, less than 1 keV, near and inside the inner electrode.

By maintaining a positive average voltage on the inner core electrodes of the electrostatic trap, and shadowing the wires composing the inner spherical electrode, these low energy electrons will be attracted to and captured by the electrostatic trap electrodes. A comprehensive computer simulation is being written to minimize the arrival of accelerated electrons at the generator shell.

VII. DISCUSSION

The purpose of this paper is to propose an electrical power generator architecture for a very low mass spacecraft destined for exoplanets. While a conceptual blueprint has been provided, a great deal of additional work is needed to translate this vision into a engineered generator qualified for space operations.

Many tests will be needed during this development path. One important experiment is to induce fission in uranium and measure the charge state of the daughters with and without a thin carbon fiber sheet stripping electrons. There are two means of performing this experiment. One is to set up an experiment at an antiproton facility such as CERN or FLAIR (in the near future). The other is to store nanograms of fissile uranium in an electrostatic trap and expose the ensemble with thermal neutrons. Such an experiment can be performed at facilities such as the neutron therapy center at the Fermi National Accelerator Laboratory or at a research reactor.

Another experiment is testing the ability of thin carbon fiber spherical shells to hold high voltage. Pictured in figure 7, Hbar Technologies, LLC has an in-house facility that can be used to perform such experiments up to 100 kV with spheres of radius as large as 20 cm.

Fig. 7. Facility for performing high voltage experiments with spherical geometries.

REFERENCES

1. Bocquet, J.P., et. al., "Prompt Fission Induced by Antiproton Annihilation at Rest on Heavy Nuclei," *Zeitschrift für Physik A Hadrons and Nuclei* **342**, No. 2, pp. 183-189, June 1992. doi:10.1007/BF01288467

2. Hofmann, P., et. al., "Fission of Heavy Nuclei Induced by Stopped Antiprotons. I. Inclusive Characteristics of Fission Fragments", *Phys Rev C* **49**, p. 2555, May 1994. doi:10.1103/PhysRevC.49.2555

3. Kim, Y. S., et. al., "Fission of Heavy Nuclei Induced by Stopped Antiprotons. II. Correlations Between Fission Fragments", *Phys Rev C* **54**, No. 5, p. 2469, November 1996. doi:10.1103/PhysRevC.54.2469

4. Ajlouni, A.W., and Mahasneh, A.A., "Atom Behavior During Nucleus Fission Process", *Journal of Applied Sciences* **7**, No. 12, pp. 1664-68, 2007.

5. Cranberg, L., "The Initiation of Electrical Breakdown in Vacuum", *Journal of Applied Physics* **23**, 518 (1952). doi: 10.1063/1.1702243

6. Hawley, R., "The Electrical Properties of High Vacuum", Chapter 4 in High Voltage Technology, Ed. L.L. Alton, Oxford University Press, London (1968).

7. Kezerasbvili, R.Y., "Solar Sail: Materials and Space Environmental Effects", Advances in Solar Sailing, Springer-Verlag, Berlin, Heidelberg (2014). doi: 10.1007/978-3-642-34907-2

8. Okuno, H., et. al., "Low-Z Gas Stripper as an Alternative to Carbon Foils for the Acceleration of High-Power Uranium Beams", *Phys. Rev. Special Topics – Acc. and Beams* **14**, 033503 (2011). doi: 10.1103/PhysRevSTAB.14.033503

9. Courant, E.D. and Synder, H.S., "Theory of the Alternating-Gradient Synchrotron", *Annals of Physics* **281**, 360-408 (1958). doi: 10.1006/aphy.2000.6012

10. Hemmati, H., Biswas, A., and Djordjevic, I.B., "Deep-Space Optical Communications: Future Perspectives and Applications", *Proceedings of the IEEE* **99**, No. 11, pp. 2020-39, December 2011. doi: 10.1109/JPROC.2011.2160609

11. Cracknell, A.P., and Hayes, L., Introduction to Remote Sensing, 2nd edition, Taylor and Francis, London (2007). ISBN: 978-0-8493-9255-9.

Nuclear and Emerging Technologies for Space
Knoxville, TN, April 6 – April 9, 2020, available online at https://nets2020.ornl.gov

STAY COOL – ALTERNATIVES FOR LONG TERM STORAGE OF LARGE QUANTITIES OF LIQUID HYDROGEN ON A MARS TRANSFER VEHICLE

Nicholas A. Morris[1], and Dr. L. Dale Thomas

[1]*301 Sparkman Dr., Huntsville, AL, 35899*

Primary Author Contact Information: 256-824-5262 nam0021@uah.edu

Improved methods for storing liquid hydrogen in larger quantities and over longer periods of time in space are becoming progressively more critical as sights are once again set on Mars. Current storage methods involve the venting of vaporized hydrogen to space, with the consequence that significant amounts of hydrogen are wasted. Extra hydrogen must be stored to account for this loss resulting in unnecessary mass penalties. Eliminating this waste can reduce overall mission mass, extend mission range, and perhaps most importantly lower mission trip times and costs. This paper explores alternative methods of storing liquid hydrogen with emphasis on missions to Mars as laid out by NASA's current design reference architecture.

I. Introduction/Background

As mankind looks to Mars once again and considers the challenges of deep space exploration, it is evident that new propulsion technologies will be needed. Nuclear Thermal Propulsion (NTP) is an attractive 21st century option to propel human exploration missions to Mars and other deep space destinations[1] due to its favorable specific impulse which reduces overall trip times, total required mission mass, and costs. Reducing trip time is particularly important for human exploration missions because of the harsh radiation environment. Although methods to shield against this radiation are being developed, simply spending less time exposed to the environment is readily achievable with improve propulsion systems such as NTP.

NASA's current design reference architecture[3] (DRA) considers the use of NTP as the main propulsion technology for both manned and unmanned Mars missions.

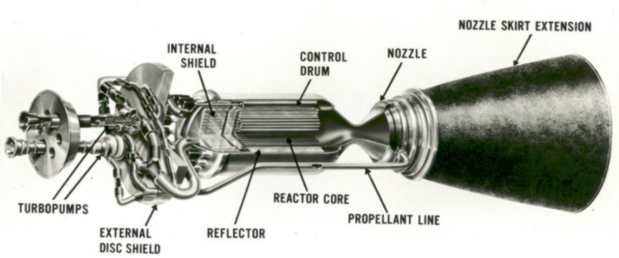

Fig. 1. An example of a nuclear thermal propulsion engine[1]

Common NTP engines (depicted in Fig. 1.) employ a nuclear reactor core to super heat pure hydrogen which is expanded through a rocket nozzle to obtain thrust. Liquid Hydrogen (LH_2) is the ideal propellant for NTP as it acts as both a coolant and a propellant. As a propellant, liquid hydrogen's low molecular weight yields a high specific impulse (I_{sp}) which exponentially reduces the overall propellant mass needed for the same ΔV mission requirement, shown by equation (1).

$$m_{propellant} = m_{inert}\left(e^{\frac{\Delta V}{I_{sp} g_0}} - 1\right) \tag{1}$$

Alternatively, by maintaining the same amount of propellant mass, a higher I_{sp} results in an increased ΔV capability (see equation (2)). This, in turn, allows the selection of shorter transfer orbits or more simply put a decrease in overall trip time.

$$\Delta V = I_{sp} g_0 \ln\left(\frac{m_{propellant}}{m_{inert}} + 1\right) \tag{2}$$

Recent work[2] has shown that NTP ΔV capability can be increased even more by seeding hydrogen propellant with heavy noble gasses, such as Argon, further reducing overall trip times. The DRA, however, currently calls for the use of pure liquid hydrogen as the propellant for the NTP engine and thus only the storage of the hydrogen propellant will be considered in this paper.

II. Problem Statement

LH_2 is a cryogenic fluid and must be stored at low absolute temperatures, approximately 14-21 K (at two atmosphere), to prevent it from changing phase to a gas, an event here forth referred to as boil-off. Boil-off is problematic when storing LH_2 for two reasons. First, gaseous hydrogen is very difficult to pump. Second, when LH_2 changes to its gaseous form inside a pressure vessel, the pressure rises and can cause the vessel to exceed its limits and fail. To prevent this from occurring, the gaseous hydrogen must be vented to return the pressure of the vessel back to acceptable limits. As a result, the vented hydrogen is lost, and the overall effective employable amount of hydrogen propellant is decreased. To make up for this event (boil-off) more than the required amount of hydrogen for an ideal zero-boil-off (ZBO) mission is needed.

This extra hydrogen is a major mass penalty. A 2011 study[4] (see Fig. 3.) shows that simply improving (reducing the amount of, not eliminating) boil-off is the single largest mass savings step in reaching the DRA's target mission mass. Completely eliminating boil-off would, of course, further increase mass savings.

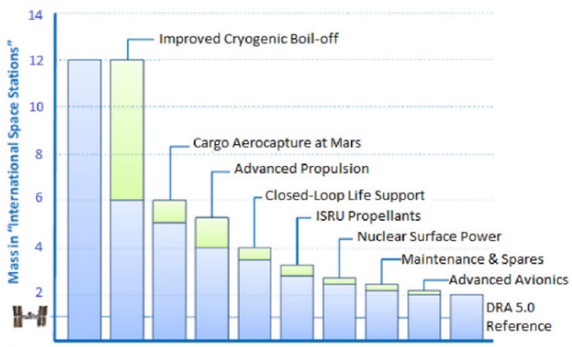

Fig. 3. Technology improvements needed to achieve DRA 5.0 reference total mission mass[4]. Improved Cryogenic Boil-off is shown as the largest step to achieve reference mass

Past works that analyze the thermal management of cryogenics in space have one key commonality, they all analyze relatively small volumes. Review of the relevant literature has been unable to identify a thorough analysis of a considerably large liquid hydrogen storage system in space, on "*the scale required for human planetary exploration,*" as JPL[11] describes it. Past research does not definitively conclude whether passive or active systems, as will be detailed in this paper, are more effective than the other. A thorough analysis of the MTV's propellant storage system through its proposed mission flight path will shed light on which of these systems are the most mass and energy-efficient and thereby the most cost effective. Results of this study will also be applicable to future deep space missions.

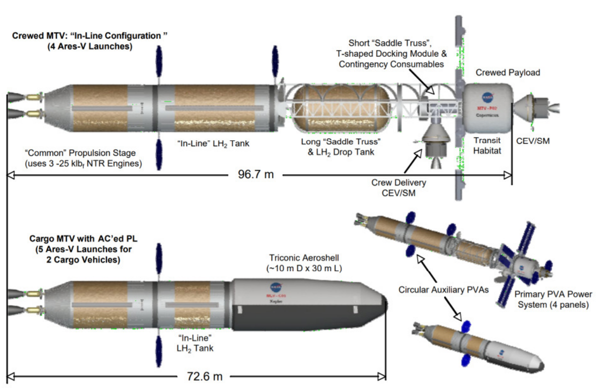

Fig. 2. The Mars Transfer Vehicle for crewed and cargo configurations as depicted in NASA's DRA 5.0

This paper provides a general analysis of a hydrogen propellant tank subjected to the environment of the Mars Transfer Vehicle (MTV), both natural and induced, in reference to the mission flight path laid out in the DRA. This paper also discusses methods to control the self-pressurization rate of the propellant tank to achieve zero-boil-off (ZBO). Non-ZBO methods and modifications to the MTV vehicle design and DRA flight path are reserved for future work. The Mars Transfer Vehicle is shown in Fig. 2. (ref. 3).

III. Thermal Analysis

A pressure control analysis using the first law of thermodynamics and the conservation of mass as done by Lin[6], et. al., shows that for a control volume that contains liquid-vapor contents, the homogenous self-pressurization (hsp) rate is,

$$\left(\frac{dP}{dt}\right)_{hsp} = \frac{\phi(Q_{net})}{V} \tag{3}$$

where ϕ is the internal energy derivative, and Q_{net} and V are the net heat into the system and the fixed cryogenic tank volume respectively. Furthermore, Lin points out that the pressure rise rate is governed by three key phenomena:

1. External heat leak
2. Fluid temperature stratification
3. Interfacial heat and mass transfer

External heat leak is evident in equation (3) (the variable Q_{net}), and will be the focus of the remainder of this paper. Both, fluid temperature stratification and interfacial heat and mass transfer have a lesser contribution and are thoroughly discussed in Lin's paper. Intermittent tank mixing is sufficient to make the effects of these two negligible.

For a constant density (thus a constant ϕ) and constant cryogenic tank volume, equation (3) suggests that tank pressure rises linearly with rising Q_{net}. In actuality, this is an exponential effect. As heat is added to the system and boil-off occurs, the overall propellant density decreases resulting in an exponential increase in ϕ and thus and exponential increase of dP/dt. However, for relatively slow pressure rates, ϕ can be taken as constant, and a linear model can be assumed.

A further analysis of Q_{net} depends entirely upon the environment in which the tank is located. For the MTV, the natural environment includes,

Q_{sol}	solar radiation
Q_{alb}	planetary albedo
Q_{IR}	planetary infrared radiation

For an unprotected tank, the total heat load can be defined as the summation of these,

$$Q_{net} = Q_{sol} + Q_{alb} + Q_{IR} \tag{4}$$

To reduce the heat leak from the natural environment, the propellant tank is covered in low solar absorbance, high infrared emittance multi-layered insulation (MLI). MLI acts as a middleman between the natural environment and the propellant tank and the resulting reduced heat leak including the tank supports and subsystems can be expressed as,

$$Q_{net} = Q_{MLI} + Q_{struts} + Q_{piping} + Q_{mixer} - Q_{out} \tag{5}$$

where

Q_{struts}	heat leak through supports
Q_{piping}	heat leak through tank piping
Q_{mixer}	heat add by tank mixer
Q_{out}	heat radiated out or removed from the system

Another heat source to be considered, specifically for NTP, is the induced gamma ray and neutron emissions from the nuclear core. This has been modeled in prior work[5], and can be expressed as Q_{NTP} and added to (5),

$$Q_{net} = Q_{MLI} + Q_{struts} + Q_{piping} + Q_{mixer} + Q_{NTP} - Q_{out} \tag{6}$$

For Q_{net} to be zero, it can be seen that,

$$Q_{out} = Q_{MLI} + Q_{struts} + Q_{piping} + Q_{mixer} + Q_{NTP} \tag{7}$$

We can further express Q_{out} as its natural and induced components,

$$Q_{out_{nat}} + Q_{out_{ind}} = Q_{MLI} + Q_{struts} + Q_{piping} + Q_{mixer} + Q_{NTP} \tag{8}$$

Equation (8) implies two methods to achieve a Q_{net} equal to zero. The first, is to reduce the right side sufficiently to equal $Q_{out_{nat}}$. These are referred to as passive methods and require no induced heat removal (i.e. $Q_{out_{ind}} = 0$). Conversely, it is not always possible to sufficiently reduce the right side of equation (8) and $Q_{out_{ind}}$ must be greater than zero. When this occurs, Active methods of heat removal, such as cryocoolers, are necessary.

Finally, in some cases the $Q_{out_{nat}}$ can exceed the right side of equation (8) and heat would need to be added to the system. If Q_{mixer} is not sufficient, strip heaters (Q_{sh}) can be used. To account for this, equation (8) becomes,

$$Q_{out_{nat}} + Q_{out_{ind}} = Q_{MLI} + Q_{struts} + Q_{piping} + Q_{mixer} + Q_{NTP} + Q_{sh} \tag{9}$$

IV. Analysis of the DRA mission

As the MTV moves through the phases of its mission, the heat loads detailed in equation (9) change significantly. To better analyze the problem and determine the optimum solution, it is important to define the MTV mission phases. The DRA proposed mission flight path is shown in figure four[3].

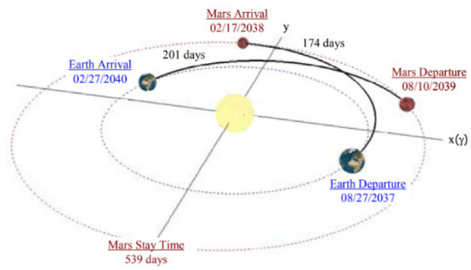

Fig. 4. Proposed flight path for 2037 crewed mission to Mars

The MTV is first scheduled to park in a cis-lunar orbit and await the crew. After some time, the MTV spends a lengthy period traveling through deep space on its way to Mars where it will park in Mars orbit and await its lengthy return trip back to Earth. These three phases are defined as:

Phase 1: Cislunar – pertaining to the Earth-Moon system, where the liquid hydrogen storage tanks spend a large fraction of the mission awaiting Phase 2 (journey to Mars). This phase is completed when the NTP engine completes its burn to enter Trans Mars.

Phase 2: Trans Mars/Earth – pertaining to the transition to Mars from Earth or vice versa, where the liquid hydrogen storage tanks coast through deep space.

Phase 3: Mars Orbit – pertaining to the orbit around Mars, where the liquid hydrogen storage tanks spend up to a year awaiting Phase 2 (return to Earth). This phase begins at the start of the second burn (to enter Mars orbit) and ends after the third burn (to enter Trans Earth).

In Phase 2, Q_{alb} and Q_{IR} are almost negligible and the right side of equation (8) can be reduced enough so that $Q_{out_{nat}}$ is greater and strip heaters will be needed. This has been shown in an analysis done by Plachta, et. al.[7] on the Titan Explorer mission. Plachta's work shows that by isolating the propellant tank's view to deep space, passive methods, such as sun shields, are enough to achieve ZBO for liquid hydrogen without the use of cryocoolers or other active heat removing systems.

As part of the same series of studies, Plachta reviews a Mars Sample Return Mission Concept[10] and concludes that due to the complications of shielding from both Q_{sol} and Q_{alb} while in a planetary orbit, it may not be possible to reduce the right side of equation (8) sufficiently for Phase 3, thus the use of active heat removal systems such as cryocoolers would be required. The results of the studies are published in a report by JPL[11]. JPL adds in their conclusion that for *"very large systems of the scale required for human planetary exploration"* the results concluded by Lin above may not be applicable and implies that a further analysis is needed.

V. Conclusions

To achieve ZBO for large quantities of hydrogen propellant on the MTV, the total net heat into the system must be small enough that the pressure rise over the period of the mission does not exceed the tank's limits. To achieve this, a more detailed analysis of the MTV's propellant tank during the DRA mission is required. Prior work[11] shows that for similar scenarios to that of Phase 2, ZBO can be achieved using passive methods only. However, for Phases 1 and 3, active methods, such as cryocoolers, may be needed.

To determine the best solution, each phase outlined in this paper should be analyzed individually and the results of various methods recorded in terms of mass, power-consumption, and complexity. Logically, the only viable solution is one that weighs less than the additional propellant and tankage needed to compensate for boil-off. As previously mentioned, non-ZBO methods and alternative flight paths than those laid out by the DRA should also be considered.

VI. Future Work

To start, a simplified steady-state model will be created to analyze the heat loads on an MTV scaled propellant tank in Earth orbit. The tank's ends will be aligned with the Sun vector and the Earth. This will allow the tank's side, the largest surface area, to be isolated to deep space. Passive methods such as MLI and sun shields will used to reduce the heat loads between the Sun and Earth and the total heat leak will be recorded. A separate model will analyze the heat loads on the same tank in the same scenario, however only MLI will be used as a passive method and in addition cryocoolers will be added. Again, the results will be recorded for comparison to the passive methods only model. Next steps include altering the geometry of the tank as well as its orbital path around the Earth and its orientation with respect to the Earth and Sun. The total mission mass, power consumption, and complexity will be measured to determine the best viable solution for each phase. Upon completion of these research tasks, the entire mission will be analyzed simultaneous in the same fashion to determine the optimum solution for the MTV following the DRA flight path. Finally, non-ZBO methods and alternate flight paths will be considered by the same metrics to determine if mass savings and mission cost can be further improved. The tools that will be used include MATLAB and Simulink in conjunction with the System Tool Kit and Thermal Desktop. To analyze the effects of the NTP engine during its several burns, the model will be combined with an existing NTP model[5].

ACKNOWLEDGMENTS

This work was supported by the National Aeronautics and Space Administration under contract number MTS_UAH_021717.

REFERENCES

1. Hall, L. Nuclear Thermal Propulsion: Game Changing Technology. NASA. http://www.nasa.gov/directorates/spacetech/game_changing_development/Nuclear_Thermal_Propulsion_Deep_Space_Exploration. Accessed Dec. 4, 2019.
2. D. Nikitaev & D. Thomas, "Seeded Hydrogen in Nuclear Thermal Propulsion Engines," AIAA Journal of Spacecraft and Rockets. (submitted)
3. Humans Exploration of Mars Design Reference Architecture 5.0. https://www.nasa.gov/pdf/373665main_NASA-SP-2009-566.pdf.
4. Braun, D. B. "Investments in Our Future: Exploring Space Through Innovation and Technology." slide 9.
5. A. Aueron, D. Thomas, & J. Cassibry, "Analytical Modeling of Radiation Attenuation and Heat Deposition in Propellant for Nuclear Thermal Rockets," AIAA Journal of Spacecraft and Rockets, March 2019.
6. Lin, C.-S., Van Desar, N. T., and Hasan, M. M. "A Pressure Control Analysis of Cryogenic Storage Systems." p. 12.
7. Plachta, D. W., Christie, R. J., Jurns, J. M., and Kittel, P. "Passive ZBO Storage of Liquid Hydrogen and Liquid Oxygen Applied to Space Science Mission Concepts." Cryogenics, Vol. 46, No. 2–3, 2006, pp. 89–97. doi:10.1016/j.cryogenics.2005.11.012.
8. Plachta, D. W., Christie, R. J., Feller, J. R., and Johnson, W. L. Cryogenic Boil-Off Reduction System Testing. Presented at the 50th AIAA/ASME/SAE/ASEE Joint Propulsion Conference, Cleveland, OH, 2014.
9. Guzik, M. C., and Tomsik, T. M. "An Active Broad Area Cooling Model of a Cryogenic Propellant Tank with a Single Stage Reverse Turbo Brayton Cycle Cryocooler." TFAWS 2011, 2011.
10. Plachta, D. W., Christie, R. J., Jurns, J. M., and Kittel, P. "ZBO Cryogenic Propellant Storage Applied to a Mars Sample Return Mission Concept." AIP Conference Proceedings, Vol. 823, No. 1, 2006, pp. 205–212. doi:10.1063/1.2202418.

11. Guernsey, C., Baker, R., Plachta, D., and Kittel, P. Cryogenic Propulsion with Zero Boil-Off Storage Applied to Outer Planetary Exploration. Presented at the 41st AIAA/ASME/SAE/ASEE Joint Propulsion Conference & Exhibit, Tucson, Arizona, 2005.

Nuclear and Emerging Technologies for Space
Knoxville, TN, April 6 – April 9, 2020, available online at https://nets2020.ornl.gov

MODELING AN OPEN CYCLE GAS CORE NUCLEAR ROCKET: CURRENT STATUS AND CHALLENGES

Rittu S. Raju[1], and John E. Foster[1]

[1]*2355 Bonisteel Blvd, Ann Arbor, Michigan, 48109*

Contact Information: (215) 303-6172, and ritzsr@umich.edu

This computational study aims to explore criticality, stability and heat transfer of a gas core nuclear rocket using a combination of commercial codes such as Fluent for flow and fissioning mass stability (vortex stabilized) and MCNP for neutronics along with an analytical formulation for the study of heat transfer to the gas. These models are self consistently coupled as the neutronics impacts Uranium fuel temperature and heat transfer. Instabilities impact not only heat transfer but also the neutronics. Simple MCNP calculations showed that the criticality can be achieved for a system with 3000 K uranium core. To better understand the system neutronics, MCNP calculations need to be done with a 50,000 K uranium cross-section. In addition to this computational work, an experimental study of radiative heat transfer from Uranium is being planned using laser ablation. These steps aim to develop a design tool suite that would be used for the realistic analysis of the feasibility of a gas core nuclear rocket.

I. BACKGROUND

Human exploration of the solar system, particularly to the outer planets can be made feasible using Gas-Core Nuclear Rocket for In-space propulsion. Gas-Core Nuclear Rockets are attractive because they feature high-impulse ranging from 2,500 to 7,000 seconds[1], and high-thrust ranging from 20,000 N to 400,000 N[2]. The gas-core nuclear rocket fuel is in a gaseous form allowing for arbitrarily high core temperatures (>10 times solid core operating temperature). Because specific impulse scales with the square root of the gas temperature, a significant increase in performance over conventional rockets is possible. Figure 1 illustrates the operation of an open cycle Gas-Core Nuclear Reactor engine, which uses uranium or plutonium as the fissioning fuel. The focus of this work is the open cycle gaseous core reactor. In Gas-Core Nuclear Rocket, the fissioning fuel reaches temperatures of more than 55,000 K, which implies that the core is actually in the plasma-like state. This plasma-like core heats a light gas such as hydrogen and then converts the high enthalpy hydrogen flow via a converging-diverging nozzle to create a high thrust and high-velocity flow. At these high temperatures, hydrogen gas dissociates leading to even further improvements in specific impulse owing to the inverse square root of mass dependence.

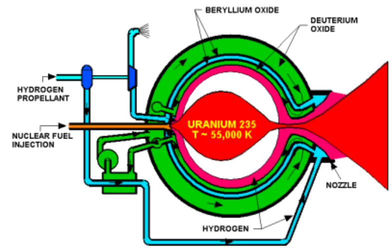

Fig. 1. An Open Cycle Gas Core Nuclear Rocket Design[3].

The Gas-Core Nuclear Rocket has the potential to solve one of the major problems facing human space exploration to Mars and beyond. The physiological effects of long-term exposure to the space environment make human exploration of the solar system challenging. But Gas core nuclear rocket has the potential to greatly reduce the trip time for a given mission as compared to chemical or electric propulsion systems. Studies show that the Gas-Core Nuclear Rocket enables roundtrip mission times of only 80-days to Mars.[2] The faster trip times greatly reduces physiological degradation associated with long-duration spaceflight. If realized, the gas core rocket can become the basic architecture for human exploration of the solar system, reaching essentially all planets with round trip times of less than a decade. Operating at high temperature (10^4 – 10^5 K), the Gas-Core Nuclear Rocket can give a specific impulse double or triple (several thousand seconds) that of a conventional solid-core nuclear rocket.

A number of technical challenges must be resolved however before Gas Core Nuclear rocket technology can become a reality. These challenges include: 1) confinement and stability of the fissioning plasma, 2) mitigation of uranium plasma erosion due to mixing and subsequent entrainment with hydrogen fuel, and 3) maximizing heat transfer from the uranium plasma to the hydrogen fuel and 4) ensuring high-temperature nozzle survivability. Past open cycle concepts have featured hydrodynamic confinement of the fissioning core. The core itself is open to the nozzle and thus nuclear fuel can be entrained and lost with the passing and subsequently exiting hydrogen flow. Hydrogen is heated radiatively by plasma emission in this concept. There have been a number of other gas core studies that focused on reactor physics, fluid flow, and heat transfer. These studies are summarized in a recent review[4].

II. MODELING STATUS AND CHALLENGES

Initial fluid flow studies were carried out in Fluent for both two-dimensional and three-dimensional cylindrical gas core nuclear rocket designs. For simplicity regarding the analysis of the hydrogen flow, the 3-D model featured a spherical obstruction with set boundaries around which gas flows. Neutronics studies were conducted in MCNP using readily available cross-sections. These studies highlighted the challenges of modeling a gas core nuclear rocket and the necessary steps needed for the realization of a realistic model.

II.A. Fluid Flow and Heat Transfer Study

The modeling design approaches used for these studies include a cylinder with a conical nozzle and Poston's study design[5]. The initial condition and inlet parameters used are similar to what is used in Ref. 5. Fluent software was primarily used to carry out this study. The input parameters used for the initial study were obtained from previous works[2, 5, and 7]. These parameters given in Table 1 will also be used in future studies.

TABLE I. Input Parameters for Initial Fluid Flow and Heat Transfer Study of a Gas Core Nuclear Rocket.

Material Properties		
Uranium at 50,000 K and 1000 atm	Density (kg/m^3)	17.8
	Viscosity (kg/m-s)	6.01e-5
	Specific Heat (J/kg-K)	1080
	Thermal Conductivity (W/m-K)	0.0192
Hydrogen at 3000 K and 1000 atm	Density (kg/m^3)	8.24
	Viscosity (kg/m-s)	4.34e-5
	Specific Heat (J/kg-K)	20100
	Thermal Conductivity (W/m-K)	0.446
Engine Parameters		
Chamber Length (m)		4
Uranium Sphere Core Radius (m)		1.2
Chamber Radius (m)		1.5
Number of Hydrogen inlets		8
Inlet Radius (m)		0.1
Nozzle Throat Radius (m)		0.3
Nozzle Exit Radius		1.2
Flow Conditions		
Hydrogen Flow Rate (kg/s)		3
Hydrogen Inlet Temperature (K)		3000
Uranium Temperature (K)		5000
Pressure (atm)		1000

A schematic of the cylindrical embodiment and the Poston's model are shown in Fig. 2 and Fig. 3 respectively. The heat transfer was modeled using just conduction. Also, the heat loss from the walls was not modeled in the initial studies.

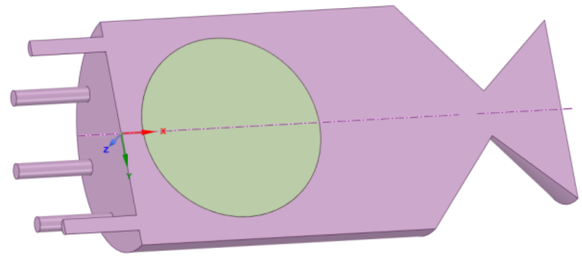

Fig. 2. Cylindrical Embodiment used for Initial Study.

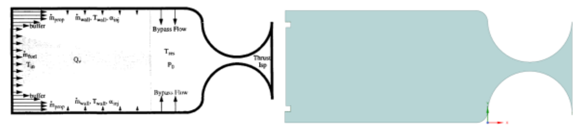

Fig. 3. Poston's Model in Paper[5] and Modeled in Fluent.

The challenges of modeling fluid flow and heat transfer in gas core nuclear rocket are (1) the geometry of the engine needs to be optimized to meet the high pressure and temperature conditions within the engine, (2) a radiative heat transfer model is necessary to describe heat absorbed by the hydrogen gas and (3) introducing the hydrodynamic confinement system into this engine design without affecting the engine's performance and criticality condition.

The current model is currently being modified to include (1) radiant heat transfer from uranium to hydrogen gas, (2) an assessment of heat loss from the walls and to the walls, (3) an optimized converging-diverging nozzle design for gas core nuclear engine as shown in Fig. 4, and (4) hydrodynamic stability analysis.

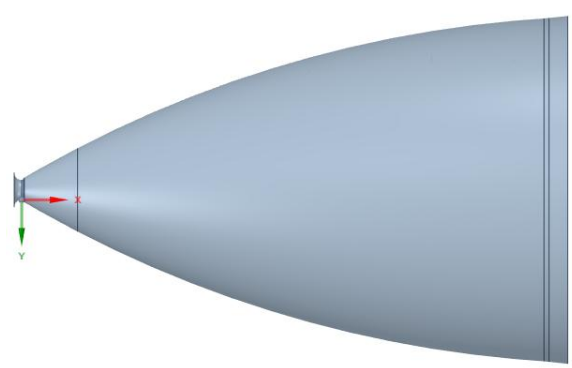

Fig. 4. Optimized Nozzle Design for an Open Cycle Gas Core Nuclear Rocket Analysis.

In addition to these computational changes, an experimental study to understand the uranium radiative heating is being planned. Previously experimental work has been done to study the radiative heat transfer from an electrically heated tungsten strip to carbon particle unseeded and seeded nitrogen[6]. The current plan is to use a laser pulse to vaporize and subsequently ionize ablated uranium 238 derived from a foil target. The uranium vapor using this approach can reach temperatures expected in the gas core reactor when it is critical. Analysis of the emission from this plasma will be compared with expected black body emission. Additionally, the interaction of this plasma with a hydrogen jet will also be investigated to look at radiative heat transfer. This experiment will be used to benchmark the radiative heat transfer model under development for this project.

II.B. Neutronics Study

A simple MCNP study has been carried out to obtain the criticality condition for this engine. A cylindrical engine with a cone-shaped nozzle was used for the analysis. Uranium 233 at 3000 K was used for the nuclear core and hydrogen propellant at 2500 K was used as a moderator around this spherical uranium core. Uranium 233 at 3000 K was used due to the readily available cross-section of uranium at this temperature. Beryllium metal was used as the reflector and the Titanium wall was used as the chamber wall for this engine. The engine is 2.8 m long and 1.2 m in radius with a core radius of 0.6 m. The reflector thickness is 0.25 m and titanium is 0.15 m thick. Although the analysis gave a keff of 1.01543, this is for the case where the cross-section of Uranium used was at 3000 K. As in the case of gas core nuclear rocket, the uranium core is at a temperature between 10,000 K to 50,000 K.

The challenge of modeling the neutronics is associated with the lack of cross-sections for uranium over the 10,000 K to 50,000 K. It may be possible to make Doppler corrections for cross-sections at higher temperatures. With this cross-section data, optimization of engine components such as the reflector will be possible.

Currently, previous neutronics studies for gas core nuclear rocket obtained uranium cross-sections at high temperatures using the NJOY code with ENDF/B-V data[7, 8]. This would be one way to obtain uranium cross-section at high temperatures. The radiative energy derived from the plasma heats the gas. This radiative transport will be modeled using a bridge code that takes reactor radiative flux and couples it to the hydrogen gas.

Although there are multiple computational challenges to this engine, the pathway is relatively straightforward. Utilizing the present-day computational tools, it may indeed be possible to realize a realistic open-cycle gas core model. With this basic model, the performance of the engine can be optimized and the feasibility of implementing the engine can realistically be contemplated.

III. CONCLUSIONS

If realized, a gas core nuclear rocket has the potential to open up the solar system for human exploration by considerably reducing the trip time. Its high specific impulse and thrust make it an attractive engine for in-space travel. The confinement of the nuclear core of this engine, heat transfer from uranium to fuel to the hydrogen propellant, uranium erosion, and the nozzle survival stands daunting challenges to the development of this engine concept. In this study, the goal is to understand the engine first using modern computational tools and then address the aforementioned technical challenges. The initial fluent analysis provided insight into the challenges of modeling a gas core nuclear rocket. It showed that a good nuclear rocket nozzle design is required to study the flow better. The radiative heat transfer from glowing uranium plasma to the hydrogen gas has to be formulated. MCNP analysis has to be done with more realistic neutron absorption cross-sections taking into account Doppler broadening at high temperatures – 10,000 to 50,000 K and uranium plasma density. The power of the reactor has to be self consistently coupled to the energy into the hydrogen gas. From this, the confinement of the engine core using hydrodynamic confinement will help us take a step towards making this engine feasible for future human space exploration.

ACKNOWLEDGMENTS

This work is supported by NASA Space Technology Research Fellowship (Grant Number: 80NSSC18K1161). We would also like to acknowledge the support of Dr. Houts (MSFC), the NASA mentor supporting this effort.

REFERENCES

1. W. E. MOECKEL, "Comparison of Advanced Propulsion Concepts for Deep Space Exploration," *NASA Technical Note*, NASA TN D-6968, Washington D. C., September (1972).

2. R. G. RAGSDALE and E. A. WILLIS, Jr., "Gas-Core Rocket Reactors – A New Look," *Seventh Propulsion Joint Specialist Conference*, AIAA, NASA TM X-67823, Salt Lake City, Utah, June 14 – 18 (1971).

3. B. PALASZEWSKI, "High Power Electric and Advanced Space Propulsion: Making the Impossible Possible," *NASA Glenn Research Center*, Lewis Field, February (2005).

4. R. S. RAJU and J. E. FOSTER, "Overview and Future of Open Cycle Gas-Core Nuclear Rocket," *Nuclear and Emerging Technology for Space Conference*, American Nuclear Society Topical Meeting, Richland, WA, February 25 – 28 (2019).

5. D. I. POSTON, "A Computational Model for an Open-Cycle Gas Core Nuclear Rocket," *Ph.D.*

Thesis, the University of Michigan, Ann Arbor, MI (1994).

6. J. R. WILLIAMS, "Radiative Heat Transfer in The Gaseous Core Nuclear Rocket," *Ph.D. These*, Georgia Institute of Technology, Atlanta, GA, May (1967).

7. M. F. TAYLOR, C. L. WHITMARSH, JR, P. J. SIROCKY, JR, L. C. IWANCZYK, "The Open-Cycle Gas-core Nuclear Rocket Engine – Some Engineering Considerations," *NASA Technical Memorandum*, NASA 0 X-67932, Atlanta, Georgia, November (1971).

8. J. E. TANNER, "Improved Gas Core Propulsion Model," Westinghouse Idaho Nuclear Co. Idaho Falls, ID.

Nuclear and Emerging Technologies for Space
Knoxville, TN, April 6 – April 9, 2020, available online at https://nets2020.ornl.gov

MODELING OF PULSED FISSION FUEL TARGET COMPRESSION

Kevin Schillo[1], Brian Taylor[2], Robert Adams,[2] and Leo Fabisinski[2]

[1]University of Alabama in Huntsville, Huntsville, AL, 35899
[2]Marshall Space Flight Center, Huntsville, AL, 35805,

Primary Author Contact Information: 813-597-1708, kjs0011@uah.edu

This paper presents recent developments in the research of the pulsed fission-fusion (PUFF) project. A fission-fusion hybrid consists of fusion fuel plasma surrounded by a liner of fissionable material. Such a system may offer a path to near-term fusion systems for terrestrial power production or spacecraft propulsion applications.

I. INTRODUCTION

In the pulsed fission-fusion (PUFF) concept, a current is passed through a liner of Li-D, which in turn surrounds a liner of fissionable material. As the Li-D implodes and compresses the fissionable material, neutrons released by fission reactions convert some of the lithium-six to tritium. The tritium and deuterium then fuse, which generates more fission reactions and more neutrons. This cycle continues until a detonation wave propagates through the target, providing a boosted fusion yield. By using fissionable material, fusion ignition may be achieved with significantly less energy input than what is required for pure D-T fusion. In addition, using the fission neutrons to breed tritium from lithium-six may offer significantly lower experimental costs compared to fusion experiments that require pure D-T targets [1, 2].

II. MODELING

Developing a comprehensive model for this process is complicated by extreme physics not generally found in other applications, and the need to perform this work without using classified sources. The implosion model must first emulate the implosion of a solid target from the impingement of a lithium liner, the generation of energy from nuclear fission and fusion reactions, diffusion of that energy throughout the target, conversion to plasma, and then plasma expansion against the magnetic fields of a magnetic nozzle

Once ignition is achieved the nuclear reaction will continue until either; the amount of fuel left to be fissioned cannot sustain criticality or the amount of energy released has caused the target to expand to where it is no longer critical. It is expected that the fusion fuel will cool almost instantly once fission energy is no longer present. These are highly intertwined and our models will address both burnup and thermal expansion. The model integrates several codes intended to evaluate the overall target while it goes through compression, burn and expansion. The DYNA2D model evaluates the solid deformation of the target into a highly compressed, supercritical mass. MCNP evaluates the criticality of the target.

III. DYNA SIMULATIONS

DYNA2D is a two dimensional lagrangian finite element software developed at Lawrence Livermore National Labs to model the strength, deformation, and compression of materials. This software serves this project as an initial model of the implosion. Energy addition is captured through an iterative process with MCNP in which the energy from nuclear reactions is added back into the DYNA2D model and rerun to capture the change in implosion.

In the PuFF demonstration model, layers of lithium deuteride, uranium, and lithium are imploded with a magnetic pressure acting on the outer surface of the outermost layer. Additional work is needed to raise the fidelity of the model. Do to lack of data, the lithium equation of state is based off of lithium deuteride literature. Improved material and equation of state properties are required. Below, the figures represent the pressure contours at several time steps in a PuFF-like implosion.

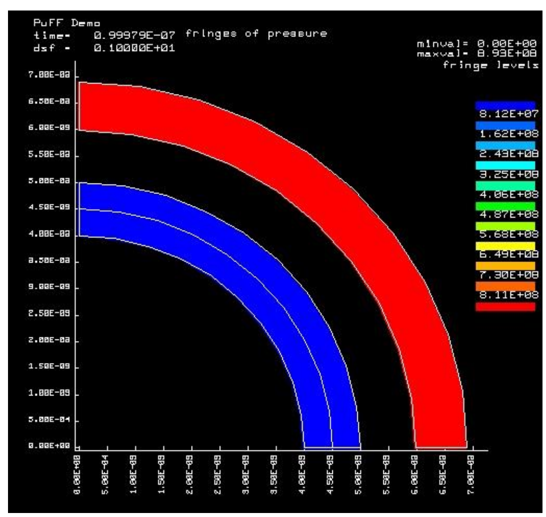

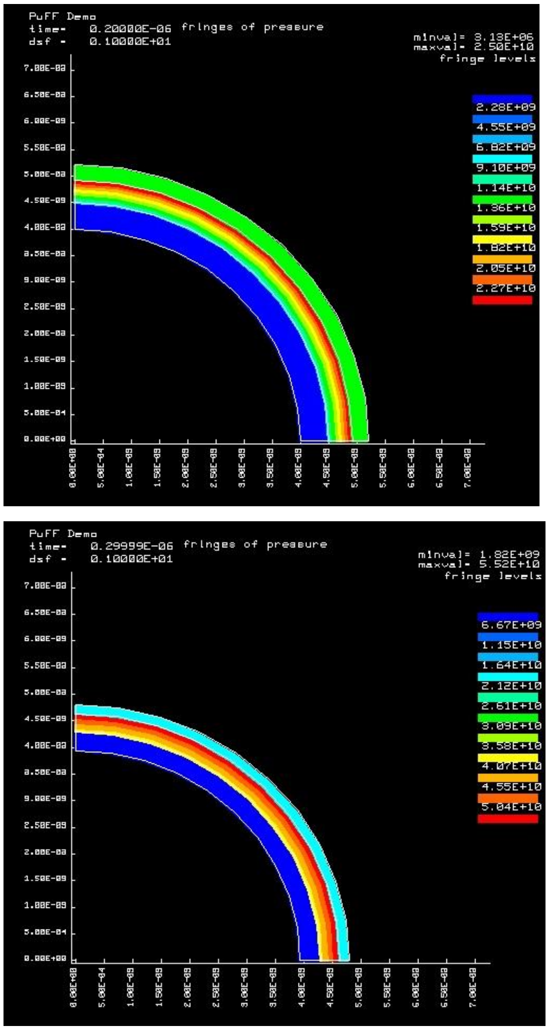

Fig. 1. Implosion of uranium-lithium target at several time steps.

A dedicated modeling computer has been procured to increase computational speed and allow for more detailed simulations with DYNA 2D. DYNA has been updated to accept heat addition through a polynomial equation of state model internal to the software. This will allow for joule and nuclear heating to be accounted for in a run by defining a heating curve for each material. Finally, a parameter space study of target implosions has begun. This problem has a large number of significant variables. The initial matrix of simulations focuses on a simplified implosion involving a constant current and single material where the current, and radii are varied. These results are analyzed with MCNP to determine k_{eff} of the compressed state. While this study will inform more complex implosion simulations, the goal is to sample the parameter space in order to work toward a minimal current and mass that reaches criticality. Since the magnetic pressure that is driving the implosion is inversely related to the square of the radius the optimum configuration will likely be a balance between minimizing initial radius in order to increase pressure while balancing the opposing need to have adequate mass for reactivity but less mass to improve acceleration and compression. Below one can see an example density contour plot of the type produced in DYNA. This density profile informs MCNP and is used to find criticality.

IV. MCNP SIMULATIONS

For the first series of simulations, the targets were assumed to be cylinders comprised of 93% enriched uranium.The radii and compression factors were varied to achieve the desired k_{eff}. Cylinders were simulated with diameters of 1, 2, and 3 cm with aspect ratios ranging from 1 to 8. The results for the 1 cm diameter target are shown in the following figure:

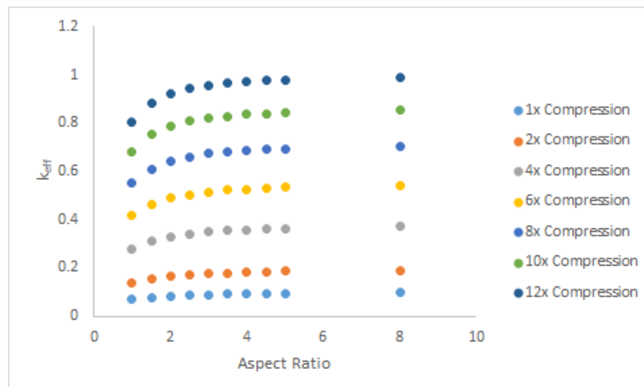

Fig. 2. Normalized k_{eff} of 1 cm diameter HEU target.

For these simulations, none of the targets examined were able to achieve a k_{eff} of 1 at any of the compression factors. This indicates that the target must have a diameter greater than 1 cm.
The results for targets that had a diameter of 2 cm are plotted in the following figure.

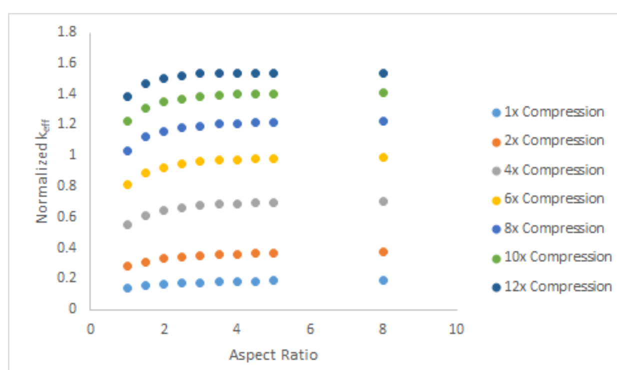

Fig. 3. Normalized k_{eff} of 2 cm diameter HEU target.

Targets with this diameter were able to achieve a k_{eff} of 1 with a compression factor as low as 8. Higher values for k_{eff} were attained with higher target aspect ratios.
The following figure provides the results for targets that have a diameter of 3 cm.

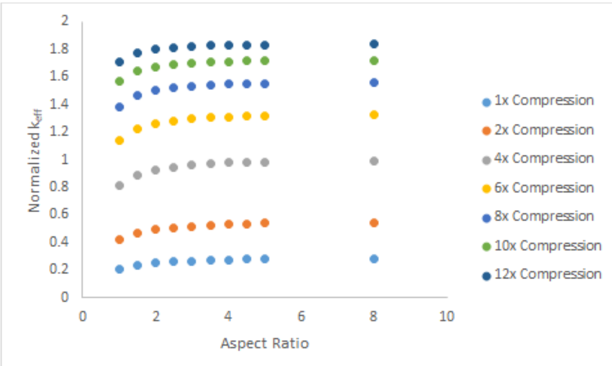

Fig. 4. Normalized k_{eff} of 3 cm diameter HEU target.

A k_{eff} of 1 was achieved for compression factors of 6. As with the other cylinder targets, a higher aspect ratio resulted in higher k_{eff}.
Once these simulations were complete, additional cases were run for targets comprised of 20% enriched uranium. These targets have the same diameters and aspect ratios as the highly enriched targets. The results for these simulations are provided in the following three figures.

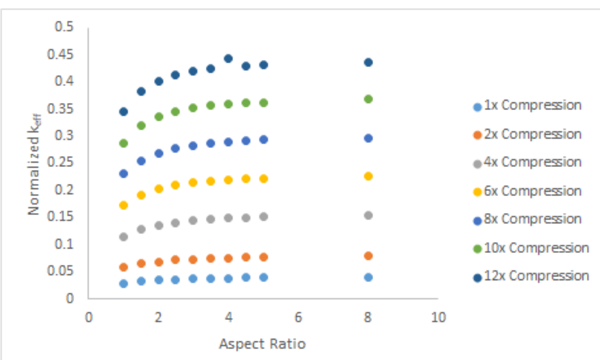

Fig. 5. Normalized k_{eff} of 1 cm diameter LEU target.

None of the 1 cm diameter targets were able to achieve a k_{eff} of 1 for this range of compression factors or aspect ratios. The following figure provides the results for targets that had a diameter of 2 cm.

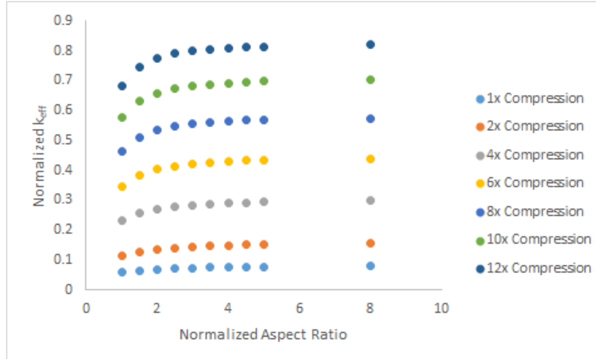

Fig. 6. Normalized k_{eff} of 2 cm diameter LEU target.

As with the 1 cm diameter targets, none of the 2 cm targets were able to achieve a k_{eff} of 1 for any of the examined compression factors or aspect ratios.
The following figure provides the results for low-enriched uranium targets having a diameter of 3 cm.

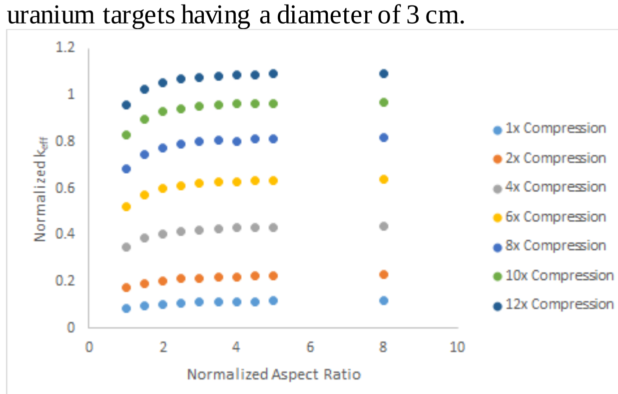

Fig. 7. Normalized k_{eff} of 3 cm diameter LEU target.

These targets were able to achieve a k_{eff} of 1 or slightly greater, but only with extremely high compression factors. This demonstrates how vital HEU will be for PUFF if target sizes are limited to the diameters, aspect ratios, and compression factors that were examined in these simulations.

V. CONCLUSIONS

The simulations presented in this paper show that criticality can be achieved for targets of high and low enriched uranium with the examined dimensions and compression factors. Future DYNA simulations will incorporate energy produced from nuclear reactions, which will likely be vital to accurately model the compression, stagnation, and expansion of the target. Future studies will also examine what current will be required to drive the target implosion and achieve the conditions observed in simulations.

ACKNOWLEDGMENTS

This work was funded by a NIAC Phase II award.

REFERENCES

[1] F. Winterberg, "Fussion-Fission-Fusion Fast Ignition Plasma Focus," *Physics Letters A*, vol. 336, no. 2-3, pp. 188-192, 2005.

[2] F. Winterberg, "On the ignition of high gain thermonuclear microexplosions with electric pulse power," *Physics of Plasmas*, vol. 11, no. 2, pp. 706-712, 2004.

Nuclear and Emerging Technologies for Space
Knoxville, TN, April 6 – April 9, 2020, available online at https://nets2020.ornl.gov

ADVANCED THERMAL MANAGEMENT CONCEPT FOR NUCLEAR-POWERED ICE MELTING PROBE

Calin Tarau[1*], Kuan-Lin Lee[1], William G. Anderson[1], Christopher G. Morrison[2] and Terry J. Hendricks[3]

[1]*Advanced Cooling Technologies, Inc., Lancaster, PA, 17601*
[2]*Ultra Safe Nuclear Corp, Seattle, WA, 98199*
[3]*NASA Jet Propulsion Laboratory, Pasadena, CA, 91109*

[*]*Calin.tarau@1-act.com 717-205-0659*

A thermal concept for the ice penetration and navigation probe to support future NASA's icy planets (e.g. Europa, Enceladus) exploration missions is developed. This thermal concept applies to both nuclear and radioisotope powered systems while the energy conversion is thermoelectric based. The thermal concept contains multiple features that can maximize the power fraction used for forward melting and mitigate a series of foreseen challenges related to icy-planetary missions. These thermal features include: (1) front vapor chamber for forward heat focusing and melting, (2) variable conductance side walls to enable lateral melting capability only when the probe gets stuck because of refreezing or meets obstacles, (3) side high-pressure steam/liquid outlets for probe maneuverability and steering (4) pumped two-phase loop for waste heat collection from the cold end of the thermoelectric convertors, transport and focus the heat at the front end of the vehicle for ice melting with minimal thermal resistance. This paper presents the preliminary design of the thermal management architecture of the melting probe for Europa ice layer penetration and presents the development of a lab-scale ice melting prototype for concept demonstration.

I. INTRODUCTION

NASA is highly interested to explore for extant life on Ocean Worlds (e.g. Europa, Enceladus), which require reliable vehicle that would directly access the subsurface liquid ocean layer underneath >30km of ice crust. Ice crust perforation can be achieved with a thermal probe that has a hot front that is supplied with enough heat so it can cancel ice subcooling, melt the ice or even sublimate the ice if ambient pressure is very low. Earth tests of such a vehicle have been successfully carried as shown in [1]. NASA is developing autonomous ice melting probes that use radioisotope to power the electronics and use the remaining waste heat to penetrate ice layer. In order to reduce penetration time, these nuclear-powered ice melting probes must have minimal footprint in vertical direction and the power fraction used for forward melting must be maximized. Advanced Cooling Technologies, Inc. (ACT) is developing a novel thermal management system that can effectively focus the waste heat to the melting front during normal ice penetration operation and mitigate a series of challenges that the probe might encounter during penetration process, including meeting obstacles, probe stuck due to ice refreezing etc.

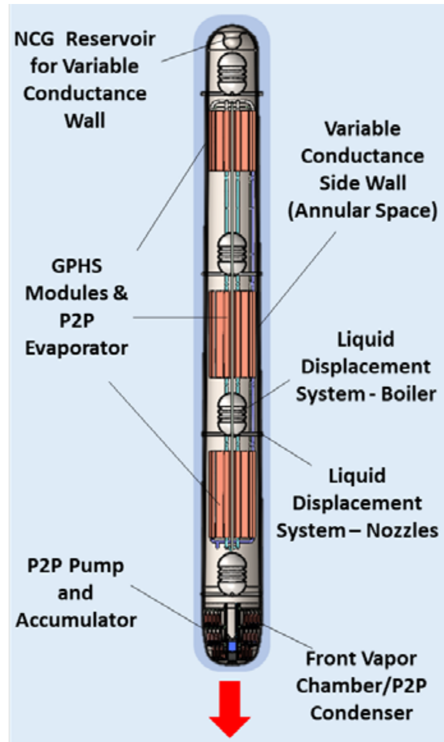

Fig 1. Preliminary thermal management system design of a nuclear-powered ice melting probe

Fig 1 above shows a preliminary thermal probe design with thermal management features. This probe design has dimensions of 26cm ID by 3m long and contains 32 GPHS modules to generate 8kW of waste heat for ice melting. Note that the thermal concept is also applicable to fission power system. Operation principle of the thermal management system is as follows: heat is provided from GPHS modules directly to thermoelectric (TEs) and the waste heat from the TEs is taken by a pumped two-phase (P2P) loop via evaporators interfacing with TE cold ends. Heat is transported via vapor flow to the condenser that is located at the bottom of the probe. Over there, P2P condenser interfaces with a front vapor chamber. The front vapor chamber in turn will focus the heat into the front of the probe for forward melting. The same front vapor chamber is extended upwards along the inside of the external wall (cylindrical) all the way to the top to form a narrow annular space. This annular extension of the front vapor chamber will contain Non-Condensable Gas (NCG) during normal operation and potentially vapor when lateral melting is needed. When thermal resistance between the front and the ice/liquid increases because of lateral freezing or other obstacles, vapor temperature and therefore vapor pressure in the vapor camber increases pushing the vapor-NCG interface upwards to heat the side walls for probe release or lateral motion. It can be seen from Fig 1 that, four sets of liquid displacement nozzles are installed to provide probe steering/lateral moving capability to avoid obstacles. More specific descriptions of thermal features are discussed in the next section.

II. THERMAL MANAGAMENT FEATURES OF ICE MELTING PROBES

II.A. Front Vapor Chamber

The front vapor chamber is a crucial component of the thermal management system since it is the main "melting" component and the main heat sink of the P2P loop. The heat is received from the P2P loop through a low thermal resistance heat exchanger that has wick at the interface which is always saturated with liquid. The heat evaporates the liquid from the heat exchanger wicked surface. The vapor will travel a short distance and condense in the wick of the inside of the front wall giving up the latent heat. This heat will conduct through the wall into the outside ice/water/environment. Optimize vapor chamber design would provide following advantages:

1. Low thermal resistance interface between P2P loop and the environment.
2. Uniform temperature distribution at melting interface.
3. Provide vapor to variable conductance walls.

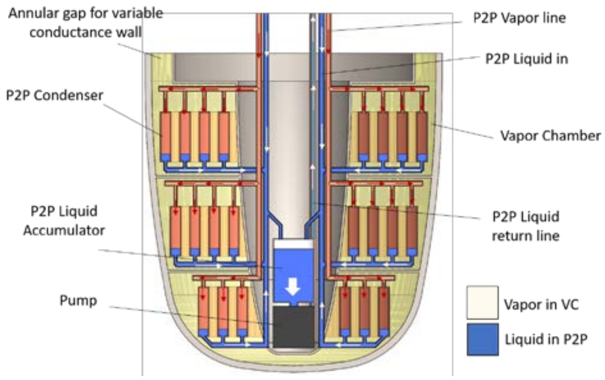

Fig 2. Compartmentalized Front Vapor Chamber and P2P Condenser

Fig 2 shows a potential vapor chamber design that integrated with P2P condenser. The front vapor chamber is elongated to increase heat transfer surface area at probe/ice interface. Also to accommodate more tubes for maximizing the heat exchange area between vapor chamber and P2P condenser, the vapor chamber is compartmentalized. Each level contains three to four toroidal tubes. This compartmentalized vapor chamber design is capable of transferring at least 15kW of heat at vapor temperature of 50°C.

II.B. Variable Conductance Side Walls

This feature involves an annular extension of the front vapor chamber upwards all the way to the rear (top) and connecting with an NCG reservoir. In other words, almost the entire probe would be blanketed by vapor and NCG that share the same volume/space. The vapor-NCG front location will be determined by vapor and NCG temperatures. Below, the feature is presented and explained based on the challenges that are solved.

1. Releasing the probe from lateral freezing: The major purpose of this feature is to passively melt the side ice when the vehicle gets stuck as a result of lateral water refreezing. When such an event occurs, thermal resistance in the front increases due to the fact that latent heat is not absorbed and also, the amount of outside liquid water increases its temperature because of sensible heating. As a result, vapor temperature increases and so does vapor pressure. Then, the vapor - NCG front moves upwards allowing the advancing vapor to heat side walls and further melt the outside ice to unblock the vehicle as Fig 3 shows. Once melting occurred and the vehicle is free to continue the forward melting and movement, vapor pressure goes back to the nominal value and the front travels back to the nominal location, just above the front vapor chamber resuming normal operation and forward melting. The system is fully passive and saves energy by minimizing its use during abnormal situations.
2. Avoiding obstacles - lateral melting: another serious challenge is the potential presence of rocks/debris/impurities in the path of the probe. In these cases, the forward melting becomes more difficult or even impossible preventing the probe from its advancement. Then, the front vapor chamber, that needs to reject the continuously incoming heat, increases vapor temperature and the NCG front moves up, as much as needed to enable heat rejection through the side walls. In other words, the probe gets hotter melting the surrounding ice and creating liquid water all around the probe. Then lateral melting and movement can start by engaging the liquid displacement nozzles, which will be described later.

3. Minimizing potential skewing: the vapor – NCG blanket that the Variable Conductance Walls feature provides will significantly increase the wall isothermality in tangential direction, minimizing the potential for skewness. In turn, this will minimize the length of the melting path/trajectory to the ice-liquid interface.

4. Heat rejection during transit: during transit to Europa the probe will be kept in "lateral melting" mode (or hot probe). In these conditions (hot probe), the entire amount of heat is rejected through the front vapor chamber and lateral walls to an external cooling loop (inside the carrier space craft) attached to the probe (and detachable once on Europa surface).

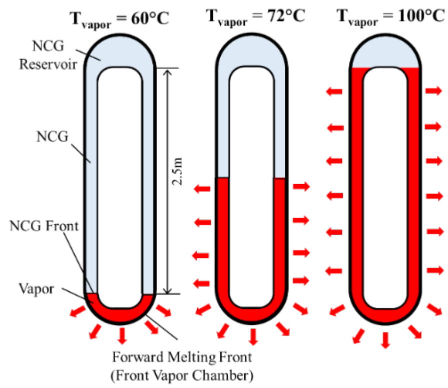

Fig 3. Operation principle of variable conductance side walls

II.D. Liquid Displacement System for Lateral Motion

This feature allows the probe to navigate through the ice in a direction other than vertical down when needed. The probe will include boilers capable of high pressure (>500atm) that are provided with nozzles to the outside environment. The high-pressure liquid nozzles would work under two different regimes:

- Two-phase water regime where the liquid is pushed out almost continuously by the vapor pressure. This regime will be used at depths where the environmental pressure is lower than the critical pressure of water (217 atm).

- Compressed liquid regime where the pressure vessel is liquid tight and volumes of liquid are pushed out into the environment intermittently (to allow recharge) by heating and cooling of the pressure vessel. This regime will be used at depths where the environmental pressure is higher than the critical pressure of water (217 atm). To be noted is that, even though the pressure is supercritical, heating of the vessel will not produce supercritical temperatures so the fluid (water) will always be in a "compressible liquid" state. Preliminary calculations show that, in high pressure environment (500atm), just by liquid displacement the probe can move entirely lateral at a rate of 1-2 mm per hour if an average heating power of 200W is applied.

II.D. Pumped Two-Phase Loop for Waste Heat Delivery

A schematic of the pumped two-phase loop system designed for waste heat collection from TEs and heat transport to the front vapor chamber is depicted in Fig 4(a). Liquid vapor phases of the coolant are separated by the wick structure within the evaporator as shown in Fig 4(b). Liquid phase will be driven by a pump and circulate within the liquid lines. Vapor phase will be generated at the evaporator, travel along vapor lines and release its latent heat at the condenser, which is located within the front vapor chamber. Wick structure of the evaporator must be properly design in such as way that it has sufficiently large capillary pressure to prevent vapor entering liquid lines at maximum heat loads [2].

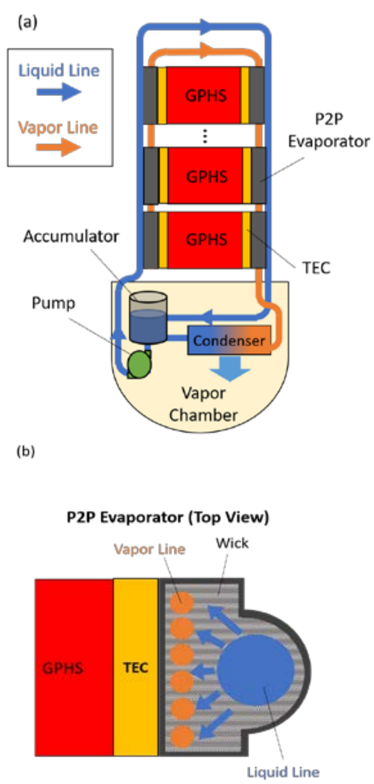

Fig 4. Pumped Two-phase Loop for waste heat delivery (a) flow path for liquid and vapor phases (b) Cross section of evaporator

II.E. Overall Thermal Resistance and ΔT Evaluation

The overall thermal resistance and ΔT from TE cold ends to the surrounding ice (ultimate heat sink) can be estimated. With 8kW of heat input, a preliminary thermal management design (P2P evaporator, condenser, loop and vapor chamber) would result in a ΔT of 62K. The heat transfer between probe and surrounding water (melted ice) was calculated based on [3]. This ΔT can be further reduced by component optimization and additional heat transfer enhancement features.

III. LAB-SCALE PROTOTYPE DEVELOPMENT

A reduced-scale melting probe prototype was built and tested. Three proposed thermal features are demonstrated by this prototype, including front vapor chamber, variable conductance wall and liquid displacement for lateral motion. The sectional view of the prototype is shown in Fig 5. This prototype consists of two shells. The inner shell contains a heater block, NCG reservoir and two high-pressure liquid outlet lines. The outer shell is the actual melting probe. Annular space between two shells is the vapor space of variable conductance walls, which will be charged with working fluid (water) and NCG (potentially argon). The vapor chamber is located at the bottom of the probe and the liquid return is achieved by fine screen mesh, as shown in Fig 5. The probe head has extruded fin structure to enhance ice/probe contact area. Flexible tubing connects between high pressure liquid source vessel (not shown in the figure) and the melting probe pipeline. High-pressure liquid pipelines penetrate the melting probe via a feedthrough from the top and exit from the side wall of the outer shell.

Fig 6 shows the experimental system built for prototype testing, which is the ice block (16” x 8” x 36”) with embedded serpentine. LN will run through the serpentine to create a subcooled ice to simulate refreezing conditions. Probe prototype will penetrate the ice from the top. Under certain power input, the axial temperature profile of the probe and the depth of penetration will be recorded during the melting process. Testing is ongoing and the test results will be presented in the conference.

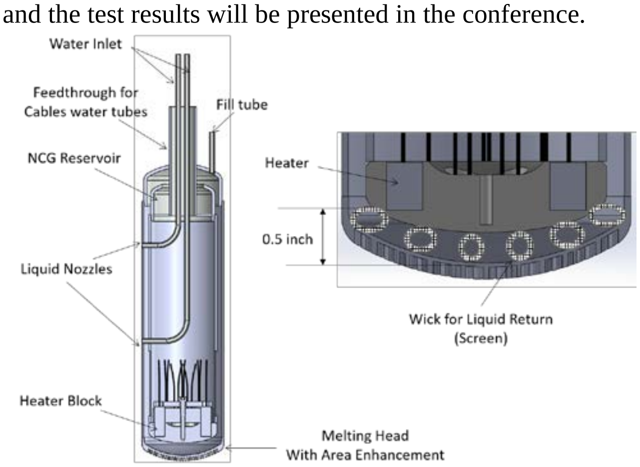

Fig 5. Cross section of lab-scale ice melting probe

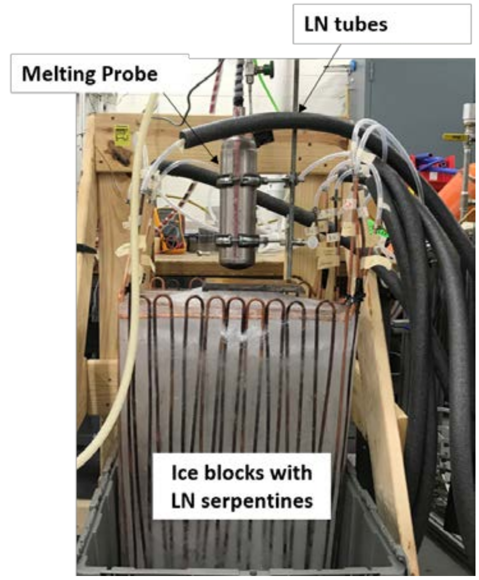

Fig 6. Experimental System for Prototype Testing

II. CONCLUSIONS

A thermal management architecture for a nuclear-powered ice melting probe for future Europa exploration was developed. The system contains multiple novel features to maximize ice penetration efficiency and mitigate foreseen challenges during the ice penetration process. A proof-of-concept prototype was built and tested in a relevant environment. Testing results will be presented in the meeting.

ACKNOWLEDGMENTS

This project is sponsored by NASA Jet Propulsion Laboratory (JPL) under an SBIR Phase I program (Contract# 80NSSC190363). The technical monitor is Terry Hendrick. Special appreciation goes to Eric Sunada. We would also like to acknowledge Philip Texter, Chris Jarmoski, Larry Waltman and Patrick Wisotzkey who have significant technical contributions on lab-scale melting probe prototype development.

REFERENCES

1. E. KAUFMANN, et al., “Melting and Sublimation of Planetary ices Under Low Pressure Conditions: Laboratory Experiments with a Melting Probe Prototype” *Earth, Moon, and Planets*, vol. 105 no. 1, p 11-29 (2009)
2. B. FURST., et al., “A Comparison of System Architectures for a Mechanically Pumped Two-Phase Thermal Control System”, *47th ICES*, 16-20 July (2017)
3. K. SCHULLER & J. KOWALSKI, “Melting Probe Technology for Subsurface Exploration of Extraterrestrial Ice-Critical Refreezing Length and the Role of Gravity”, *Icarus*, 317 (2019) p.1-9

Nuclear and Emerging Technologies for Space
Knoxville, TN, April 6 – April 9, 2020, available online at https://nets2020.ornl.gov

ADVANCED WASTE HEAT RECOVERY TECHNOLOGY BY THERMO-RADIATIVE CELL FOR NUCLEAR SPACE POWER APPLICATIONS

Jianjian Wang[1*], Chien-Hua Chen[1], Richard Bonner[1], and William G. Anderson[1]

[1]*Advanced Cooling Technologies, Inc., Lancaster, PA 17603*
[*]*Jianjian.Wang@1-act.com* *717-490-2387*

In order to satisfy the long-lasting and high energy/power density requirements for NASA deep space exploration missions, Pu-238 has been identified as one of the most suitable radioisotope fuels for GPHS modules since the 1960s. The availability of Pu-238 is currently extremely limited. The limited availability suggests that efficiently using the heat generated by the GPHS is very important and critical for NASA space applications. However, the efficiency of the most widely used radioisotope thermoelectric generators is only about 6-8%, which means that a significant amount of energy is dissipated as waste heat via radiators such as metallic fins. In deep space, the extremely cold universe (3 K) provides a robust heat sink. Even for a heat source with a temperature below 373 K, the corresponding Carnot efficiency can be more than 99%. In this paper, we show a proof-of-concept demonstration of using a thermo-radiative cell, a new technology concept conceived in 2015, to convert heat to electricity. A reversed I-V characteristic between thermo-radiative cell and photovoltaic cell is also experimentally demonstrated for the first time. The predicted efficiency of thermo-radiative cells is significantly higher than thermoelectrics at peak power output, and can be even higher at reduced power output. Integrating thermo-radiative cells with radio-isotope heating units (high-grade heat) or radioisotope power system (RPS) radiators (low-grade waste heat) could provide a new way to significantly increase the energy efficiency of Pu-238 or other radioisotope fuels.

I. INTRODUCTION

Traditionally, there are two classes of thermal-to-electrical energy conversion systems: static and dynamic. The key benefit of static thermal-to-electrical energy conversion systems, like thermoelectrics, thermophoto-voltaics, and thermionics, is that no moving parts are involved in the system. Dynamic thermal-to-electrical energy conversion systems, like Stirling, Brayton and Rankine cycle engines, involve repetitive motion of moving parts containing various working fluids. The operation of these thermal-to-electrical energy conversion systems in deep space requires a high temperature heat source which is usually supplied by General Purpose Heat Source (GPHS) modules. In order to satisfy the long-lasting and high energy/power density requirements for the deep space exploration missions, Pu-238 has been identified as the most suitable radioisotope fuel for GPHS modules since the 1960s [1].

However, the bulk production of Pu-238 in the US was stopped in 1988. Although DOE is expected to be able to produce 1.5 kg Pu-238 per year by 2026 for NASA, there are still many uncertainties, and DOE is facing many challenges to meet this production goal. In addition, due to the highly technical nature of the Pu-238 production process and the long time required (~2 years) for technical staff training, the unit price of Pu-238 is very high, ~$8 million per kilogram [2,3]. NASA's budget can only support one radioisotope power system (RPS) mission every 4 years [3]. The extremely limited availability and high cost of Pu-238 suggest that efficiently using the heat generated by the GPHS is very important and critical for NASA space applications. However, the efficiency of multi-mission radioisotope thermoelectric generator, which is a thermoelectric RPS, is only about 6%. Even though the dynamic thermal-to-electrical energy conversion systems (e.g. Stirling RPS) can achieve 25% or even higher efficiency, there is still a significant amount of energy dissipated as wasted heat via radiators such as metallic fins. Harvesting energy from this waste heat not only improves the total energy utilization efficiency of GPHS, but also significantly reduces the mass of the required RPS.

For any thermodynamic energy conversion system, from ideal Carnot heat engine to photovoltaics, thermophotovoltaics, thermionics, or thermoelectrics, there must be a high temperature heat source and a low temperature heat sink. The heat source temperature ranges from 800-1200 K in thermoelectrics to near 5800 K in photovoltaics. The high temperature in these heat sources is necessary due to the relatively high temperature heat sinks (~300-500 K) used in these energy converters since larger temperature differences between the heat source and heat sink usually give higher energy conversion efficiency. In deep space, the extremely cold background temperature of around 3 K provides a robust heat sink. Even for a waste heat source with a temperature below 373 K, the corresponding Carnot efficiency can be more than 99%. Here we are imagining an energy converter that can convert part of the waste heat from the primary convertors to electricity and dump the rest of the waste heat into deep space by radiation (the only choice to reject heat in this deep space). Such a device belongs to the general emissive energy harvester (EEH) which was proposed by Byrnes et al. in 2014 [4]. The EEH is a device that has high emissivity in the "atmospheric window" at 8-13 μm and low emissivity for other wavelengths. Since the atmosphere is almost transparent for radiation wavelengths between 8 μm and 13 μm, the earth's surface temperature is 275-300 K and the outer space temperature is only 3 K, so the EEH (at the earth's ambient temperature) will emit far more thermal radiation than it receives from the outer space. The imbalance of the emitted and the absorbed thermal radiation can be converted into an imbalance of charge carrier motion in the EEH, i.e., generating electricity (Fig. 1).

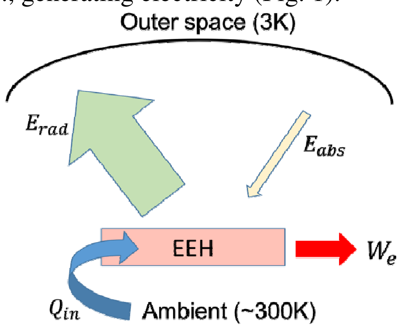

Fig. 1. Principle of emissive energy harvester (EEH).

Based on the general EEH idea, Strandberg [5] proposed a new technology concept, termed the thermo-radiative (TR) cell, to convert heat into electricity and reject the unused heat via thermal radiation. The thermo-radiative cell is essentially made of semiconductor P-N junctions and operated at an elevated temperature (325 K to 475 K, or even higher temperature depends on the accessible waste heat source temperature) compared to its surroundings (3-150 K in cold universe). It is well-known that P-N junctions are widely used in photovoltaic (PV) cells to convert solar radiation energy to electric power. In a photovoltaic cell, since the solar surface temperature is much higher than the cell temperature, more photons are absorbed by the PV cell than emitted by the PV cell. In a thermo-radiative cell, the surrounding temperature is lower than the cell temperature, thus the generated voltage has an opposite sign to the photovoltaic cell. When the device is connected with a load, the current direction in the thermo-radiative cell is also opposite to that of a photovoltaic cell (Fig. 2).

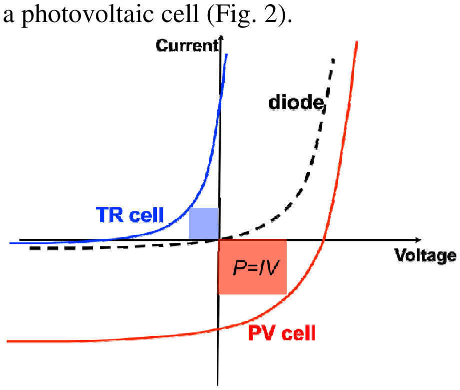

Fig. 2. The voltage and current directions in PV and TR cells are opposite. Both can generate power (P=IV <0).

II. THEORETICAL PREDICTION OF THERMO-RADIATIVE CELL PERFORMANCE

Power density and energy efficiency are the two most important parameters for any power generation devices. For deep space applications, the heat sink temperature can vary from 3 K (when the TR cell faces the deep space) to 100-150 K (when the TR cell faces some cold planets or their satellites). The power density of the thermo-radiative cell increases with the heat source temperature. The efficiency of the thermo-radiative cell varies with the cell voltage or the power density. The efficiency of the thermo-radiative cell can be analyzed by the principle of detailed balance [6-8], which was used to derive the famous Shockley-Queisser limit for photovoltaic cell.

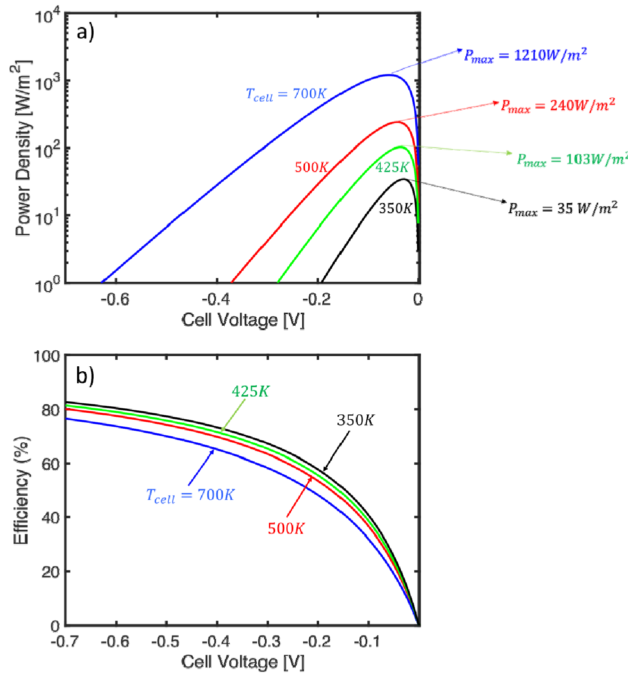

Fig. 3. (a) Power density and (b) Efficiency of the TR cell as a function of cell voltage at different temperatures.

Assuming a thermo-radiative cell with a bandgap 0.1 eV, its output power density and efficiency at different temperatures are calculated and shown in Fig. 3. The peak power density ranges from several tens of Watts per square meter (at 350 K) to over one thousand Watts per square meter (at 700 K) (Fig. 3a). For thermo-radiative cells operating at 500 K (near the low-grade waste heat upper limit), the generated electrical power density is on the same order of magnitude as photovoltaic cells. When the cell temperature reaches 700 K (medium-grade waste heat), the generated power density is several times higher than the state-of-the-art power density achieved in photovoltaic cells. The generated electricity could be used to supply power for the power electronics on spacecraft. Although the thermo-radiative cell efficiency increases with the magnitude of the cell voltage (Fig. 3b), the power density generated at those very large efficiency ranges (e.g., >50%) is low, except when the thermo-radiative cell is operated at relatively higher temperature (e.g., 700 K). Therefore, the efficiency near those peak power outputs is more useful (10%-35%). For low-grade waste heat recovery, the efficiency at peak power output is above 12%, which is significantly higher than the 6-8% efficiency of state-of-the-art thermoelectric RPS.

III. EXPERIMENTAL DEMONSTRATION

III.A. Thermo-Radiative Cell System Setup

For NASA space applications, the extremely cold universe (3 K) will serve as the heat sink for the TR cell energy conversion process. However, achieving such low temperature is difficult and requires expensive equipment. For terrestrial proof-of-concept demonstration, liquid nitrogen-based heat sink is chosen to mimic the cold universe. The radiation power from a black surface is proportional to the 4th power of temperature. For a heat sink at either 77 K or 3 K and a thermo-radiative cell at a temperature of low-grade waste heat, the net outgoing radiation (emitted minus absorbed) power from the TR cell surface is almost same for both cases. Therefore, it is accurate enough to mimic the cold universe heat sink with liquid nitrogen-base cryogenic system. The TR cell is kept near room temperature or mildly heated to a temperature corresponding to the typical low-grade waste heat temperature (less than 100□).

The thermo-radiative cell performs best with low bandgap semiconductors. There are a few good semi-conductor candidates that are commercially available and suitable for working as thermo-radiative cells for low-grade waste heat recovery. These candidates are InSb, $Hg_{1-x}Cd_xTe$, and $InAs_{1-x}Sb_x$, with appropriate x. Usually semiconductor bandgap decreases with temperature. Therefore, for high temperature operation, there are more semiconductor choices (e.g., InAs). HgCdTe commercial photodiode has been selected as the thermo-radiative cell in this demonstration, due to its wide tunable bandgap range and commercial availability.

The HgCdTe photodiode we used is covered with an immersion lens, so that the field of view (FOV) can be controlled. We placed a planar cold plate (liquid nitrogen cooled) at a finite distance from the cell and ensure that cold plate surface completely covers the FOV of the HgCdTe thermo-radiative cell. The cold plate is made of aluminum with embedded copper tubes. Liquid nitrogen flows through the copper tubes to maintain the aluminum plate surface at low temperature. The surface temperature is adjustable from room temperature down to around 77 K. The surface temperature is controlled by the flow rate of the liquid nitrogen in the copper tube. An ultra-black foil is covered on the top surface of the cold plate. It aims to minimize the reflections from the environment to the thermo-radiative cell since it has very low reflectance from visible light to long-wavelength infrared (LWIR).

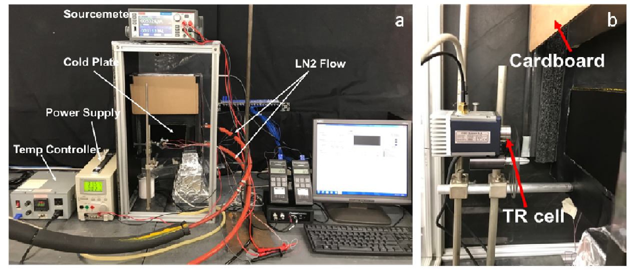

Fig. 4. (a) Experimental setup. (b) Side view of TR cell.

Fig. 4 shows the integrated thermo-radiative cell measurement system. During the measurements, a cardboard sheet is controlled manually to block/unblock the view of the thermo-radiative cell. The system is placed in a chamber during the measurement which is flowed with dry nitrogen gas to maintain a positive pressure and reduced humidity inside, which could avoid the water vapor in the ambient entering into the chamber as well as minimize the condensation on the cold plate.

III.B. TR Cell ON/OFF Response Demonstration

Initially, the cell and the cold plate are both at ambient temperature. At this point, there should be zero net radiation from the thermo-radiative cell to the cold plate. The measured output electrical signal of the thermo-radiative cell is almost zero as expected. As we continuously decrease the cold plate surface temperature by controlling the liquid nitrogen flow rate, the output electrical signal continuously increases. If we use cardboard to suddenly block the view of the cell to the cold plate, we observed that the electrical signal suddenly drops to zero. This is because the cardboard and the thermo-radiative cell are at the same temperature. In other words, the thermo-radiative cell changes from the "ON" state when it faces to the low temperature cold plate, to the "OFF" state when it suddenly faces to the ambient temperature cardboard. This ON/OFF response is clearly showed in Fig. 5.

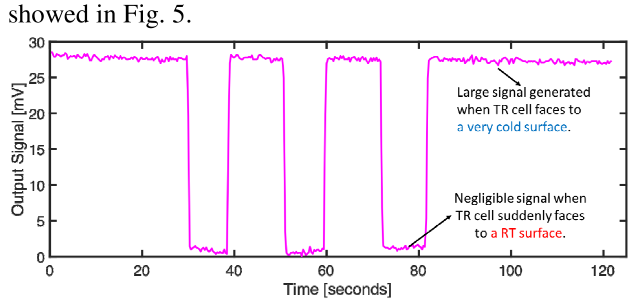

Fig. 5. A measurement curve when the cold plate is at -50C and the TR cell is at ambient temperature.

III.C. TR Cell I-V Characteristic Demonstration

We compared the I-V curves of the cell under three different conditions. Under the first condition, the cell is in thermal equilibrium with the ambient. In this case, the I-V curve passes through the origin point, i.e., when the bias V=0, the current I=0 (the blue curves in Fig. 6). The cell shows the standard p-n junction behavior under dark condition. As we heated up the cell and controlled the plate to the cryogenic temperature, the cell works in the thermo-radiative cell mode. The I-V curve moves upwards from the thermal equilibrium curve, i.e., when the bias V = 0, the short-circuit current is positive (the black curves in Fig. 6). When we kept the cell at ambient temperature and heated up the plate temperature, the cell works in the (thermo-)photovoltaic mode. The I-V curve moves downwards from the thermal equilibrium curve, i.e., when the bias V = 0, the short-circuit current is negative (the red curves in Fig. 6).

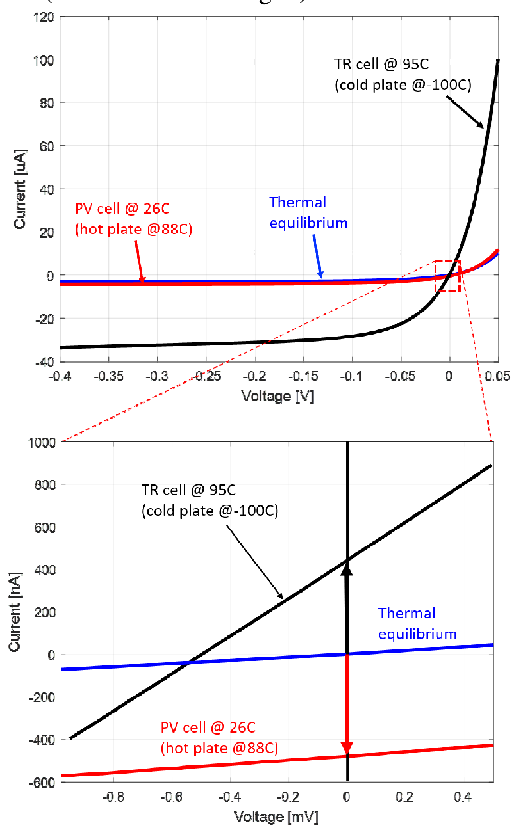

Fig. 6. I-V measurement of the cell under three conditions: PV mode, TR mode, and thermal equilibrium.

To the best of our knowledge, this is the first experimental demonstration of the reversed current-voltage characteristics between a thermo-radiative cell and a photovoltaic cell. The demonstration clearly indicates the feasibility of using thermo-radiative cells for power generation. For example, we can integrate thermo-radiative cells with RPS radiators to harvest the low-grade waste heat, i.e., providing additional electric power for RPS.

IV. CONCLUSIONS

In summary, thermo-radiative cell is a new waste heat recovery technology that is extremely suitable for space power applications. Usually it is difficult to harvest energy from low-grade waste heat since the temperature difference between the terrestrial ambient and low-grade waste heat is small, and the heat dissipation at low temperature is more difficult. However, in deep space, since thermo-radiative cell can easily make use of the cold universe as the heat sink (3 K to 150 K), it makes low-grade waste heat recovery much easier. In addition, it is passive with no moving parts, and does not require maintenance. It could potentially serve as an easy add-on to the radiator panels without changing the current RPS design. The predicted efficiency of thermo-radiative cells is significantly higher than thermoelectrics at peak power output, and can be even higher at reduced power output. Integrating thermo-radiative cells with radioisotope heating units or radioisotope power system radiators could provide a new way to increase the energy efficiency of Pu-238 or other radioisotope fuels. To the best of our knowledge, the reverse current-voltage characteristics between thermo-radiative cell and photovoltaic cell are experimentally demonstrated for the first time.

ACKNOWLEDGMENTS

This SBIR Phase I program was sponsored by NASA under contract No. NNX17CS05P. We would like to thank Wayne Wong of NASA Glenn, and Jean-Pierre Fleurial of NASA JPL for their helpful comments and suggestions on integrating thermo-radiative cells with NASA spacecraft.

REFERENCES

[1] Schmidt, G.R., Sutliff, T.J., and Dudzinski, L.A. "Chapter 20-Radioisotope Power: A Key Technology for Deep Space Exploration," Radioisotopes–Applications in Physical Sciences

[2] News from Nuclear Science and Engineering Department, Oregon State University, http://ne.oregonstate.edu/rebuilding-supply-pu-238

[3] "Space Exploration: Improved Planning and Communication Needed for Pu-238 and Radioisotope Power Systems Production," US Government Accountability Office Report, #GAO-17-673

[4] Byrnes, S.J., Blanchard, R., and Capasso, R. "Harvesting renewable energy from earth's mid-infrared emissions," PNAS, 111, 3927-3932, 2014

[5] Strandberg, R. "Theoretical efficiency limits for thermoradiative energy conversion," J. Appl. Phys., 117, 055105, 2015

[6] Hsu, W.-C., Tong, J.K., Liao, B., Huang, Y., Boriskina, S.V., and Chen, G. "Entropic and near-field improvements of thermoradiative cells," Sci. Rep., 6, 34837, 2016

[7] Shockley, W., and Queisser, H.J. "Detailed balance limit of efficiency of p-n junction solar cells," J. Appl. Phys. 32, 3, 510–519, 1961

[8] Santhanam, P. and Fan, S. "Thermal-to-electrical energy conversion by diodes under negative illumination," Phys. Rev. B, 93, 161410, 2016

Nuclear and Emerging Technologies for Space
Knoxville, TN, April 6 – April 9, 2020, available online at https://nets2020.ornl.gov

RADIOISOTOPE BREEDING FOR POSITRON MICROFUSION PROPULSION

Ryan W. Weed[1], Balachandar Ramamurthy[1], and Joshua R Machacek[1]

[1]*Positron Dynamics Inc, Mojave, Ca, 93501*

Primary Author Contact Information: ryan.weed@positrondynamics.com

A microfusion propulsion concept has been proposed that utilizes this annihilation 'knock-on' process, where a pulse of monoenergetic positrons is injected into a small volume of a metallic substrate loaded with high density of Deuterium. Neutrons from the DD fusion events are thermalized in a blanket surrounding the engine core filled with ^{78}Kr. gas, undergoing a neutron capture reaction, producing ^{79}Kr. This radioisotope is enriched and deposited on a cryogenic surface, providing a source of moderated positrons for further pulsed beam production. Here, we discuss the feasibility and initial simulation results of the required engine core geometry, neutronics, radioisotope breeding dynamics, positron source production.

I. INTRODUCTION

Nuclear fusion-based propulsion concepts hold great promise for increasing delta-V capability of spacecraft and significantly reducing transit times for manned spaceflight missions within the solar system[1]. Magnetic confinement fusion (e.g. ITER) and Inertial Confinement Fusion (e.g. NIF) require large magnet mass and/or large driver systems in order to achieve ignition conditions in fusion fuel[2]. Antimatter-matter annihilation has the ability to deliver large amounts of energy without requiring massive driver systems. Early antimatter-fusion concepts relied on antiproton-proton annihilation to generate fusion ignition conditions[3], however, production and trapping of sufficient quantity of antiprotons remains a challenge[4]. Positrons are lighter and can produced from radioisotopes during a beta decay process[5]. While positrons are easier to create compared to antiprotons, positron-electron annihilation produces gamma rays, which are not efficient at heating fusion fuels, due to their low interaction cross section. This has limited the positron to annihilation-thermal propulsion concepts[6] which require unrealistic amounts of trapped positrons to generate significant thrust.

In the 1990's, Morioka suggested that Deuterons trapped in metal lattice defects may be able to receive kinetic energy from positron-electron annihilation gamma-rays[7], similar to the Mossbauer nuclear excitation process[8]. Recent experimental work shows that positron-electron annihilation in deuterated metal substrates can indeed transfer kinetic energy to a trapped deuteron, causing Deuterium-Deuterium fusion events to occur[9]. This mechanism gives positrons the ability to inject pulses of large power density in fusion fuels, generating the conditions required for ignition.

I.A. Propulsion Concept

In the Radioisotope Positron Propulsion (RPP) concept, a focused and pulsed positron beam generates microfusion reaction products which exit through a magnetic nozzle, producing thrust. Neutrons from these fusion reactions are captured in a nozzle blanket to produce a positron-emitting radioisotope, which is enriched and deposited onto a source layer, producing more positrons and more thrust. This 'breeder' fuel cycle avoids the need to store large amounts of antimatter and allows for launch with a minimal amount of radioisotope[10].

I.B. Microfusion Ignition

Previous work with ion-beam driven inertial confinement fast ignition gives us a rough order-of-magnitude requirement for energy deposition requirement to initial a fusion burn in Deuterium-Deuterium fuel. In the fast ignition scheme, it is estimated that a Deuteron beam of approximately 10^{18} ion/cm^2 would achieve ignition in a 10nm thick Palladium foil, loaded with D clusters at a 10% packing fraction[11]. To estimate the positron pulse requirements, we need to know the momentum transfer probability of this impulse interaction, which compares the spin averaged differential cross section of the impulse interaction with the dominant 2-gamma annihilation process:

$$R \equiv \frac{d\sigma_R}{d\sigma_{2\gamma}} = \frac{e^2}{2m^2}\sqrt{\frac{M_D}{m}}\,|I^2|, \qquad (1)$$

where M_D and m are the mass of the Deuteron and positron, respectively, and I describes the S-matrix for the impulse interaction. Neutron measurements from DD fusion reactions in Deuterium gas loaded Pd substrate, using a ^{22}Na positron source indicate the impulse interaction probability is approximately R ~.01. From this, we estimate a 400ps pulse of 10^{12} positrons on a 50-micron beam spot would produce ignition conditions.

Analysis of Lawson Criteria and results from 0-D Energy balance and 2-D PIC code simulations predict similar positron beam requirements[12].

I.C. Radioisotope Enrichment

Using a (n,γ) reaction in this manner to generate a positron beam was originally proposed by Mills in 1990's who estimated that 10-100 atm blanket of pressurized Kr will be sufficient to thermalize these hot neutrons within a reasonable length scale (<1m) [13,14]. Mills envisioned that the Kr would then pass into the cryogenic isotope enrichment stage, allowing for very high source specific activities (>kCi/g). The Mills enrichment method utilizes an oscillating carrier gas (e.g. He) in combination with periodic heater elements to achieve very high separation factors in a single stage[13].

II. ENGINE CORE DESIGN

The engine core not only brings together the fusion driver and the fusion fuel, but also serves to regulate and dissipate waste heat, direct fusion particles to generate thrust, and finally to capture energetic DD neutrons, producing the radioisotope source of positrons. The interplay between these design elements result in complex trade-offs[12]. The geometry of the engine core is dominated by the neutron capture blanket, as shown in Figure 1.

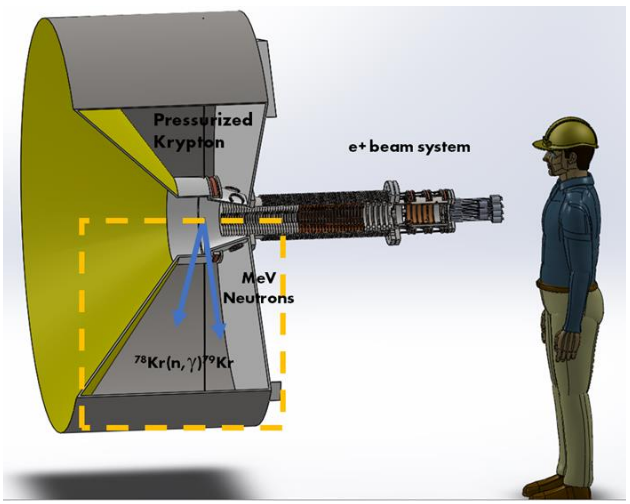

Fig. 1. Cutaway of engine core section.

Initial nozzle design covered approximately 2π of the fuel target with a 1-meter thickness gaseous Krypton layer Later iteration of this design included a ‘hot section’ and ‘cold section’ with varying Kr density but maintained the overall shape that maximizes solid angle to the fuel target.

Monte Carlo N-particle Code[15] (MCNP Version 6.2 with ENDF/B-VII.1 Cross Sections) was used to determine neutron transport characteristics in the engine core.

III. RADIOISOTOPE BREEDING

^{79}Kr positron source breeding follows the linear set of coupled differential equations, with N_{78} and N_{79} representing the amount of ^{78}Kr and ^{79}Kr in grams, respectively:

$$\frac{\partial N_{78}}{\partial t} = -A * N_{78}N_{79} \quad (2)$$

$$\frac{\partial N_{79}}{\partial t} = A * N_{78}N_{79} - \lambda N_{79} \quad (3)$$

where λ is the decay rate (λ=8E-6 s^{-1} for ^{79}Kr) and A is a constant describing positron beam production, transport to fusion target, fusion characteristics and neutron capture properties. If we define the number of neutrons generated per incident positron as n_p and the probability of neutron capture in the ^{79}Kr blanket per incident neutron as η_c, then equation 3 becomes:

$$\frac{\partial N_{79}}{\partial t} = \lambda N_{79}\{\ln(2)\,\beta\varepsilon_m T n_p \eta_c \Omega N_{78} - 1\}, \quad (4)$$

with β the branching ratio for positrons emitted per decay of ^{79}Kr, T represents the accumulator and transport efficiency, ε_m the moderator efficiency, and Ω the solid angle of the ^{79}Kr blanket. From equation 4 we see that the breeding requirement is:

$$\ln(2)\,\beta\varepsilon_m T n_p \eta_c \Omega\, N_{78}^0 > 1, \qquad (5)$$

where $N_{78}^0$is the initial amount of ^{78}Kr. Equation 5 does not explicitly depend on the initial amount of ^{79}Kr, however, it is likely that the accumulator and transport efficiency, T, will drop to zero at arbitrarily small values of N_{79}^0, due to finite trap and accumulator lifetimes as well as limitations to the ^{79}Kr enrichment throughput. To include this in our model, we assume that accumulator and trap efficiency depends on the amount of ^{79}Kr, such that $T = [1 - e^{\frac{-N_{79}}{\kappa}}]$.

In this model, κ corresponds to the amount of ^{79}Kr that will produce the number of positrons required to reach ignition in the target (N_{pos}) within the trap/accumulator lifetime, τ. A realistic upper limit for trap/accumulator lifetimes is on the order of 100 secs based on previous work with low pressure accumulator stages[16]. Given the branching ratio of ^{79}Kr of $\beta = 0.07$ and $N_{pos} = 10^{12}$ per pulse the transport efficiency, T, rises rapidly to unity when the amount of ^{79}Kr is above 10 µg.

IV. POSITRON SOURCE/MODERATOR

The propulsion system cannot support an arbitrarily large amount of ^{79}Kr due to several factors:

- Heat load and neutron damage in source, blanket, nozzle, magnets
- Cooling, compression, bunching timescales
- ^{79}Kr isotope enrichment throughput
- Positron self-absorption in source layer

The driving limitation will likely be reduction in moderator efficiency when the thickness of ^{79}Kr-rich source layer approaches the thermalization length of the energetic positron emitted during decay of ^{79}Kr. This process is modeled using PENELOPE a Monte-Carlo simulation of electron and positron energy loss in solid materials.

Additionally, the source/moderator surfaces must be maintained at approximately 100K during operation. Heat load into the source layer was estimated using the PENELOPE simulation results and the Beer-Lambert law for gamma-ray absorption using In general, the heat load from gamma ray absorption will be much lower than the heat load from positron thermalization:

$$\frac{E_{abs}^{pos}}{E_{abs}^{\gamma}} \sim \frac{\beta}{\left[1-e^{-\left(\frac{\mu}{\rho}\right)\rho T}\right]} \gg 1. \quad (6)$$

V. RESULTS

V.B. Neutron Capture Estimates

A representative example of MCNP simulation results for 10atm pressurized Kr blanket is shown in Fig 2, below.

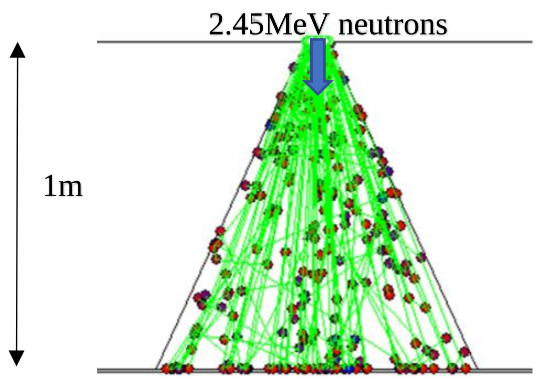

Fig. 2. PENELOPE simulation results for ^{79}Kr emitted positrons into solid Kr layer.

After running MCNP over several different Kr pressures, we found the neutron capture probability, η_c, to scale $\eta_c \sim 0.013\ atm^{-1}m^{-1}$. This scaling was used in the radioisotope breeding system model and helped determine optimal blanket sizing for a given mission application.

V.B. Radioisotope Breeding

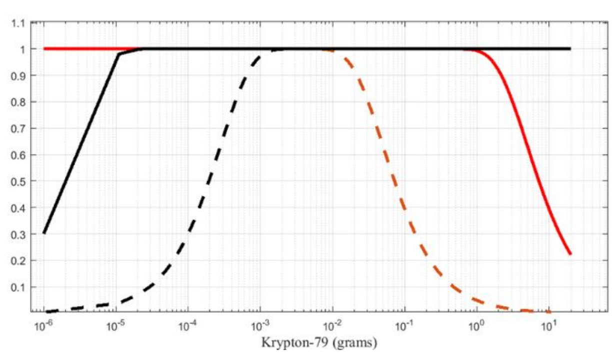

Fig. 3. Transport efficiency model. The dotted lines represent trap/accumulator lifetime of 1 sec and ^{79}Kr enrichment of 1%. Solid lines represent 100 sec trap/accumulator lifetime and 100% enrichment.

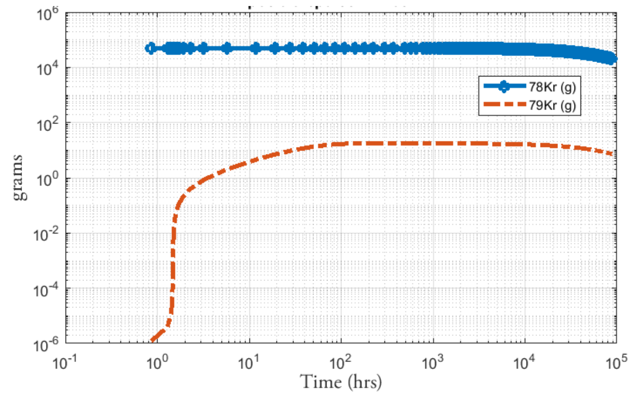

Fig. 4. Amount of ^{78}Kr and ^{79}Kr versus time from MATLAB RPP model.

Using the breeding model described above a time-series output was generated in MATLAB. From Fig. 4, we see that the initial breeding period lasts less than a week, increasing the amount of ^{79}Kr from 1ug to more than 10g. The ^{79}Kr breeder system can be turned off for days at a time, without losing the ability to restart the engine. Over long periods of operation, the engine core will run out of ^{78}Kr as the ^{79}Kr decays into Bromine and is filtered out of the fuel cycle. The beginning of this process can be seen at times >10^4 hours in Fig. 4.

V.C. Positron Source Layer

To determine the fraction of positrons that escape the frozen Kr layer, we performed PENELOPE simulations of positron implantation and reflection from a Tantalum backing. The reflector is placed adjacent to the source layer in order increase positron flux towards the beam output. PENELOPE simulations indicate the 40% of incident positrons will be reflected towards the moderator for a planar geometry using a Ta reflector. Additionally, the simulation results (Fig. 5) indicate that nearly all the positrons are thermalized in the source layer when the thickness is above 200um.

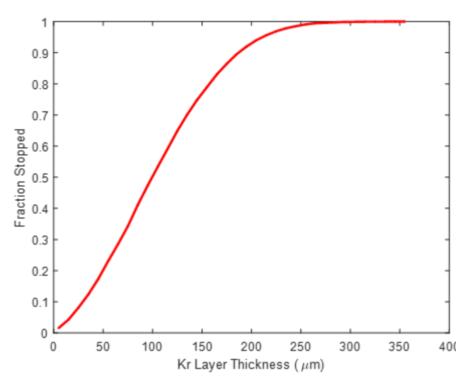

Fig. 5. PENELOPE simulation results for ^{79}Kr emitted positrons into solid Kr layer.

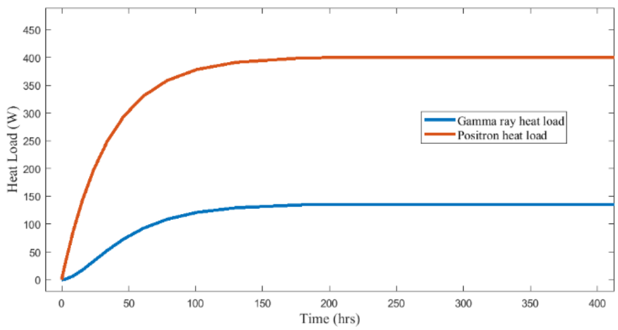

Fig. 6. Heat load vs time for gamma rays and positrons for 100cm^2 square source area, 25% enrichment.

The heat load to the source layer in this example is ~5W/cm^2, with a maximum ^{79}Kr activity of 2.5x10^{17} Bq. With the source layer temperature of <100K, radiative heat transfer away from the surface is minimal, therefore active cooling must be applied. Modern Pulse Tube Cryocoolers could apply the required cooling power at cryogenic temperatures[17]. Additional cooling could also be applied flowing low temperature D_2 gas through microchannels in the coldhead structure.

VI. CONCLUSIONS

We have described a radioisotope breeding design that could lead to the most intense positron beams ever produced. A propulsion system based on this fuel cycle would be capable of providing very high specific impulse (>10^5 sec) and specific power (>10kW/kg) on a variety of manned and un-manned spacecraft, enabling very high delta-V missions throughout our solar system.

While this work focused on the neutron capture, breeding requirements and source characteristics; more experimental work is planned to determine if pulsed positron beams can actually produce ignition in fusion targets. The ignition problem is not unique to RPP - the high temperature and radiation environment presents a common challenge for surrounding materials amongst various fusion projects. We hope to leverage the progress being made, particularly in high temperature superconducting magnets, and the understanding of fusion facing materials and their damage characteristics.

ACKNOWLEDGMENTS

Some material presented here was supported by NASA under award 80NSSC18K0910.

REFERENCES

1. Meyer, Mike, et al. "In-space propulsion systems roadmap." National Aeronautics and Space Administration, Office of the Chief Technologist (2012)
2. Tabak, M., et al. Review of Progress in Fast Ignition, Physics of Plasmas 2005
3. Kramer, K. et al. “Antimatter-initiated microfusion: Direct energy conversion for propulsion applications” AIP Conference Proceedings, 608, 787-788 (2002)
4. Mansoulié, Bruno, and GBAR Collaboration. "Status of the GBAR experiment at CERN." *Hyperfine Interactions* 240.1 (2019): 11.
5. Krause-Rehberg, Reinhard, and Hartmut S. Leipner. *Positron annihilation in semiconductors: defect studies*. Vol. 127. Springer Science & Business Media, 1999
6. Smith, G. NIAC Phase I Final Report “Positron Propelled and Powered Space Transport Vehicle for Planetary Missions”
7. Morioka, “Nuclear Fusion Triggered by Positron Annihilation in Deuterated Metals”, Il Nuovo Cimento, Vol107a, N12, 1994
8. Cassidy, D.B., et al, "Resonant versus nonresonant nuclear excitation of 115In by positron annihilation," Physical Review C, Vol 64 054603, October 2001
9. Weed, R., et al. "Positron-electron annihilation momentum transfer to trapped deuterons." *AIP Advances* 9.11 (2019): 115109.
10. Weed, R., et al. "Positron propulsion for Interplanetary and Interstellar Travel." *Journal of the British Interplanetary Society* 72 (4), 110-115 (2019)
11. J. C. Fernandez, B. J. Albright , K. A. Flippo et al., “Progress on Ion based fast ignition” Journal of Physics: Conference Series (2), 022051 (2008)
12. Weed, R. et al. “Radioisotope Positron Propulsion – NASA Innovative Advanced Concepts Phase I Report” NASA Technical Reports Server, Report HQ-E-DAA-TN67893, (2019)
13. Mills Jr, A. P. "Physics with many positrons." *Rivista del Nuovo Cimento della Societa Italiana di Fisica* 34.4 (2011): 151-252.
14. Mills Jr, A. P. "Suitability of ^{79}Kr as a Reactor-Based Source of Slow Positrons." *Nuclear science and engineering* 110.2 (1992): 165-167
15. Briesmeister, Judith F. "MCNPTM-A general Monte Carlo N-particle transport code." *Version 4C, LA-13709-M, Los Alamos National Laboratory* (2000)
16. Greaves, R. G. & Surko, C. M. “Positron trapping and the creation of high-quality trap-based positron beams” Nucl. Instruments Methods Phys. Res. Sect. B Beam Interact. with Mater. Atoms 192, 90–96 (2002)
17. Shaoshuai Liu , Zhenhua Jiang , Lei Ding , Haifeng Zhu , Qi Huang , Yinong Wu. “Impact of operating parameters on 80 K pulse tube cryocoolers for space applications” International Journal of Refrigeration (2018)